FABRICATION OF ELECTROCHEMICAL BIOSENSORS FOR THE DETERMINATION OF PHENOLIC COMPOUNDS BY EXPERIMENTAL AND COMPUTATIONAL METHODS

Kwanele Winterose Kunene

(Reg. No: 20803990)

Submitted in fulfilment of the requirements of the degree of Master of Applied Science in Chemistry in the Faculty of Applied Sciences at the Durban University of Technology

January 2018

DECLARATION

I, **Kwanele Kunene** declare that the thesis submitted for the degree of Master of Applied Science in Chemistry at the Durban University of Technology is the result of my own investigation and has not already been accepted in substance for any degree, and is not being concurrently submitted for any other degree. All the work was done by the author.

Student Name: Kwanele Kunene

Student Signature [redacted] Date:.25/01. /2018…

Supervisor Name: Professor K. Bisetty

Signature: [redacted] Date:.25/01. /2018…

Co-Supervisor Name: Dr S Kanchi

Signature: [redacted] Date:.25/01. /2018…

DEDICATION

Traveler there is no path

The path must be forged as you walk.

Antonio Machado

Dedicated to the memory of my late father (Madoda Maxwell Kunene) who always supported me, whatever path I took.

ACKNOWLEDGEMENTS

This thesis became a reality with the kind of support and help of many individuals. I would like to extend my sincere thanks to all of them.

Foremost, I want to offer this endeavour to **GOD** almighty for the wisdom, strength, peace and good health enabled me to complete this research.

I would like to extend my sincere gratitude and appreciation to my supervisor, **Prof K Bisetty** for his patient guidance, practical advice, multiple revisions, and consistent encouragement throughout the work. There is a quiet force in his sweet smile, which gave me power through my master's study. I am very proud and lucky to have him as my academic advisor. I would also like to express my gratitude and appreciation to my co-supervisors **Dr. S Kanchi** and **Myalowenkosi Sabela** for their encouraging words during a difficult period. **Mrs. Mavis Xhakaza**, **Mpume Cele** and **Avy Naicker** for their help during experimental analysis. I'm highly indebted to my second family at the **University of Latvia** and **University of Lithuania** for their guidance and supervision, especially to **Prof Donalts Erts, Dr. Roman Viter, Prof Arunas Ramanavicius, Daniel Jevdokimov and Povilas Genys.**

I want to express my gratitude to my family especially my mother, **Makubheka Kunene**, **Mbalie Kunene, Lihle and Khwezi Mbambo** for their encouragement and motivation to finish this research; to my beloved and supportive twin, **Dasie** who is always by my side when I need her the most and my son, **Zosukumizizwe** who served as my inspiration to pursue this journey. I would like to give my deepest sense of gratitude to **Zama Khumalo** for his constant understanding and support throughout this journey. I would also like to express my sincere gratitude to **Ms. Mathonsi, Mr. Njabulo Kudla and Yusuf Mia.**

Many thanks go to my friends Dennis Walthew (Mr. D), Sandile Mgiqi, Mzo Dandala (Ntsaka), Nosipho Cele, Athika Darumas, Bayo Tri, Deepa Sharma, Avenal Finlayson, Teo Gherkenashvili, Benjie Mokhine, Lethukuthula Buthelezi, Ncomeka Mgxadeni, Slungile Nxumalo, Talent Makhanya, Londie Mkhize, Mxolisi Cele, Ntokozo Ntsaba, Palisa Mothibe, Sindisiwe Muthwa, Nonhlanhla Khomo, Freddie Ncube, Queen Ngubane, Menzi Mtshali, Mike Mathe, Hlengiwe Hlongwane, Zinhle Shabalala, Neli Xulu, Nkanyezi Kubheka, Zamo

Makhanya, Zibuyile Mposula, Funanani Ravuluvulu, Bhekie Mgobhozi and Jackie Mathanzima, for their consistent support throughout this work and for believing in me.

I would like to acknowledge the financial support of National Research Fund (NRF) and AESOP scholarship.

ABSTRACT

The polyphenolic compounds of interest, bisphenol A (BPA) and its analogue bisphenol S (BPS) used in the plastic industry to manufacture baby bottles and beverage containers, were used in this study. They are generally used in the manufacture of polycarbonates, epoxy resins and unsaturated polystyrene resins. There is a growing concern in the public and scientific community about these organic compounds due to their endocrine disrupting activity and negative toxic impact on the wildlife. This has encouraged scientists to embark on research to find a sensitive and selective technique that will adequately determine these compounds even in trace amounts.

The experimental research strategy adopted in this work was supported by computational methods. This work was conducted in two stages; Firstly, a sensitive EC biosensor was developed using a carbon screen printed electrode fabricated with the combination of silver doped zinc oxide nanoparticles with multiwalled carbon nanotubes (MWCNTs) and laccase enzyme. The EC behaviour of BPA towards the fabricated biosensor was investigated using cyclic voltammetry and differential pulse voltammetry under optimum experimental conditions. Secondly, a novel and selective PEC sensor was developed for the first time to detect BPS based on the vertically aligned ZnO nanorods (ZnO NRs) with a molecularly imprinted polypyrrole (PPy). Amperometric, cyclic voltammetry and impedance spectroscopy were used for the investigation of the photo induced electrochemical behaviour of BPS.

Different characterisation techniques such as ultra-violet visible spectroscopy, fourier transform infrared spectroscopy, scanning electron microscopy, transmission electron microscopy, photoluminescence, Raman spectroscopy, grazing incidence X-ray diffraction and diffuse reflectance were used to characterize the synthesized nanostructures.

Results revealed that the fabricated EC and PEC sensors exhibited good catalytic activity towards the determination of BPA and BPS respectively, in samples extracted from plastic water bottles.

For the EC method, a low detection limit of 0.08 μM for BPA in a linear range 0.5 to 2.99 μM was detected. However, in the case of BPS, a highly selective PEC method was attained linearly ranging from 2.5 to 12.5 μM with a much higher limit of detection of 0.7 μM.

Experimental results were further supported computationally for a better understanding of the optical properties of ZnO NRs-polypyrrole complex. Computational results were in good agreement with experimental results.

TABLE OF CONTENTS

LIST OF TABLES

LIST OF FIGURES

LIST OF REACTION SCHEME

LIST OF ACRONYMS AND SYMBOLS

Ag-ZnO NPs	Silver doped zinc oxide nanoparticles
BPA	Bisphenol A
BPC	Bisphenol C
BPS	Bisphenol S
BPF	Bisphenol F
CA	Chronoamperometry
CD	Compact disc
CE	Capillary electrophoresis
CVD	Chemical vapour deposition
CV	Cyclic voltammetry
CPs	Conducting polymers
C-SPE	Carbon screen printed electrode
DVD	Digital versatile disc
DMF	Dimethylformamide
DFT	Density functional theory
EFSA	European Food Safety Authority
EC	Electrochemical
EDCs	Endocrine disrupting chemicals
EP	Epoxy resin

ECD	Electron capture detector
EIS	Electrochemical impedance spectroscopy
EDX	Energy-dispersive X-ray spectroscopy
FT-IR	Fourier-transform infrared spectroscopy
FID	Flame ionization detector
FTO	Fluorine doped Tin oxide
GC	Gas chromatography
GIX-RD	Grazing Incidence X-ray Diffraction
HPLC	High performance liquid chromatography
HPV	High production volume
ITO	Indium tin oxide
LC	Liquid chromatography
MWCNTs	Multiwall carbon nanotubes
MIP	Molecular imprinted polymer
MS	Mass spectroscopy
NIP	Non imprinted polymer
mV	Millivolts
mHz	Megahertz
PEC	Photo electrochemical
PLD	Pulsed laser deposition
PC	Polycarbonate

PVC	Polyvinyl chloride
PBS	Phosphate buffer
PDA	Photodiode array
PPy	Polypyrrole
PPO	Polyphenol oxidase
PL	Photoluminescence
Pt wire	Platinum wire
rpm	Rotations per minute
Si	Silicon
SPE	Screen-printed electrode
SEM	Scanning electron microscopy
TEM	Transmission electron microscopy
TGA	Thermogravimetric analysis
UV-Vis	Ultraviolet visible spectroscopy
VS	Vapour solid
VLS	Vapour liquid solid
ZnO NRs	Zinc oxide nanorods
ZnO NPs	Zinc oxide nanoparticles

LIST OF CONFERENCE PRESENTATIONS

Poster Presentations

2nd International Conference Functional Materials and Nanotechnologies held at University of Tartu, Tartu, Estonia, Europe, 24th – 27thApril **2017**. **"**Development of Novel Nanostructured Photo-electrochemical Platform for Chemical Sensing".

Oral Presentations

75th Latvijas Universitates koference held in University of Latvia, Riga, Europe. 3rd to 5th February **2017. "**Synthesis of nanostructured ZnO for Sensors Applications".

5th COST action workshop held in University of Latvia, Riga, 22th to 23th, May **2017.** "Photo electrochemical Detection of Bisphenol Using ZnO nanorods."

CHAPTER 1

INTRODUCTION

This chapter provides details about properties of phenolic compounds and their detection methods. The compounds of interests, Bisphenol A (BPA) and its analogue Bisphenol S (BPS) are discussed. In addition, electrochemical and photo electrochemical biosensors for detection of these phenolic compounds are presented for pharmaceutical and environmental applications. This is followed by the aims and objectives and a brief outline of the thesis.

1.1 Phenolic compounds

Phenolic compounds are aromatic molecules containing hydroxyl, methyl, amide or sulphonic groups attached to the benzenoid ring structure. They are the main plant metabolites with diverse structures. Due to its organoleptic and nutritional properties, it has been used in food products and plant derivatives and other important practical applications (Cheynier, Tomas-Barberan and Yoshida 2015). Phenolic compounds are classified according to their chemical structure as shown in **Table 1.1.** Most phenolic compounds are the derivatives of phenol, including adipic acid, caprolactam and bisphenols.

Table 1.1 Classification of phenolic compounds.

Classification	Examples
Phenol	catechol, hydroquinone and thymol
Phenolic acids	gallic and salicylic acids
Acetophenones	tyrosol and *p*-Hydroxyphenylacetic acid
Naphthoquinones	juglone and plumbagin
Chromones	umbelliferone and aesculetin
Xanthonoids	mangiferin
Stilbenoids	resveratrol
Chalconoids	quercetin
Lignans	enterolignans enterodiol and enterolactone
Halogenated algal phenolic compounds	kaviol A and colpol

Maffini and co-worker has reported the controversy associated with phenolic compounds as endocrine disruptors and their widely known positive effects on human health (Maffini *et al.* 2006). Enhanced detection methods for phenolic compounds (e.g., bisphenols) are required due to more conclusive evidence on health hazards or to address these concerns resulting in the need to monitor and control phenol concentrations and ensure that they are within the recommended safe limits in food and beverage products.

Bisphenols comprises of two hydroxyphenyl groups, with most of them based on benzhydryl, with the exception of bisphenol S, P, and M. BPA is well known representative of this group, often referred to as bisphenol. These chemical compounds are originated naturally due to the degradation of humid substances, tannins and lignins and industrial processes, including the production of drugs, textiles, dyes, pesticides and paper (Neilson *et al.* 1991). These are the main source of phenolic compounds in the environment. Previous research shows that BPA and BPS are endocrine disruptors (Wang *et al.* 2009). Endocrine disrupting activity is due to the presence of the alcohol group on the benzene ring in phenolic compounds. These compounds mimic hormones. They are widely used in the production of plastics, plasticizers, drugs, dyestuffs, explosives, pesticides, detergents, stabilizers and antioxidants (Gabriel *et al.* 2007; Opeolu, Fatoki and Odendaal 2010). They are released into the environment by different industries. This study is therefore aimed at BPA and its analogue BPS, chosen as the compounds of interests for the fabrication of the electrochemical biosensor and photo electrochemical sensor that is used mainly in the plastic and wood industry.

The increasing health and safety risks associated with BPA and BPS as endocrine-disrupting chemicals (EDCs) are gaining widespread recognition. EDCs are commonly employed in the manufacturing of polycarbonate (PC), epoxy resin (EP) and unsaturated polystyrene resins. The end products are usually used to manufacture plastic food containers, food can linings, powder paints, and dental fillings. These compounds are normally found in baby bottles, and containers that store foods and beverages, and water supply pipes. The sewage treatment industries also release these chemicals into streams and rivers, resulting in an increase of surface waters and sediments. Polyvinyl chloride (PVC) pipes that are used for tap water supply is another possible route exposure of this EDCs. There is a growing concern about the human exposure of EDCs because of their endocrine disrupting properties.

Literature studies reveal a number of commonly used analytical techniques such as capillary electrophoresis (CE), spectrophotometry, liquid chromatography (LC), and gas chromatography (GC) for the determination of phenolic compounds (Kuch and Ballschmiter 2001; Vílchez *et al.* 2001; Stuart *et al.* 2005). These techniques have low limits of detection (LODs). However, they require the use of classy and expensive instrumentation and require complex pre-treatment, cumbersome and time consuming sample pre-treatment, expensive equipment and skilled persons to operate (Mayorga-Martinez *et al.* 2012). There is a growing interest in finding a precise, sensitive and rapid method for the detection of phenolic compounds and its derivatives. Lately, these problems have been overcome by the introduction of sensor and biosensor technologies. Electrochemical and photo electrochemical sensors and biosensors are considered to be a preferred choice for such applications. This technique offers advantages compared to the conventional method such as reagent-less detection, portability, low cost instruments and non-trained personal.

The nature of materials used to modify the surface of the electrode determines the performance of the electrochemical sensor, which are the broader goals of this study. For this purpose, the choice of materials with improved electrocatalytic activity and interaction with the analyte, will be investigated in this work.

However, an extensive literature survey revealed that the direct detection of phenolic compounds on the bare electrode results in oxidation of polyphenol and the formation of dimers that leads to electrode fouling (Iwuoha *et al.* 2004). Therefore, in order to overcome this problem, fluorine doped tin oxide (FTO) and screen printed electrode (SPEs) modified with ZnO with shapes ranging from nanoparticles to nanorods, have been used as the alternative nanomaterials in this investigation with a view to enhancing the signal compared to traditional electrodes. Accordingly, this study focuses on developing a sensitive and selective photo electrochemical sensor and a laccase-based biosensor for the detection of BPS and BPA. These biosensors have the potential to offer a sensitive, cheap, rapid and simple determination of BPA and BPS related to the food and beverage industries.

1.2 Aims and Objectives

Aims:

This study is aimed at developing an electrochemical biosensor and photo electrochemical sensor for the sensitive and rapid detection of phenolic compounds, BPA and BPS using experimental and computational methods.

Objectives:

- To synthesize nanostructures of Ag-ZnO NPs and ZnO NRs.
- To characterize the synthesized nanostructures by UV-Vis spectroscopy, transmission electron microscopy (TEM), scanning electron microscopy (SEM), Fourier transform infrared (FT-IR), Raman spectroscopy, cyclic voltammetry (CV), electrochemical impedance spectroscopy (EIS) and Grazing incidence X-ray diffraction (GIX-RD).
- To develop an electrochemical biosensor for BPA by immobilizing the enzyme laccase onto the surface of screen printed electrode modified with Ag-ZnO/MWCNTs.
- To develop the photo electrochemical (PEC) sensor by polymerization of polypyrrole onto the surface of FTO modified with ZnO NRs.
- To characterize the biosensor and (PEC) sensor by cyclic voltammetry (CV) and electrochemical impedance spectroscopy (EIS) and to optimize the sensor parameters such as sensitivity.
- To investigate the electrochemical behaviour of phenolic compounds on a bare and modified electrode.
- To apply the developed biosensor and PEC sensor for the detection of phenolic compounds by cyclic voltammetry and amperometry.
- To validate experimental method using computational methods by DFT calculation.

1.3 Thesis outline

Following the introduction, further chapters of the thesis are outlined below:

Chapter 2: Gives general reviews of bisphenol occurrences and their detection using analytical techniques, the current improvements in the use of nanomaterials and conducting polymeric materials for improved sensor and biosensor applications are also highlighted. Numerous synthesis methods for ZnO nanostructures are discussed in detailed.

Chapter 3: In this chapter, theoretical principles underpinning the experimental and computational methodologies employed in this study are presented along with synergies between both methodologies**.**

Chapter 4: A description of the experimental and computational methodologies for the synthesis of the nanostructured ZnO, conducting polymer, biosensor and (PEC) sensor construction, characterization and application of the developed biosensor/sensor for the determination of BPA and BPS are presented in this chapter.

Chapter 5: This chapter deals with the experimental and computational results along with a discussion. Furthermore, characterization of the two nanostructures, Ag-ZnO synthesized by co-precipitation method and ZnO NRs synthesized by the hydrothermal method are discussed extensively. The results for the electrochemical and structural characterization of BPA and BPS are also discussed in this chapter.

Chapter 6: A summary of the main results using computational and experimental works are described here. The results are also correlated and associated with each other in order to obtain concluding remarks and highlights. Future work and recommendations are also briefly proposed to improve significant and interrelated works for the advancement of early BPA detection using computational and biosensor experimental techniques.

References: The references used in this thesis are enclosed.

CHAPTER 2

LITERATURE REVIEW

This chapter highlights the general reviews associated with BPA and BPS. A review of recent analytical methods including biosensor applications particularly aimed at the bio-recognition use of enzymes is also presented. Recent sensor studies of BPS using photo electrochemical and electrochemical methods are highlighted. The focus of this review is aimed at novel applications of nanomaterials such as zinc oxide in combination with an assembly of polymers in the application of sensor architecture in BPA detection.

2.1 Bisphenols

Bisphenols are compounds that share the basic chemical structure of two phenol groups, with hydroxyl moieties at the para positions joined by a carbon or sulfur bridge (Xue, Wan and Kannan 2016). BPA and BPS are widely produced chemicals around the world, reaching a capacity of 6.4 billion pounds since 2003 (Richter *et al.* 2007). They have been used as the starting material in the manufacture of epoxy resin and polycarbonate plastic (Fernández *et al.* 2009). Extensive literature studies reveal that BPA is an endocrine disruptor chemical (EDC), which raises great concern about their uses (Bonefeld-Jørgensen *et al.* 2007; Okada *et al.* 2008). The U.S. government and retailers have banned products containing BPA because of its carcinogenic effects. Consequently, this has shifted to the use of its analogues such as BPS and bisphenol F (BPF) for industrial and other applications (Skledar and Mašič 2016). These alternatives, however, have similar chemical structures to BPA and are expected to possess similar toxic effects.

However, since 1940 bisphenols have been generally used as a starting material in the production of polymers such as epoxy resins, polysulfone, polyacrylate and polycarbonate for the polymerization of polyvinyl chloride plastics (PVC) as the inhibitor and an antioxidant in the synthesis of the flame retardant tetrabromobisphenol-A as a precursor (Geens, Goeyens and Covaci 2011).

BPS and BPC are the most used analogues of BPA because of their higher thermal stability (Lotti *et al.* 2011). BPS is used in BPA–free products, but research reveals that BPA-free products are not safe implying that BPS is just as harmful as BPA (Kinch *et al.* 2015). However, BPA have a wide application as summarized in **Table 2.1** (PlasticsEurope 2007).

Table 2.1 Summary of several BPA applications.

Application class	Application
House hold equipment	Electrical panel, switches, light bulbs, kitchen tools, hairdryers, blades
Architecture	Coating of ceramic, corrosion protection, concrete reinforcement, floor covering
Medical practice	Lenses, dialysis instrument, armamentarium, dental restoration
Automotive	Light covers, automotive paint
Food & beverage	Beverage cans, silverware, food storage containers, jar sealer
Leisure and safety	Sports helmets, goggles, visor, tennis /ski/golf/gear
Entertainment & Communication	Mobile phone housings, CDs, DVDs, computer circuit boards

2.1.1 Properties of Bisphenols

The physical and chemical properties of bisphenols such as high molecular weight, pKa, water solubility and melting points play an important role because they control transportation and the fate of contaminants in the environment. Lui and co-workers revealed that the rejection efficiency of EDCs by membranes are strongly dependent on the physicochemical properties of EDC's (Liu, Kanjo and and Mizutani 2009).

2.1.2 Types of bisphenols

BPA and BPS were chosen as the compounds of interest in this study. These two chemicals were chosen because they are high production volume chemicals (HPV chemicals) and they are found in many plastic products.

2.1.2.1 **Bisphenol A (BPA)**

The plastic monomer and plasticizer Bisphenol A shown in **Figure 2.1** (4,4'-isopropylidenediphenol; CAS No 80-05-7) is one of the most toxic phenolic compounds (Vandenberg *et al.* 2007). It was first discovered as a synthetic estrogen in the 1890s and was reported to have the efficacy of estrogen in stimulating the female reproductive system in rats in the 1930s (Rochester 2013). The reports suggested that BPA is the endocrine disruptor because it causes the negative effects in the environment and humans (Pivnenko *et al.* 2015). This industrial chemical is used in the manufacture of epoxy resins and polycarbonate plastics.

It is found in many plastic products like toys, beverage containers, eyeglass lenses, ski gear, dental polymer, water pipes, armamentarium, and home electronics (Olea *et al.* 1996; Richter *et al.* 2007). In addition, human exposure to BPA occurs through diet, inhalation of household dust and dermal exposure (Larsson *et al.* 2014). Exposure to BPA has been associated with the increase of chronic illnesses (Iwakura *et al.* 2010). The reports revealed that BPA changes gene functions even at low concentrations, this results in the silence of critical genes (Bernal and Jirtle 2010; Weng *et al.* 2010).

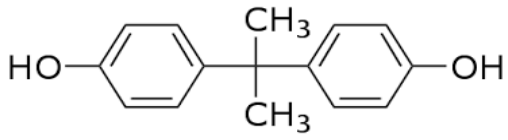

Figure 2.1 Bisphenol A (BPA).

2.1.2.2 **Bisphenol S (BPS)**

Bisphenol S shown in **Figure 2.2** (Bis (4-hydroxyphenyl) sulfone; CAS No 80-09-1), an analogue of Bisphenol A (BPA) was first produced in 1869 as a dye (Glausiusz 2014). It is commonly used as epoxy adhesives, surface metal protection and in polymer reactions as a reagent (Viñas *et al.* 2010). BPS has a wide variety industrial application in cleaning industry as a fastening agent, an electroplating solvent, and integral of phenolic resin (Rochester and Bolden 2015). BPS is used as a colour developer and in products advertised as "BPA-free as a replacement of BPA (Gao *et al.* 2015).

It is also present in paper products such as envelopes, receipts and airline boarding passes (Liao, Liu and Kannan 2012), personal care products like hair care products, make up, body wash, and toothpaste. It is also detected in food dairy products, meat, vegetables, canned foods, cereals (Liao and Kannan 2013). BPS is the significant organic compound that can be used to inhibit the oxidation of other molecules, as a monomer for polyester and epoxy resin because of its outstanding properties to produce commodity plastics and composition materials with excellent properties (Viñas *et al.* 2010). BPS is well known endocrine disrupting compound (EDC), because its interfere with the normal activity of estrogen, then lead to adverse health effects (Cao, Zhuang and Liu 2014). Limited studies have shown that BPS possess acute toxicity, genotoxicity, and estrogenic activity, similar to BPA (Grignard, Lapenna and Bremer 2012). Latest evidence suggests that BPS is able to induce alterations in embryonic nervous and endocrine systems (Kinch *et al.* 2015). BPS is currently not regulated and used without

restriction. Toxicological data on BPS are scarce and no *in vivo* or *ex vivo* study has evaluated their effects on any physiologic function in humans or other mammals (Eladak *et al.* 2015).

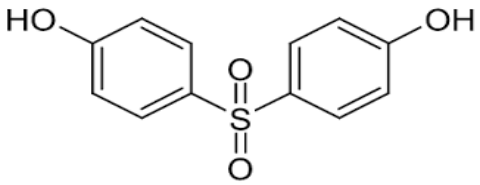

Figure 2.2 Bisphenol S (BPS).

2.2 Analytical detection of bisphenols

Different analytical techniques (shown in **Table 2.2**) have been used for the quantification of phenolic compounds. These analytical techniques are coupled with different detectors such as ultraviolet (Yakimova *et al.* 2012a; Zhang *et al.* 2013), mass spectrometry (MS) (Wissiack, Rosenberg and Grasserbauer 2000; Sambe *et al.* 2006), flame ionization detection (FID) (Sarafraz-Yazdi, Dizavandi and Amiri 2012), electron capture detection (ECD) (Bagheri and Saraji 2001), chemiluminescence (Tsukagoshi *et al.* 2002).

Table 2.2 Analytical methods for quantification of phenolic compounds.

Analytical method	Reference
Gas chromatography (GC)	(Chawla *et al.* 2012)
Liquid chromatography (LC)	(Chawla *et al.* 2012)
High performance liquid chromatography (HPLC)	(Watabe *et al.* 2004; Ou *et al.* 2006)
Spectrophotometry	(Lupetti, Rocha and Fatibello-Filho 2004)
Capillary electrophoresis (CE)	(Fonseca *et al.* 2001; Tsukagoshi *et al.* 2002)

2.2.1 Gas chromatography (GC)

GC is an ideal technique because of its unrivalled high resolution and easy coupling with sensitive and selective detectors. The detection of phenolic compounds using detectors such as FID, ECD MS has been reported (Kuch and Ballschmiter 2001). The use of solid-phase micro extraction (SPME) followed by gas chromatography with flame ionization detector (SPME-GC-FID) to determine phenol and cresol in waste water and urine have been reported in the literature (Sarafraz-Yazdi, Dizavandi and Amiri 2012). A method for detection of chlorophenols was developed, based on solid-phase extraction gas chromatography-electron

capture detector (SPE-GC-ECD) for an aqueous sample (Yakimova *et al.*). The disadvantage of these techniques is that it requires pre-concentration and derivatization (Bagheri and Saraji 2001).

2.2.2 High performance liquid chromatography (HPLC)

HPLC is the most popular method used for the quantification of phenolic compounds, as reported by several authors (Watabe *et al.* 2004; Ou *et al.* 2006; Arribas, Martínez-Fernández and Chicharro 2012), coupled with different detectors such as Ultraviolet/visible (UV-Vis) and photodiode array (PDA) (Klejdus *et al.* 2005; Bisetty *et al.* 2011). The HPLC application is based on the chemical properties of phenolic compounds such as hydrophobicity, hydrophilicity and molecular weight. Low amounts of the analytes are detected even in the presence of interference (Valls *et al.* 2009). HPLC separation is based on the distribution of analytes between stationary and mobile phases. The reverse phase is the most widely used technique for separation of phenolic compounds due to its wide application range, its simplicity and it can be able to analyse compounds of various polarity and molecular mass (de Rijke *et al.* 2006).

2.2.3 Capillary electrophoresis (CE)

The quantification of phenolic compounds using capillary electrophoresis with chemiluminescence as a detector have been reported in the literature (Fonseca *et al.* 2001; Tsukagoshi *et al.* 2002), using different chemiluminescence reagents such as such as luminol (Tsukagoshi *et al.* 2002), peroxyoxalate (Hashimoto *et al.* 1999), and Ru(II) complex (Tsukagoshi *et al.* 2002).

These techniques are sensitive. However, they require the use of the classy and expensive instrument and require complex pre-treatment and trained persons to operate (Yu *et al.* 2011; Chawla *et al.* 2012; Mayorga-Martinez *et al.* 2012). In this regard electrochemical methods have been highly preferred due to their portability, excellent sensitivity (in low ppb levels), automation, short analysis time, low power consumption, inexpensive equipment and the possibility of in situ analysis (Yu *et al.* 2011; Fan *et al.* 2012).

Numerous electrochemical techniques for the detection of phenolic compounds have been reported, but amperometry is the most commonly used technique (Ding, Ayon and García 2007). Electrochemical methods have been improved especially, for the detection of phenols

in environmental samples and food. In this regard, biosensors based on polyphenol oxidase (PPO) tyrosinase and laccase are the preferred methods that are used for the detection of phenols (Rubianes and Rivas 2000; Li *et al.* 2014; Zhou *et al.* 2014). Amperometric detection of BPA using tyrosinase on multiwalled carbon nanotubes (MWCNTs)-cobalt phthalocyanine (CoPc)-silk fibroin (SF) composite modified glassy carbon electrode (GCE) have been reported (Yin *et al.* 2010). Electrochemical detection of phenolic compounds with magnetic nanoparticles tyrosinase modified screen printed electrode was reported (Alkasir *et al.* 2010). The voltammetric behaviour of BPA at a screen printed electrode modified with laccase–thionine–carbon black has been reported (Portaccio *et al.* 2013). Moreover, screen printed electrodes modified with nanomaterials were used for the electrochemical detection of phenolic compounds.

2.3 Biosensors

A biosensor is an analytical device used for analysis of the analyte that combines a biological component with a transducer to produce a signal proportional to the analyte concentration. It has many applications in health care, industrial process control, military applications and environmental monitoring (Rodriguez-Mozaz, de Alda and Barceló 2005). Belický and co-workers reported four features of a biosensor namely: transducer, signal amplifier, processor, and display (Belický, Katrlík and Tkáč 2016) as shown in **Figure 2.3**.

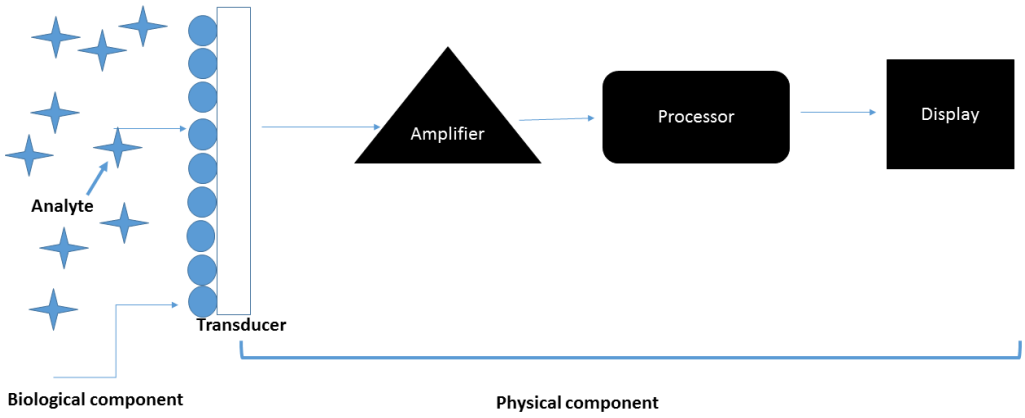

Figure 2.3 Schematic representation of a biosensor.

2.3.1 Components of a biosensor

A biosensor consists of a physical component and biological component. The physical component includes the transducer and the amplifier, while the biological component includes the recognition elements such as enzymes or antibodies. The biological component has two significant functions.

- It identifies the analyte.
- It interacts with the analyte and produces a signal that is detected by the transducer.
- The biological component properties are sensitive and they have the ability to detect and analyse the analyte. Normally the biological component is immobilized onto the transducer. The accurate immobilization of the enzymes improves their stability and results in the repetitive use.

Recognition elements are also known as bio-components interact with the analyte of interest to produce an effect measurable by the transducer. Enzymes, antibodies, receptors, organelles, and microorganisms have been used as a biological sensing element. The choice of the recognition element normally depends on the analyte of interest and the recognition element should have a high binding affinity for the target as well as stability. Biosensors are classified according to their recognition element, as shown in **Table 2.3**.

Table 2.3 Classification of sensor and biosensor.

Recognition element	Sensor
Enzyme	Enzymatic biosensor
Whole cells	Whole-cell biosensor
Antibodies	Immunosensor
Nucleic acids	Genosensor

The physical component has three features, this includes the amplifier, processor and the computer for the display of results. The transducer converts the physical change into an electrical signal. This signal is then amplified by the amplifier and then processed by the processor. The processed signal is then interpreted and displayed in the computer.

2.3.2 Types of biosensor

There are different kinds of biosensors such as, amperometric, potentiometric, conductometric, colorimetric, optical and piezoelectric (Pohanka and Skládal 2008; Mehrotra 2016). Electrochemical and optical are the most common methods followed by piezoelectric (Luong, Male and Glennon 2008).

2.3.2.1 **Amperometric biosensors**

Amperometric biosensors are based on measuring the current associated with oxidation or reduction of an analyte involved in the electrochemical reaction usually at the constant potential. These biosensors have a high sensitivity and wide linear range. The ongoing research on new sensing concepts coupled with various technological innovations have opened the door to a widespread environment use of amperometric biosensor. Amperometric biosensor is commonly used where the enzyme is combined with nanomaterials such as nanoparticles and carbon nanotubes (Chauhan and Pundir 2011).

2.3.2.2 **Potentiometric biosensors**

Potentiometric biosensors involve the detection of the analytes by measuring the potential difference between the working electrode and the reference electrode separated by a selective membrane, ion-selective electrode normally used as a transducer (Lei, Chen and Mulchandani 2006). The potentiometric biosensor is sensitive and selective due to the use of ion-selective electrode (ISE). The use of stable and correct reference electrode is always compulsory and challenging to maintain, this limits the application of potentiometry in biosensors (Ciosek and Wróblewski 2011).

2.3.2.3 **Conductometric biosensors**

Conductometric biosensors focus on measuring the conductance change of the biological component occurring between a pair of metal electrodes. During chemical reactions, ions or electrons are either formed or consumed and this causes the complete change in the electrolytic conductivity of the solution. This complete change is measured and monitored during the progress of a reaction. Conductometric biosensors have advantages over other types of biosensors - they can be produced through low-cost and simple thin film standard technology, there is no need for a reference electrode and low power consumption and differential mode

measurements allow cancellation of interferences (Jaffrezic-Renault and Dzyadevych 2008). Anh and co-workers detected diuron, atrazine, desisopropylatrazine, and desethylatrazine using a conductometric tyrosinase biosensor (Anh *et al.* 2004).

2.3.2.4 Colorimetric biosensors

Colorimetric biosensors employ a simple and fast technique, in which a dye substance is used in order to create a colour. The response signals are visible instead of a mechanical transducer (Zhai *et al.* 2013).

2.3.2.5 Optical biosensors

Optical biosensors measure the absorbed and radiated light of a biochemical reaction. Optical fibers are used to guide the light waves (Gerard, Chaubey and Malhotra 2002). Phenolic compounds have been detected using these biosensors (Abdullah *et al.* 2006).

2.3.2.6 Piezoelectric biosensors

Piezoelectric biosensor employs piezoelectric effect to analyze the change of pressure, acceleration, temperature, strain, or force by converting them to an electrical charge. They are commonly used to detect toxic compounds.

2.3.3 Biosensors for the detection of phenolic compounds

In environmental monitoring, the biosensor is used for selective detection of various chemical compounds such as phenolic compounds, heavy metals and pesticides etc. It is vital to monitor these toxic compounds because they are a threat to human and animal life. There has been a growing interest to monitor phenolic compounds and its derivatives by using portable and low-cost devices. The usage of an enzymatic sensor to detect phenols has increased over the past decade due to their irregular properties. Enzymes are catalysts, they speed up a chemical reaction (Cajthaml *et al.* 2009). Previous reports revealed that phenolic compounds have been detected using enzymes like tyrosinase, horseradish peroxidase and laccase compounds (Li *et al.* 2006; Mei *et al.* 2015; Wu *et al.* 2016).

One of the challenges facing the biosensor development is the efficient signal capture of the biological recognition event (transduction). In order to improve the performance of biosensors, different modifiers are used. Nanomaterials and conducting polymers are commonly used as

the modifiers. Nanomaterials are materials of which a single unit measures between 1 and 1000 (10^{-9} meter) but is usually 1—100 nm (the usual definition of nanoscale (Buzea, Pacheco and Robbie 2007). They are classified as inorganic nanoparticles. An inorganic nanoparticle includes quantum dots, metal and metal oxides such as silver, copper oxide, titanium oxide, iron oxide and zinc oxide.

2.4 Zinc oxide (ZnO)

Zinc oxide has gained remarkable interest in the field of electrochemical sensing due to its exceptional properties such as a wide range of radiation absorption, photo stability and high electrochemical coupling coefficient (Segets *et al.* 2009). ZnO is a widely used semiconductor metal oxide that has a wurtzite crystal structure that contributes to its unique optoelectric properties (Zhao, Wang and Mao 2004). ZnO has a wide band gap of (3.37 eV), a large excitation binding energy (60 eV) and exhibits near UV emission (Zhao, Wang and Mao 2004). ZnO is used in electronics, optoelectronics, laser technology, ceramic industry, biomedicine and as a sensor. The diversity of ZnO structures shows that ZnO is a material with prospective applications in the nanotechnology field. They are three types of zinc oxide dimension structures that include one dimensional (1D), two dimensional (2D), and three dimensional (3D) structures (Kołodziejczak-Radzimska and Jesionowski 2014). 1D structures is one of the major group, comprising nanowires (Huang *et al.* 2001; Banerjee *et al.* 2003), nanorods (Frade, Jorge and Gomes 2012), ribbons (Botello-Méndez *et al.* 2007), needles (Wahab *et al.* 2007), rings (Kong *et al.* 2004), belts (Lu, Chang and Fan 2006), tubes (Lu, Chang and Fan 2006) and combs (Wang and Song 2006). ZnO can be synthesized and results in 2D structures and this includes nanopellets (Chiu *et al.* 2010; Soltaninezhad and Aminifar 2011) and nanosheets (Ma and Sasaki 2010). The 3D structures include snowflakes (Polshettiwar, Baruwati and Varma 2009), coniferous urchin-like (Zhao, Wang and Mao 2004), and flowers (Shi *et al.* 2013).

2.4.1 Basic properties of ZnO

ZnO has three crystal structures this includes hexagonal wurtzite, sphalerite structure and halite (NaCl-type) as shown in **Figure 2.4**. Wurzite is thermodynamically stable under controlled conditions. The sphalerite is metastable while halite is stable under extreme pressure (~2 GPa) (Sokolov *et al.* 2010).

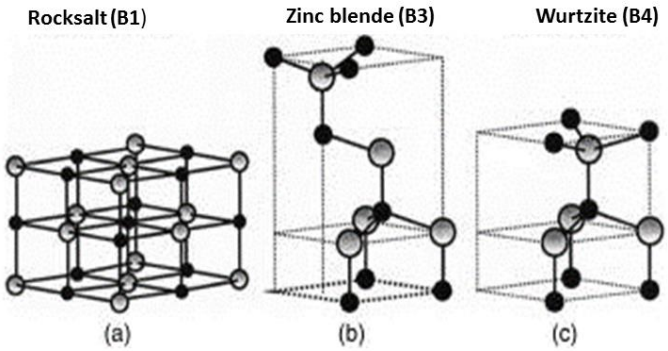

Figure 2.4 ZnO crystal structures: cubic rock salt (a), cubic zinc blende (b) and hexagonal Wurtzite (c) (Espitia *et al.* 2012).

Understanding the fundamental physical properties is vital to the rational design of functional devices. Investigation of individual ZnO nanostructures properties is very crucial for developing their potential as the building blocks for future nanoscale devices.

2.4.2 Mechanical properties

The mechanical properties of ZnO such as hardness, elastic modulus, piezoelectric and fracture toughness can be determined using different technique. ZnO has the estimated hardness of 4.0 on the Mohs scale (Gordon 2000). It has a small elastic modulus constant compared to other semiconductors metals. Piezoelectric property of ZnO has been studied for application in nanodevices (Agrawal and Espinosa 2011). The piezoelectricity lies in its crystal structure, in which the oxygen atoms and zinc atoms are tetrahedrally bonded. ZnO has the highest piezoelectric tensor. This makes it a significant material for various applications, which entail large electromechanical coupling.

2.4.3 Electrical properties

ZnO is a direct and wide gap (~3.3 eV) semiconductor metal. The wide band gap plays an important role in various applications such as sustaining large electric fields and lower electron noise (Özgür *et al.* 2005).

2.4.4 Synthesis of ZnO

Zinc oxide has diverse structures that have a wide range of properties. The fabrication of zinc oxide is classified as, bottom-up and top-down methods. In the top-down method, the nanostructures are synthesized by removing crystal planes which are already present on the substrate. Physical techniques, such as photolithography and mechanical stamping are used in top-down methods. A bottom up synthesis method involves the stacking of atoms to each other to produce the nanostructures onto the substrate which gives rise to crystal planes. This synthesis method is based on vapour phases or solutions. The bottom-up fabrication techniques include atomic layer deposition, co-precipitation, electrodeposition, hydrothermal, vapour deposition, sol-gel, and pulsed-laser deposition. This technique makes it attainable to achieve products with different morphology and structure. **Table 2.4** summarizes different techniques with their advantages and disadvantages. These methods are fully illustrated below. In this work, both co-precipitation method in an aqueous medium (wet method) and hydrothermal method was used for the synthesis of ZnO NPs and NRs respectively.

2.4.4.1 **Vapour deposition**

In this method, zinc and oxygen vapour mixture react with each other forming ZnO one-dimensional (1D) nanostructures such as zinc oxide nanowires. Vapour-solid (VS) and vapour-liquid-solid (VLS) growth mechanisms are commonly used to achieve numerous structures as shown in **Figure 2.5**. The VLS mechanism was first discovered in the early 1960s (Wagner and Ellis 1964). In the VLS mechanism, the metallic catalyst is used. The catalyst dimension and location determine both the diameter and the position of the structure (Hao *et al.* 2006). Several researchers used VLS mechanism to synthesize different shape nanostructures. Haung and co-workers produced nanowires (Huang *et al.* 2001), while Gudiksen and co-workers produced nanowire superlattices (Gudiksen *et al.* 2002) and nanotree (Dick *et al.* 2004). The VS mechanism analysis is achieved without the catalyst by producing complex structures such as nanobelts and nanohelices (Kong and Wang 2003).

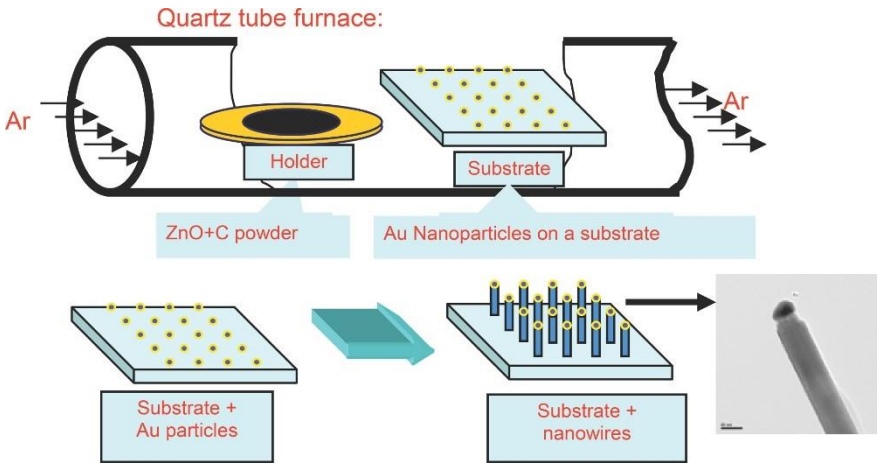

Figure 2.5 Schematic diagram for fabrication of nanowires using the catalytic VSL growth method (Willander, Zhao and Nur 2007).

2.4.4.2 **Sol-gel Method**

This is a wet-chemical technique that uses a chemical solution or colloidal particles to produce an integrated network (Angelopoulos 2001). This method involves the reacting of zinc salts such as (zinc chloride, zinc acetate and zinc nitrate) with an organic solvent such ethanol, and propanol to produce 3D metal oxide (Rani *et al.* 2008). The chemical transformation involves two reactions: hydrolysis and condensation (Rechberger and Niederberger 2017). The precursor zinc acetate is commonly used with ethanol as the solvent, then a base is added into a reaction in other to control the morphology and structure of the particles. The use of bases such NaOH, KOH and LiOH have been reported in the literature (Meulenkamp 1998; Yang *et al.* 2005; Hasnidawani *et al.* 2016). Zhang and co-workers prepared ZnO NPs from zinc acetate dissolved in methanol and lithium hydroxide as the base (Zhang *et al.* 2008). Wong and Searson used zinc acetate and 2-propanol with sodium hydroxide to synthesize ZnO (Wong, Bonevich and Searson 1998). The sol-gel method is most common because it is inexpensive, reliable, repeatable, and simple (Švegl, Orel and Hutchins 1997). Nanoparticles which are synthesized by this route, show good optical properties.

2.4.4.3 **Atomic layer deposition**

The Atomic layer deposition is a film deposition technique that is based on the successive use of self-terminating gas–solid reactions. It a subgroup of the chemical vapour deposition (CVD) technique (Puurunen 2005). The reacting precursors are introduced into a reaction chamber by a sequence. The growth occurs layer by layer by using the gas as a source. The growth of material layers by ALD consists of four characteristic steps. The precursor enters at one end of the chamber where the molecules adsorb onto the surface substrate that is surrounded by a heater. In order for a reaction to proceed in a self-limiting manner the operating temperature needs to be set. The precursor can decompose or not be reactive enough if the temperature is too high or too low. A great advantage of the technique is thus to allow the use of highly reacting precursors and to lower the deposition temperature as compared to classical CVD.

2.4.4.4 **Hydrothermal synthesis**

In this method metal oxide crystals are produced from aqueous metal salt solutions through heating (Adschiri, Hakuta and Arai 2000). The formation of metal hydroxide or metal oxide is due to the equilibrium reaction of a metal salt in water with various temperature as shown in **Figure 2.6**. This method is simple and environmentally friendly. Low temperature is used to carry out the reaction mixture in the autoclave. The crystal nuclei are formed due to heating and cooling. Hydrothermal method has countless advantages such as performing reactions at low temperatures, the high degree of crystallinity of the product formed, and the high purity of the material obtained and the various shapes and dimensions of the resulting crystals depending on the composition of the starting mixture and the process temperature and pressure (Baruwati, Kumar and Manorama 2006; B Djurisic, Y Chen and H Leung 2012). Different materials were used to synthesize various morphology of ZnO (Xu *et al.* 2004).

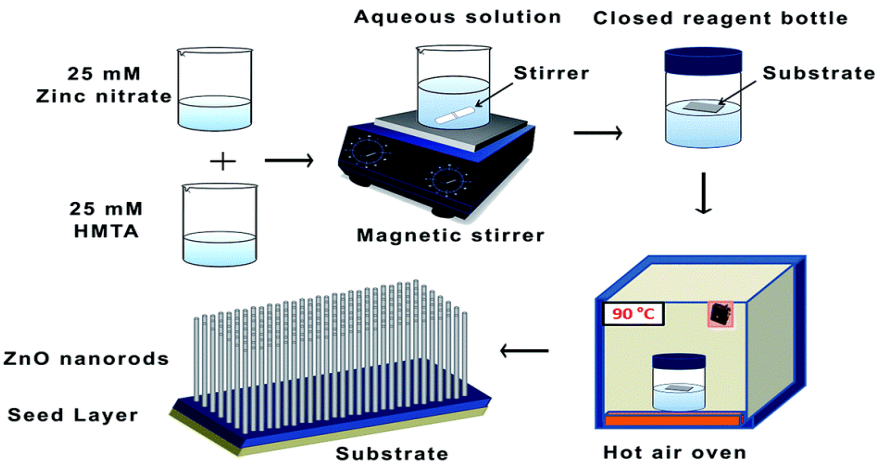

Figure 2.6 Process steps followed for the synthesis of hydrothermally grown (Gaddam *et al.* 2015).

2.4.4.5 **Co-precipitation method**

This method involves (shown in **Figure 2.7**) the dissolving of a salt precursor, e.g. $AlCl_3$ to make Al_2O_3, $Y(NO_3)_3$ to make Y_2O_3, and $ZrOCl_2$ to make ZrO_2. The metal hydroxide of the corresponding salt precursor is usually formed during the process and precipitate from water by adding a basic solution. The resulting chloride salts, i.e., NaCl or NH_4Cl, are then washed away and the hydroxide is calcined or dried after filtration or centrifugation and is washed again to obtain the final oxide. Kumar and co-workers have reported the synthesis of ZnO, using zinc sulphate and sodium hydroxide as starting materials (Kumar *et al.* 2013), while, Singh and co-workers synthesized ZnO NPs with different morphologies by using different salts precursors (zinc chloride, zinc nitrate and zinc acetate) and ammonium hydroxide (Singh, Kohli and and Singh 2013). Nanoparticles synthesized by this method usually have different morphology, the morphology depends on the concentration of cations, the presence of counter ions, and pH of the solution.

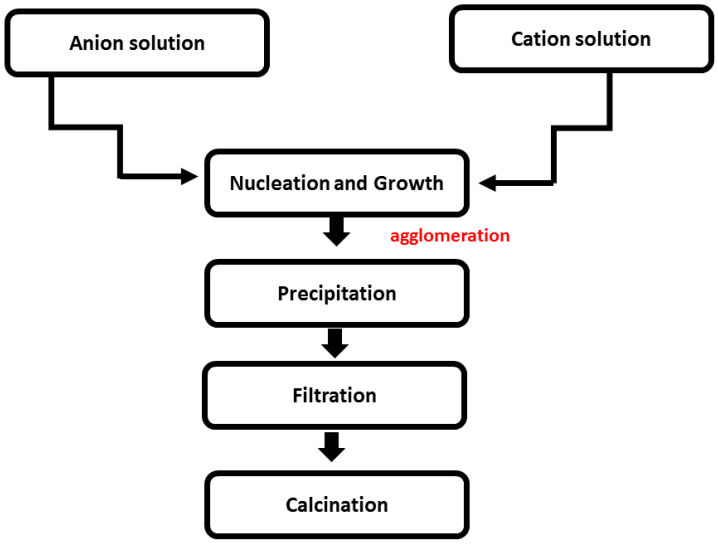

Figure 2.7 The process step in the co-precipitation method.

2.4.4.6 **Electrodeposition method**

This method (shown in **Figure 2.8**) uses a very low cathode voltage or current to produce the ZnO thin film on any conductive substrate such as a transparent conducting oxide (COŞKUN *et al.* 2009) or any other metal plate (Wang *et al.* 2005). In this method, the film thickness, morphology and optical properties can be controlled by the several operating parameters: current density, applied potential, deposition time and the concentration of the electrolytic bath. This process uses zinc nitrate solutions (Mahalingam *et al.* 2005) or zinc chloride solutions (Cembrero *et al.* 2004). Since then, several groups investigated the substrate effect on the ECD-grown ZnO. For example, Fahoume and co-workers found diameter sizes of the particles grown on a copper substrate were larger than the particles of the film deposited on ITO/glass, these diameters ranged between 7 and 10 μm (Fahoume *et al.* 2006). Cembrero and co-workers investigated ZnO films on GaN and FTO substrates and they found that GaN substrates produce perfectly oriented ZnO columns of higher dimensions than using FTO coated glass substrates (Cembrero *et al.* 2004). The cathodic electrodeposition technique has been recognized as an effective method for the production of ZnO thin films due to its simplicity, low temperature process, high deposition rate, low cost technique and suitability for large area substrate.

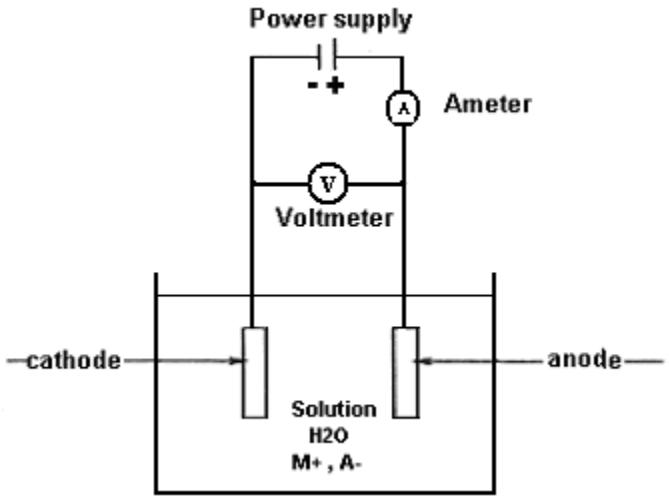

Figure 2.8 A schematic showing the electrodeposition technique (Al-Bat'hi 2015).

2.4.4.7 Pulsed-laser deposition

This method uses a pulsed laser beam for vapourizing a sample to be deposited as a thin film on a substrate. The thin films are grown up to several thousand angstroms (Å) thick. Various substrate and lasers have been used in the literature for the synthesis of zinc film. Substrates such as indium tin oxide (Saito *et al.* 2011), sapphire (α-Al_2O_3), silicon (Si), glass and polycarbonate (PC) have been reported in the literature together with a different pulsed laser (Han *et al.* 2008; Franklin *et al.* 2011; Kaur, Mitra and and Yadav 2015). It is well known that the crystalline quality of ZnO films depends on the substrate properties. Therefore, it is interesting to compare the structural features of the epi-layers deposited on different substrates.

2.4.4.8 Spray pyrolysis

Spray pyrolysis deposition is a well-known and commonly used technique for thin film processing. Two major interests in this method are the operating at atmospheric pressure and the deposition on a large surface. The compressed gas or ultrasonic waves are used for transformation of the solution to a droplets stream. The droplets are sprayed onto a heated surface where they react to form a solid film. Thereafter, the properties of the used solution and the thermodynamics at the interface droplet/substrate are crucial parameters controlling the spray deposition processes and the deposited films properties. It is a quite simple method due to the use of air without a vacuum system which is present in most deposition techniques (sputtering, CVD, evaporation, ablation laser, etc.)

Table 2.4 ZnO synthesis techniques and their comparison with respect to their advantages, and disadvantages

Technique	Advantage	Disadvantage	Reference
Vapour deposition	Controllable product composition, simple process.	The use of high reaction temperature	(Zhao, Wang and Mao 2004)
Hydrothermal synthesis	The reaction is carried out at low temperature and cost nanometer-size particle can be obtained by this method, different morphologies form by adjusting the reaction time.	It is impossible to observe the crystal as it grows. The need of expensive autoclaves	(Chen, Jiao and Cheng 1999)
Spray pyrolysis	Simple, cheap method, easy to operate technique.	Oxidation of sulfides when processed in air atmosphere, difficulties with growth temperature determination, and spray nozzle become cluttered	(Perednis and Gauckler 2005)

2.4.5 Applications of ZnO

Zinc oxide has many applications due to its diverse properties, both chemically and physically. It plays a significant role in a wide range of applications, it has been used to manufacture lasers and ultraviolet radiation generation because of its high binding energy of excitons of 60 meV (Chen *et al.* 2001). ZnO has been used in electronics and electrotechnology industry, photocatalysis, pharmaceutical and cosmetic industry due to it extraordinary properties (Kołodziejczak-Radzimska and Jesionowski 2014). ZnO is a non- toxic material with a high isoelectric Point (IEP) of ~9.5, that makes it applicable for absorption of proteins with low IEPs through electrostatic (Zhang *et al.* 2004; Liu *et al.* 2005; Yakimova *et al.* 2012a). ZnO is one of the most promising materials for biosensor application because ZnO nanostructures have numerous unique advantages such as high specific surface area, non-toxicity, chemical stability, electrochemical activity, and high electron communication features (Zhang *et al.* 2004; Wang *et al.* 2006). ZnO nanostructures have been employed in different kinds of sensors such as a chemical sensor, biological sensor, reductive and oxidation sensor. Lately, the attention has been dedicated toward the application of ZnO in biosensing because of its high isoelectric point (9.5), biocompatibility, and fast electron transfer kinetics. Such features advocate the use of this exciting material as a biomimic membrane to immobilize and modify biomolecules. This reveals that zinc oxide can be used in the fabrication of an electrochemical biosensor. ZnO has been investigated intensively for solar cells and nanogenerators applications (Keis *et al.* 2002; Pietruszka *et al.* 2015), biosensors, cosmetics and drug-delivery systems (Rasmussen *et al.* 2010), electronic devices (Schlettwein *et al.* 2000; Huang *et al.* 2001). Different ZnO structures have various applications, **Table 2.5** below summarizes the morphology and application of some ZnO nanostructures. **Figure 2.9** shows the summarized applications of ZnO.

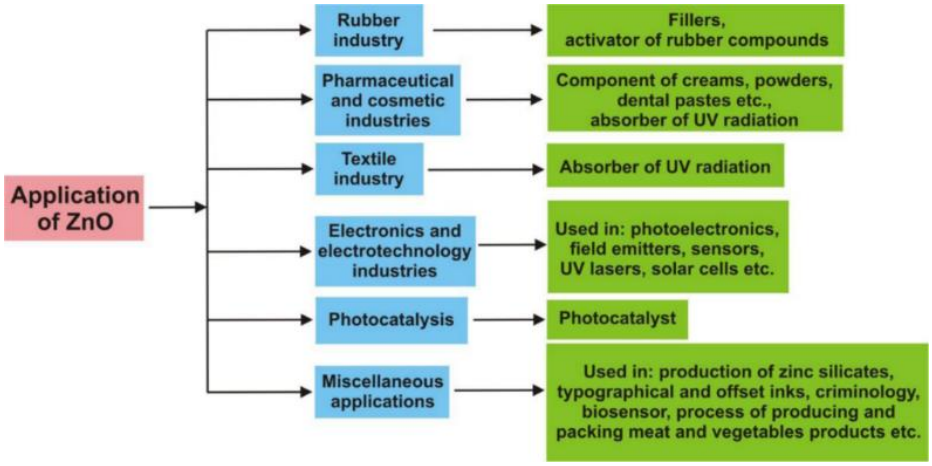

Figure 2.9 Schematic showing the applications of ZnO (Kołodziejczak-Radzimska and Jesionowski 2014).

Table 2.5 Applications of the different morphology of ZnO.

Morphology	Application	Reference
Zinc powder	solar cell, UV shielding	(Keis *et al.* 2002)
Zinc nanowires/nanorods	gas sensor, piezoelectric, nanogenerators	(Hossain *et al.* 2005; Wang and Song 2006)
Flower like zinc oxide	photocatalyst, photovoltaic	(Kansal *et al.* 2011; Sharma, Dalal and Mahajan 2016)
Zinc nanocombs	sensor, electrochemical devices	(Bhakat and Singh 2012; Pan and Zhao 2015)
Zinc nanobelts	sensor, resonators	(Gao *et al.* 2005; Hossain *et al.* 2005)
Zinc urchin like	photocatalyst, solar cell, biofuel cells	(Elias *et al.* 2012; Zhou *et al.* 2016)

2.5 Conducting Polymers

Conducting polymers also referred as synthetic metals because of their properties such as semiconductors, electronic, magnetic and optical characteristic similar to metals (Mu and Wang 2016). Conducting polymers (CPs) have attracted much attention since their discovery in 1977. They have countless advantages compared to non-conducting polymers, due to their electronic and optical properties. Conducting polymers such as poly(carbazole), polyaniline, poly (para-phenylene vinylene), polypyrrole, and poly(thiophene) have been reported in the literature (Ates, Karazehir and Sezai Sarac 2012). The presence of conductivity in CPs arises from the presence of conjugated double bonds along the backbone of an otherwise insulated structure. In conjugation, the bonds between the carbon atoms are alternatively single and double bonds. Every bond in the backbone contains a localized 'sigma' (σ) bond, which forms a strong chemical bond and every double bond also contains a less strongly localized 'pi' (π) bond.

CPs are extensively used in bio-analytical science because of their biocompatibility and charge transport characteristic (Geetha *et al.* 2006; Ferreira *et al.* 2011).

Lately, the combination of conducting polymers with nano-materials have opened extensive possibilities for novel applications. Numerous scientists have conducted research on conducting polymers in sensor evaluation (Adhikari and Majumdar 2004; Ahuja and Kumar 2009). Polypyrrole (PPy) was used in this study because of the interaction with (BPS).

CPs are the most important organic materials. They are called conducting polymers due to its electrically conductive, exceptional physical properties. CPs are the new useful materials (Naveen, Gurudatt and Shim 2017). Literature revealed that conducting polymers have different applications and are classified into groups: electronic (Angelopoulos 2001), electromechanical (Otero 2000), and optoelectronic (Otero 2009).

2.5.1 Chemistry of polypyrrole

PPy is an organic polymer that is formed by polymerization of pyrrole. (PPy) was first reported by Weiss and co-workers in 1963 (McNeill *et al.* 1963). Literature reveals that PPy is a conducting polymer, and it have other related members such as polyacetylene, polyaniline, poly (*p*-phenylene), and polythiophene (Vernitskaya and Efimov 1997; Shayeh *et al.* 2015). PPy has drawn the attention of researchers because of its wide application range in different fields as the prospective electrode material, sensor and biosensor. PPy has been the centre of research because of its tremendous properties like high conductivity, stability in the oxidised state, and fascinating redox properties. The simplicity of the synthesis method and availability of the monomers are also attractive features of PPy. Chemical and electrochemical synthesis are two methods that are used for the synthesis of PPy. During chemical synthesis, chemical oxidants such as copper (II) and iron (III)) salts are widely used. Previous reports reveal that polymers synthesized by this methods have a stable structure and higher crystallinity than those synthesised electrochemically (Vernitskaya and Efimov 1997). Electrochemical methods have numerous advantages over chemical methods, viz.,

2.5.1.1 The electroactive film is attached to the electrode surface and having high conductivity,

2.5.1.2 it is easy to control the thickness of the film, and the

2.5.1.3 properties of the film are controlled during preparation.

2.6 Enzymes

Enzymes are very large biological molecules (usually protein) that speed up chemical reactions. Without the enzymes, a chemical reaction occurs slowly as to be insignificant. Like any catalyst, enzymes are not consumed, nor do they change the equilibrium of a chemical reaction. Enzymes are more specific which makes them different from other catalysts. Some molecules such as inhibitors and activators normally affect the enzyme activity. Inhibitors decrease enzyme activity, while activators increase activity. Other factors affecting enzyme activity are temperature, pressure, chemical environment like pH and concentration of the substrate. Laccase (Lac) enzyme was used in this study due to its catalytic activity towards phenolic compounds.

2.6.1 Laccase

Laccase (see **Figure 2.10**) is one of the most popular enzymes since the nineteenth century. Lac was first studied by Yoshida in 1883 from the juice of the Chinese lacquer tree (Thurston 1994). However, Bertrand and Laborde in 1896 revealed that laccase is a fungal enzyme (Thurston 1994). Lac is a copper-containing enzyme that catalyzes oxidation and reduces reactions of molecules that are found in living and non-living systems, aromatic amines, phenols and polyphenols (Madhavi and Lele 2009). Lac belongs to a blue copper protein or blue copper oxidase group, while other enzymes are from the plant ascorbate oxidase and mammalian plasma protein ceruloplasmin (Thurston 1994). It has the capability to oxidize phenols and reduce molecular water (Madhavi and Lele 2009). This enzyme is found in various plants, microscopic organisms and fungi, and it promotes the oxidative coupling of phenols and monolignols. Laccase has been widely studied because of its distinctive characteristics and has numerous uses in farming, manufacturing, medical and environmental applications (Morozova *et al.* 2007; Arora and Sharma 2010).

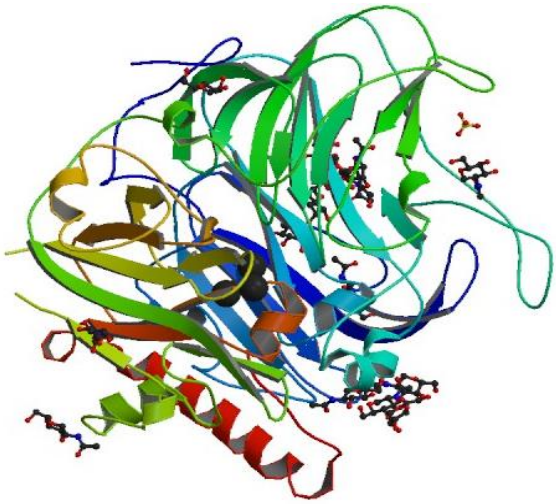

Figure 2.10 Image of laccase from Botrytis aclada at 1.67 A resolution (Osipov *et al.* 2014).

2.6.1.1 **Laccase characteristics**

The laccase enzyme contains a molecular weight of 60–80 kDa with an isoelectric point of 4–7. Lac has four copper atoms (type 1 (T1), type 2 (T2) and type 3 (T3). These copper atoms form the active site of the enzyme, and they are categorized into three groups, and this depends on the features attained by UV/visible and electron spin resonance (ESR) spectroscopy (Piontek, Antorini and Choinowski 2002):

- type 1 copper (T1), it is characterized by the intense blue colour with an absorption peak at around 600 nm and is ESR detectable;
- type 2 copper (T2), is colourless because it does not show an intensity on the UV/visible region but its detectable in ESR spectroscopy; and,
- type 3 copper (T3), has a weak absorption peak at 330 nm and is not detectable by ESR spectroscopy (Durán *et al.* 2002; Madhavi and Lele 2009).

2.6.1.2 **Applications**

Lac has the ability to oxidize a wide variety of phenols that have been used in numerous industrial sectors. Laccase is normally used in textile industries (Morozova *et al.* 2007), waste treatment to remove colour (Almansa *et al.* 2004; Junghanns *et al.* 2005), food production (Morozova *et al.* 2007), and in biofuel cells development (Tan *et al.* 2009). It has wide applications in the field of the biosensor (Zhang *et al.* 2007; Di Fusco *et al.* 2010) and environmental (Tang *et al.* 2008), and medical applications (Quan and Shin 2004; Ferreira *et al.* 2009).

2.6.1.3 **Immobilization of laccases in biosensors**

Laccase has to be robust and recyclable in order to be a sustainable industrial catalyst, and this is achieved by treating the enzyme. Immobilization is one of the most considered treatments. Immobilization is described as the enzyme attachment to an insoluble support (Arıca, Altıntas and Bayramoğlu 2009). The most common used immobilization treatment includes chemical linkage or entrapment method (Durán *et al.* 2002). The immobilization treatment is very significant because it has benefits including, the extended use of the sensor, prolonged storage and stability (Liu *et al.* 2006). A number of immobilization methods have been reported in the literature (Rodríguez-Delgado *et al.* 2015), including covalent coupling, adsorption, cross-

linking, encapsulation and entrapment (Brena, González-Pombo and Batista-Viera 2013; Zucca and Sanjust 2014).

CHAPTER 3

THEORETICAL PRINCIPLES

This chapter focuses on the theoretical principles underpinning the computational and experimental studies carried out in this study. The role of computational chemistry in biosensors is highlighted. Furthermore, the equations and rigorous foundation of density functional theory (DFT) in relation to biosensor construction are presented. This is followed by the electrochemical and structural techniques used to characterize the morphology of the fabricated nanomaterials.

3.1 Computational chemistry

Computational chemistry is a branch of chemistry, that utilizes high-performance computers to solve chemical problems. In terms of sensors, computational simulations predominantly help to simulate the optimized structures of material recognition, to better understand the interaction between the substrate materials and target analyte, to compute the interaction or adsorption energy, and to observe the structural, electronic, optical, and vibrational properties of the employed materials and molecules. Density functional theory (DFT) will be discussed here.

3.1.1 Density functional theory (DFT)

DFT is the most commonly used method in computational chemistry. DFT calculations are used to observe the impact of particle size on the structure and molecular features of nanomaterials (Fadeel 2014). DFT has been widely used to study and predict electronic structures such as conductivity and other related properties of transition metal complexes (Harvey 2006) as well as macromolecules such as DNA duplexes (Tsukamoto *et al.* 2009). It is also useful in the modeling and prediction of interaction energies.

DFT, a scheme of classical first-principles, is commonly employed to calculate the atomic or molecular properties at the ground-state level. DFT is also known as *a minimum-information* theory. Instead of dealing with the many-body wave function $\Psi\ (r_1 \ldots\ldots, r_N)$, DFT leads to the direct calculation of the simplest electronic properties of atoms or molecules, i.e. the electronic density. DFT has been established as one of the main tools for calculating the properties of solid-state physics and molecules since 1980 (Fiolhais, Nogueira and Marques 2003).

DFT was established by Hohenberg, Kohn, and Sham through their classic papers for justifying the replacement of the many-body wave function by one-electron orbitals (Hohenberg and Kohn 1964; Kohn and Sham 1965; Lundqvist and March 2013). Hohenberg and Kohn demonstrated a couple of theorems (Hohenberg and Kohn 1964) in which the first theorem specified that the electron density has a significant influence on the external potential (to within an additional constant), while the second was for several positive definite trial density (rt) i.e.$\int \rho t\ (\mathbf{r})d\mathbf{r} = \mathrm{N}$ then $\mathrm{E}\ [\rho t] \geq E_{\mathrm{o}}$. They successfully provided a direct proof of the aforementioned theorem in which the first theorem was expanded to involve schemes with degenerate states in proof contributed by Levy (Levy 1979, 1982; Dreizler and da Providencia 2013).

From the first Hohenberg and Kohn theorem, it can be defined that the trial density establishes a sole trial of Hamiltonian and therefore, the wave function remains to be (Ψ); $\mathrm{E}[\rho t] = \langle \psi t|H|\psi t\rangle \geq \mathrm{E_o}$ derived from the Schrödinger equation on variational theorem (**Eq. 3.1**).

$$\left[E[\rho] - \mu(\int \rho\ (\boldsymbol{r})d\boldsymbol{r} - N)\right] = 0\delta \tag{3.1}$$

The density and ground state energy refer to the minimum of several functional, $E[\rho]$, dependent on the restriction that the density covers the correct electrons number. Herein, the Lagrange multiplier corresponds to the electronic chemical potential (μ).

Equation 3.1 limits the DFT to discover on the ground state level particularly. A minor addition permits the variation with regards to an excited state which can be assured orthogonal to the ground state. The wave function is necessary in order to accomplish this knowledge of the ground state level. These couple of theorems set the basic equation of DFT (Harrison 2003).

The abovementioned statement establishes the notable fact that there is a universal functional, $E[\rho]$, which is independent of an external potential. If the functional form is already identified, it could be involved in **Eq. 3.1** and subsequently optimized to obtain the obvious density at the ground state level of energy (Harrison 2003). The original DFT theorem is applied for observing the electronic energy on the ground-state level of a molecule. Subsequently, a feasible theory of DFT was further established by Kohn and Sham who formulated an approach analog to the Hartree-Fock (Fahoume *et al.* 2006) method in terms of structure (Young 2001).

In this study, since several integrals of DFT parts could not be done analytically, as consequence, there is a step to evaluate the integrals over atomic orbitals, using interpolation of the numerical atomic basis set of grid points. DMol3 has three options of qualities to define the accuracy of integral calculations, which are Coarse, Medium, and Fine. The combination of the spin and charge densities from the previous iteration is taken into account in order to increase the speed of SCF convergence. Further, a direct inversion of the iterative subspace (DIIS) sub-technique implemented under DMol3 is also applied to enhance the SCF speed performance (Cremer and He 1996). This method enables to minimize the error by approximating a significant error for the density function. As result, it reduces the iteration numbers with efficient compelling the convergence and allows the next estimated density functional to be closer with the actual ground state density without exploring full SCF iterations for each estimation at the density (Jensen 2016).

3.2 Experimental characterisation techniques

The characterisation techniques used in this research are electrochemical techniques such as cyclic voltammetry (CV), chronoamperometry and electrochemical impedance spectroscopy (EIS); morphological and structural techniques namely ultraviolet spectroscopy, scanning electron microscopy (SEM), transmission electron microscopy (TEM), fourier transform infrared (FT-IR), Raman spectroscopy, photoluminescence (PL), grazing incidence X-ray diffraction (GIX-RD) and diffuse reflectance.

3.2.1 Electrochemical techniques

Voltammetric and impedimetric techniques were used in this study, these techniques are discussed below.

3.2.1.1 Cyclic Voltammetry (CV)

Cyclic voltammetry known as linear scan voltammetry is one of the most famous electrochemical techniques that is categorized under sweep techniques that are used in various areas of chemistry. It has a wide-ranging application in redox reactions, understanding chemical reaction reactants and electrochemical properties of analytes. Cyclic voltammetry requires the three electrochemical cell comprising a working electrode, auxiliary electrode, and reference electrode. The various potential is applied to the working electrode during the voltammetric analysis at a fixed scan rate while monitoring the current in both the reverse and

forward reaction. The important parameters such as redox and electrochemical properties of the sample are usually obtained from the cyclic voltammograms. Parameters such as cathodic and anodic peak currents (i_{pc} and i_{pa}) as well as anodic and cathodic peak potentials (E_{pa} and E_{pc}). **Figure 3.1** shows the classic cyclic voltammograms demonstrating these parameters. These parameters give the information about the analyte, like the nature of the electrochemical process whether it is quasi-reversible, irreversible or reversible. It also predicts the reaction time on how fast the reactions are.

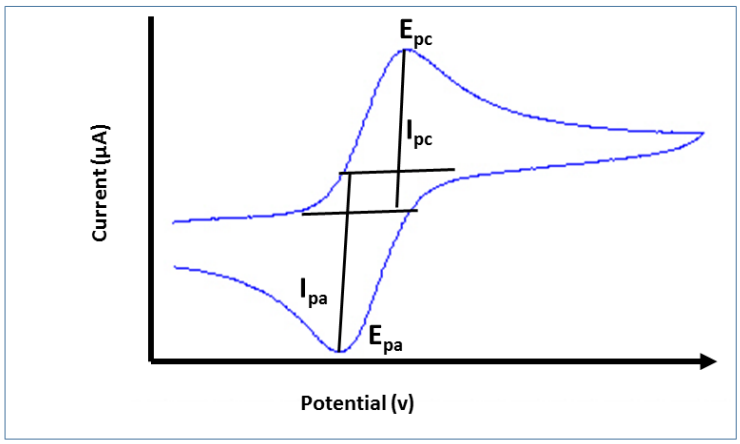

Figure 3.1 Cyclic voltammogram illustrating basic parameters.

3.2.1.2 **Chronoamperometry**

Chronoamperometry (CA) is an electrochemical technique in which the potential of the working electrode is kept constant and the resulting current occurring at the electrode is monitored as a function of time (Girault 2004). The experimental analysis is diffusion controlled, after some time the molecules species that reaches the electrode are reduced (oxidized). There must be enough applied potential to cause the oxidation/ reduction of the compound of interest. The number of molecular species determine the generated current oxidized or reduced in the electrode. The chronoamperometry is based on the Cottrel equation which defines the current-time dependence for linear diffusion control.

$$I = nFACo\frac{\sqrt{\mathrm{D}}}{\pi t} \tag{3.2}$$

Where,

I = current

n = number of electrons

A = area of the electrode

C_0= concentration

D = diffusion coefficient

t = time

The Cottrell equation can be used to calculate the diffusion coefficient, surface area of an electrode or the concentration of the analyte in solution.

Figure 3.2 shows the amperograms.

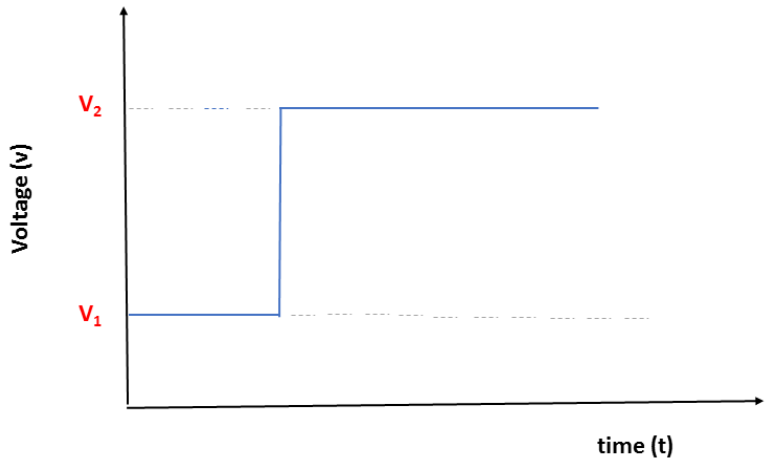

Figure 3.2 Amperometric curve.

3.2.1.3 **Electrochemical impedance spectroscopy (EIS)**

Electrochemical impedance spectroscopy (EIS) is the widely used characterization technique to examine the surface of the modified and unmodified electrode. It is used to analyse the in-depth electrochemical behaviour of the modified electrode using both the individual and mixed components. The features of the impedance are discussed in terms of Nyquist plots which are used to analyse the contributions of dissimilar components of the cell.

The Nyquist plot as shown in **Figure 3.3** is a plot of imaginary impedance, Z'' (ω), versus real impedance, Z' (ω) components that initiate mostly from the capacitance and the resistance of

the cell. The diffusion characteristics and electron transfer kinetics are extracted from the shape of the impedance spectrum. Semicircles of the curves correspond to the electron-transfer resistance (R) and the double layer capacity (C).

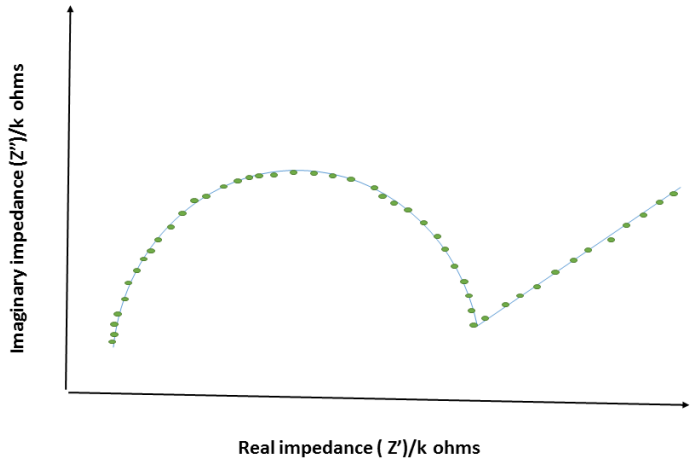

Figure 3.3 Nyquist plot.

3.2.2 Morphological and structural techniques

The spectroscopic and morphological techniques such as Ultraviolet Visible spectroscopy (UV-Vis), Fourier transform infrared (FT-IR), Scanning Electron Microscopy (SEM), Transmission Electron Microscopy (TEM), Raman Spectroscopy, Photoluminescence (PL), Grazing Incidence X-ray diffraction (GIX-RD) and Diffuse reflectance were employed in this study.

3.2.2.1 Scanning electron microscopy (SEM)

Scanning electron microscopy (SEM) is one of the versatile microscopic technique that is used in research and is capable of producing two-dimensional images. SEM uses the focused beam of the energized electrons to produces a range of signals on the surface of the sample. The carbon coated sample holder is normally used because its conducts electrical signals. These signals give a properties information such as chemical composition, morphology and crystalline structure of the sample. The information of the sample is measured in the selected area, and the two-dimensional image is then produced to show morphology. The key requirement for the effective analysis includes the electrically conductive sample and direct placing of conductive materials such as carbon and metals on the SEM and coating the non-metallic sample with a gold metal. Most of the scanning electron microscopes (SEM) have an

energy dispersive spectrometer (EDX) detection system, which identifies and shows most of the spectra and the elemental composition of the sample. In this work, SEM was used to determine the morphology of ZnO NRs.

3.2.2.2 **Transmission electron microscopy (TEM)**

Transmission electron microscope (TEM) is one of the sophisticated microscopic techniques that is mostly used in the scientific industry. TEM investigates the structural and chemical properties of the sample down to the atomic level. It is used in the research area to understand and manipulate the properties and the behaviour of the nanostructured materials. The TEM is used in the investigation of the size, distribution and the morphology of synthesized nanostructure materials. It has the same working principle as an optical microscope. The beam of electrons, produced by the high voltage electron emitter, interacts with the sample and magnifying magnetic lenses, focused at the viewing screen. In this research work, the size, morphology and the crystallinity of the materials were investigated by TEM.

3.2.2.3 **Raman Spectroscopy**

Raman spectroscopy is the analytical technique that is used to study vibrational, rotational and low-frequency modes in the system. Raman spectroscopy is widely used in chemistry to give a structural fingerprint for molecular identification. It relies on the monochromatic light, such as inelastic and Raman scattering. The laser will cause excitation and hence cause molecular vibrations, photons in the system, resulting in the energy of the laser photons being shifted up or down. The shifting gives information about the vibrational modes in a system. Raman spectroscopy was used to examine the nanomaterial's composition.

3.2.2.4 **Photoluminescence (PL)**

Photoluminescence (PL) spectroscopy known as fluorescence spectroscopy is the analytical technique commonly used for characterization of the optical and electronic properties of semi-conducting materials. The light is illuminated into the sample, and then it's absorbed and regenerates excess energy into the materials in the process called photo-excitation. Excess energy gradually spread out and disappear in the sample through the luminescence and, this luminescence is called photoluminescence. Therefore, photoluminescence is the spontaneous emission of light from the material under optical excitation. This light is then collected and evaluated spectrally and temporally. The material properties are analysed through the spectral

content and the intensity of the photoluminescence. The electrons within the sample jump into an excited state, this is caused by the photoexcitation process.

3.2.2.5 **UV-Visible spectroscopy**

UV/Vis spectroscopy is a quantitative analytical technique that is used for the determination of coloured samples, such as the element in d-block of the periodic table, conjugated chemical compounds that contain carbon, and large biological molecules. The analysis is normally carried out in an aqueous solution however gases and solids are also studied. The basic operation in UV/Vis entails the passing of light over the sample and measuring the wavelength of light that reaches the detector. The wavelength provides the crucial information about the number of molecules, concentration and the chemical structure. Analytical information is shown in terms of transmittance and absorbance. Normally the light of certain wavelengths and energy are emitted on the sample, which absorbs a certain amount of energy from the incident light. The absorbance of the sample is then measured using the photodetector. To determine the concentration of the absorbing species in the solution, Beer-Lambert plot is applied as shown in **Figure 3.4**.

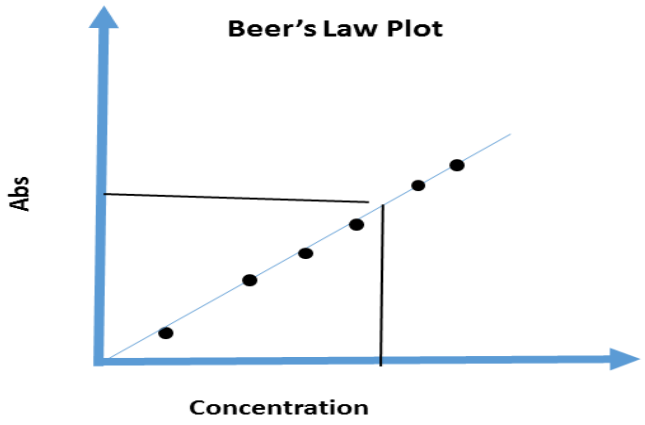

Figure 3.4 Beer's Lambert Plot.

3.2.2.6 **Fourier transform infrared (FT-IR)**

Fourier transform infrared spectroscopy (FTIR) is a vibrational spectroscopic technique generally used to identify functional groups of the organic and inorganic materials. It is normally used to obtain an infrared spectrum of the sample in a complete range of wave numbers simultaneously. This method operates by collecting the signal of each wave number

separately where it differs from a dispersive method. The great signal-to-noise ratio of FT-IR method makes its superior to dispersive infrared. It is an indispensable method for material characterization.

3.2.2.7 **Grazing incidence X-ray diffraction (GIX-RD)**

Grazing Incidence X-ray diffraction (GIX-RD) is a low-angle analytical technique that is used for characterizations and identification of the sample based on diffraction pattern. The GIX-RD is a powerful tool in the study of crystallinity and atomic structure of materials and forms an integral part of the comprehensive characterization study of the consolidated composite carbon material. It is used extensively in the determination of the Bravais lattice types and unit cell dimensions. X-ray diffraction methods can be classified into two types: spectroscopic and photographic. The spectroscopic technique known as X-ray powder diffraction is the most widely used diffraction method, which can replace most photographic methods, photographic techniques. However, photographic methods are used to determine unknown crystal structures. In XRD, crystalline solids are bombarded with a collimated x-ray beam which causes crystal plane atoms, serving as diffraction gratings, to diffract x-rays in numerous angles. Each set of crystal planes or Miller indices (hkl) with inter-plane spacing (d_{hkl}) can give rise to diffraction at only one angle. The diffraction angle is defined by Bragg's law, where the diffracted x-ray is measured and plotted against the corresponding Bragg angles (2θ) to produce a diffractogram.

$$n\lambda = 2d\sin\theta \qquad (3.3)$$

Where:

λ = wavelength of the X-rays

d = spacing of the planes in the crystal

2θ = angle of diffraction

The intensities of the diffraction peaks are proportional to the densities of the abundance of the corresponding crystal facets in the material lattice. Diffractograms are unique for different

materials and can therefore qualitatively be used in material identification. In this study, XRD was used to examine the crystallinity of the metal oxide nanoparticles.

3.2.2.8 **Diffuse reflectance**

Diffuse reflectance spectroscopy is related to UV-vis spectroscopy because both use visible light to stimulate outer shell electrons to empty orbitals. The difference in these methods is that UV-vis spectroscopy measures the transmittance of light, while diffuse reflectance measures the reflected light. Diffuse reflectance technique gathers and examines the scattered light. It is normally used to measure powders and particles. There is no sample preparation. Diffuse reflectance technique is normally used for the determination of energy band especially semiconductors metals. It is the best method for determining energy band gap, this technique is based on Kubelka–Munk function. Its permits the detection of the indirect forbidden energy gap.

CHAPTER 4

MATERIALS AND METHODS

This chapter details the research design used in this study. The experimental and computational study that was conducted will first be described, particularly highlighting the development of the sensitive and selective photo electrochemical sensor and the electrochemical biosensor using nanostructures. Subsequently, both qualitative and quantitative analysis that was conducted, will be described in-depth including the optimized parameters.

4.1 Experimental methods

4.1.1 Instrumentation

4.1.1.1 Electrochemical techniques

(a) Electrochemical measurements were carried out using two different electrochemical instruments: a portable USB-powered 910 PSTAT mini potentiostat (Metrohm, Durban, SA) was used in combination with the PSAT software (for cyclic voltammetry and differential pulse voltammetry) using the three-electrode system as shown in **Figure 4.1**. ZnO modified screen printed electrodes were used as the working electrode, Pt wire and Ag/AgCl as the counter electrode and reference electrode respectively. The potentiostat was computer-controlled and therefore the experimental modes were selected from the software and specified during its operation. The pH measurements were performed with a 781 pH/ion meter coupled with an 801 stirrer (Metrohm, Herisau, Switzerland). The electrochemical experiments were carried out in a phosphate buffer solution at a controlled room temperature of 20°C.

(b) Chronoamperomertry (CA) and cyclic voltammetry (CV) measurements were carried out using the Autolab potentiostat (model PGSTAT 100, Ecochemie B.V., Utrecht, Netherlands). Electrochemical impedance spectroscopy (EIS) was conducted on the Autolab potentiostat combined with Frequency Response Analyzer (FRA) software in the two electrode system. The ultraviolet lamp with the wavelength of (365 nm) and the intensity of 3 MW was used as an irradiation source. Modified and unmodified fluorine doped tin oxide (FTO) with the thickness of 2.2 mm and sheet resistance < 10-15Ω were used as the working electrodes, Pt wire and a saturated Ag/AgCl was used as the counter and reference electrode respectively. The bath sonicator (100 W, 40 kHz) was used to sonicate the conducting glass (FTO). Plasma Cleaner

PDC-002, Supplier HARRICK PLASMA, USA) was used to remove organic compound on the surface of the substrate. Zinc oxide seed layer was deposited on the conducting substrate by using the spin coater MF-002, ELMI, LABOTEK and the Controller - GSL-1100X-LD muffle furnace was used to dry the seeded substrate.

Counter electrode (CE): also known as auxiliary, allow the current to pass through.

Working electrode (WE): is the electrode in an electrochemical system on which the reaction of interest occurs, it normally used in conjunction with the counter electrode.

Reference electrode (RE): it allows the measurement of the potential of the working electrode without passing current through.

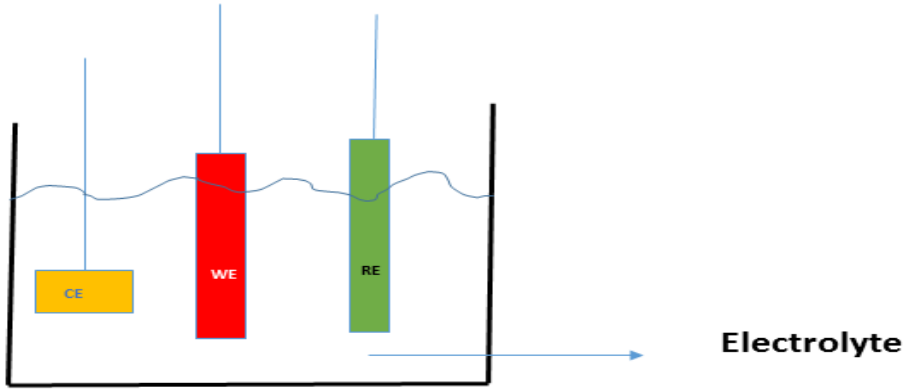

Figure 4.1 Three-electrode electrochemical cell system.

4.1.1.2 **Characterisation techniques**

The functional groups present in the synthesized ZnO NPs were investigated by Fourier transform infrared (FT-IR) spectrophotometer at wavelengths ranging from 4000 cm^{-1} to 400 cm^{-1} (Perkin-Elmer, Midrand, South Africa). The crystallinity and atomic structure of the synthesized ZnO NRs were investigated by the Grazing Incidence X-ray diffraction (GIX-RD) using a Bruker D5000 Advance diffractometer. Morphological analysis of ZnO NRs was examined by scanning electron microscope (SEM) (Hitachi, S-4800) and EVO HD15, equipped with a LaB6 emitter and coupled with energy dispersive X-ray (EDX, OXFORD instruments) and JEOL JIB-4000 Transmission electron microscopy from Germany, Europe. The crystallinity of ZnO NRs was investigated by the Raman spectrometer equipped with a confocal microscope (Leica), analysis was performed at room temperature using the argon laser at 488nm. The optical characteristics of the ZnO NRs were investigated using photoluminescence (PL) measurements with a nitrogen laser at 337nm using Ocean optics hr 2000 +, equipped with UV-Vis light source and UV-Visible spectra were recorded in the wavelength ranging 300 to 600 nm with VARIAN Cary 50 spectrophotometer.

4.1.2 Reagents and materials

Sodium dihygrogen phosphate (NaH_2PO_4), disodium hydrogen phosphate ($Na_2HPO_4.7H_2O$), sodium hydroxide (NaOH), bisphenol A (BPA), multiwall carbon nanotubes (MWCNTs), zinc gluconate ($C_{12}H_{22}O_{14}Zn$**)**, catechol ($C_6H_4(OH)_2$), 4-aminophenol ($H_2NC_6H_4OH$), 2-nitrophenol ($C_6H_5NO_3$), phenol (C_6H_5OH), 4,4-sulfonyldiphenol ($C_{12}H_{16}O_4S$), silver nitrate ($AgNO_3$) and sodium acetate ($C_2H_3NaO_2$) were purchased from Sigma Aldrich (Durban, SA). Sulphuric acid (H_2SO_4), ethanol (C_3H_6O), ammonia (NH_3), acetone (C_3H_6O) (absolute, 99.9%) were supplied by Capital Lab Supplies (Durban, SA). Bisphenol S (BPS), bisphenol C (BPC), ethanol (C_3H_6O), Zinc acetate dihydrate ($C_4H_{10}O_6Zn$), hexamethylenetetramine ($C_6H_{12}N_4$), 2-propanol (C_3H_8O), ethanolamine ($HOCH_2CH_2NH_2$) and zinc nitrate hexahydrate ($Zn(NO_3)_2 \cdot 6H_2O$) were purchased from Sigma Aldrich (Riga, Latvia). All reagents were of analytical grade and were used as obtained. Deionized water used for preparation otherwise stated. Screen printed electrode and the conducting glass Fluorine doped tin oxide (FTO) were supplied by Metrohm, Durban, SA and Sigma Aldrich, Riga, Latvia respectively.

4.1.2.1 Preparation of working solutions

(i) Preparation of phosphate buffer solution

Phosphate buffer solution of 0.1 M was prepared by dissolving 0.5999 g of sodium dihygrogen phosphate (NaH_2PO_4) and 0.7098 g disodium hydrogen phosphate ($Na_2HPO_4.7H_2O$) separately in 250 mL deionized water, then mixing the salt solutions according to Henderson Hasselbalch equation to obtain the required pH using a 0.01 M NaOH and HCl solution to adjust pH. The pH meter was then calibrated with buffer solutions with pH 7 and pH 4. The phosphate buffer solution was used and stored in a refrigerator at 4^{o} C for not more than 2 weeks.

(ii) Preparation of 5 M bisphenol A stock solution

A 5 M stock solution of bisphenol A (BPA) was prepared in ethanol (absolute) and kept in a refrigerator at 4 °C. A fresh 5 mM solution of BPA was then prepared from the first stock solution using a standard dilution method in a deionized water. The electrochemical properties of BPA were examined in 0.1 M PBS using cyclic voltammetry (CV) method.

(iii) Preparation of 1 M bisphenol S stock solution

A 1 M stock solution of bisphenol S (BPS) was prepared in ethanol and kept in a refrigerator at 4 °C. A fresh 0.01 M second stock solution was prepared from the first stock solution in PBS and a 0.001 M third stock solution from the second one was prepared in PBS. The electrochemical behaviour of BPS was examined in 0.1 PBS using chronoamperometry (CA) method.

(iv) Preparation of laccase (Lac) enzyme solution

A solution of Laccase was prepared by adding 3 mg of Lac into 1mL of 0.1 M phosphate buffer, pH 6.5. The enzyme was adsorbed on the electrode surface modified with Ag-ZnO NPs and MWCNTs by dropping 10 µL of the enzyme solution on it and allowed to dry at 4^{0} C for 3 hours. After drying, the electrodes were covered with 5 µL of glutaraldehyde and left to dry at room temperature for 10 minutes in order to avoid enzyme leakage.

4.1.3 Synthesis of nanostructures

The disposable screen printed electrode and conducting glass fluorine doped tin oxide (FTO) were used as a working electrode. ZnO NPs synthesize by co-precipitation method was used to modify the SPE, while ZnO NRs were synthesized by simple hydrothermal method (Amin *et al.* 2012).

4.1.3.1 Synthesis of Ag-ZnO NPs/ZnO NPs by Co-precipitation method

The Ag-ZnO NPs and ZnO NPs was prepared according to the previous report with slight modification (Siva Vijayakumar *et al.* 2013). Briefly, a mixed solution of 100 mM of zinc gluconate and 1 mM silver nitrate were prepared in 50 mL of deionized water by dissolving approximately 3.400 g and 0.0400 g respectively. Thereafter, 25% of ammonia solution was added drop-wise until a white precipitation was formed, then a few more drops were added further till the clear solution was obtained. To this solution, 1.25 mL of 0.1 M acetate buffer was added drop-wise and stirred until a white precipitate was formed. The resulting precipitate was washed with 100 mL deionized water, followed by 10 mL acetone and then centrifuged. Finally, the residue was oven dried overnight at 110 ^{o}C. ZnO NPs were prepared for control purposes using a similar procedure.

4.1.3.2 Synthesis of ZnO NRs by Hydrothermal method

ZnO NRs were prepared by a simple hydrothermal method according to previous work (Gurav *et al.* 2014). This was achieved by using the two-step process: (i) the seed layer preparation and (ii) the hydrothermal growth of nanorods.

(i) Preparation of a seed layer

Conducting glass fluorine doped tin oxide (FTO) was used as a substrate for the synthesis of ZnO NRs by hydrothermal method. The first step involves, cleaning of the substrate by sonication in isopropanol and deionized (DI) water sequential for 10 min each and subjected to plasma treatment for 15 min in order to eliminate organic traces. ZnO seed layer was grown on FTO substrate using the sol-gel method (Foo *et al.* 2014).

The precursor solution was prepared by dissolving 2.2 g zinc acetate in 20 mL of 2-propanol stirring at 50 ^{o}C, and 20 mL of 2-propanol was then mixed with ethanoline in the separate beaker. The resulting mixture was then added dropwise into the zinc acetate mixture under

constant stirring for 20 min. 20 µL of the prepared solution was then deposited on the substrate using a spin coating method (30 s at 3000rpm). The uniform seed layer was obtained after three layers of deposition, then the seeded substrate was annealed at 350 ^{o} C for 2 h in order to transform zinc acetate to ZnO.

(ii) ZnO hydrothermal growth

The hydrothermal growth of ZnO NRs was achieved by following the typical procedure, equal molar ratio aqueous mixture of 50 mM zinc nitrate and hexamethylenetetramine mixture were prepared in 5ml deionized water under stirring. The prepared solution was then transferred to a Teflon-lined stainless autoclave and the seeded substrate was then placed horizontally in the autoclave and heated at 95 ^{o}C for 4 h. At the end of the reaction, the obtained nanostructure was allowed to cool to the room temperature, rinsed with deionized water and calcined at 450 °C for 3 h using the furnace. A typical flowchart for ZnO NRs synthesis using hydrothermal method is shown in **Figure 4.2**.

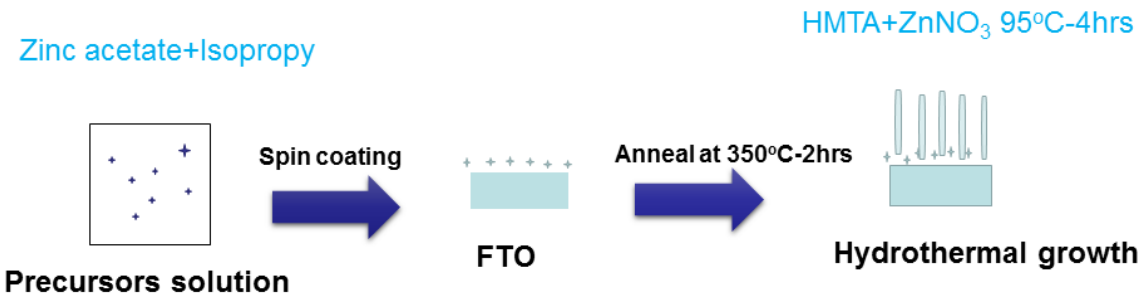

Figure 4.2 The schematic design for the fabrication of the ZnO NRs by hydrothermal synthesis.

4.1.4 Structural characterization techniques

4.1.4.1 UV-Visible spectroscopy

The optical properties of ZnO NPs were analysed using the VARIAN Cary 50 spectrophotometer in the wavelength ranging 200 to 800 nm. ZnO NPs powder was prepared in ethanol. The single beam instrument was used with a 1 cm cell path length.

4.1.4.2 Photoluminescence (PL)

The photoluminescence of ZnO NRs was studied at room temperature using Ocean optics hr 2000 + software, with a nitrogen laser at 337 nm, equipped with UV-Vis light source and integrating sphere. There is no sample preparation, the synthesized nanostructure is placed in the sample holder and the laser light is passed through the sample.

4.1.4.3 Fourier transform infrared (FT-IR)

The characterization of synthesized ZnO NPs and Ag-ZnO NPs were performed using the Fourier transform infrared (FT-IR), recorded in a wavelength between 4000 cm^{-1} to 400 cm^{-1} using Perkin-Elmer model. Sample was prepared using a KBr disk method by mixing KBr with ZnO NPs in the ratio of (1:0.01).

4.1.4.4 Scanning Electron Microscope (SEM)

The surface morphology of the modified electrode with ZnO NPs, Ag-ZnO NPs, Lac/Ag-ZnO NPs/MWCNTs were characterized using the scanning electron microscopy (SEM) model EVO HD15, equipped with a LaB_6 emitter and coupled with energy dispersive X-ray (EDX, OXFORD instruments). Morphology of ZnO NRs and MIP/ZnO NRs were analyzed by scanning electron microscopy (SEM) model Hitachi, S-4800 operating with an accelerating voltages of 5 to 10 kV, with a maximum resolution of 5 μm. The sample was mounted on the stub of the metal with the adhesive tape and then observed in the microscope.

4.1.4.5 Grazing Incidence X-ray diffraction (GIXRD)

The crystallinity of ZnO NRs was investigated using Grazing Incidence X-ray diffraction (GIXRD), a Bruker D5000 Advance diffractometer (voltage 40 KV; current 40 mA). The XRD spectra were recorded in the range 20-80 using 2degrees. The synthesized ZnO NRs were placed in the 2 mm thick sample holder that has 20 mm square hole centre. About 10-20 mg of the nanostructure was placed in the double scotch tape over the hole, then spread and smoothed flat.

4.1.4.6 Raman spectroscopy

The Raman spectroscopy studies have been carried out using Renishaw 1000 spectrometer, equipped with a UV-coated CCD camera and excited with the argon laser at wavelength 488 nm. The spectra were collected through Leica microscope. There is no sample preparation for powder sample. Nanorods were grown on the conducting glass, so the analysis were first performed on the glass in order to determine the Raman features of the glass before taking the Raman spectra of the sample.

4.1.4.7 Transmission electron microscope

The size distribution and morphological properties of ZnO NRs were investigated by transmission electron microscope of JEOL JIB-4000 (Germany) operating at 30 KV acceleration voltage. The sample was prepared by dispersing ZnO powder in deionized water, placing a few drops of the dispersed solution onto carbon films, and then leaving the films to dry at room temperature.

4.1.5 Fabrication of sensors

The fabrication of the electrochemical sensor was investigated using two different electrodes, carbon screen printed electrode (SPEs) and fluorine doped tin oxide (FTO). Both of these electrodes were first pre-treated before modification. The C-SPE was first washed with ethanol, then rinsed in deionized water and kept in 0.01M hydrochloric acid. FTO was cleaned first by sonication in isopropanol and deionized (DI) water sequentially for 10 min each and subjected to plasma treatment for 15 min in order to eliminate organic traces.

4.1.5.1 Preparation and fabrication of Lac/Ag-ZnO NPs/MWCNTs/C-SPE for detection of BPA

During the first step, a homogenous paste was achieved by mixing 2.0 mg of MWCNTs, 2.5 mg of Ag-ZnO NPs or ZnO NPs with 2 mL of DMF: H_2O (1:1) as a dispersion medium of the mixture and sonicated for 3 h (Fanjul-Bolado *et al.* 2008). The presence of 50 % of water in the solution allows modifying C-SPEs due to its compatibility with the ink composition. It is important to note that pure DMF solution of MWCNTs are not suitable to modify the most of plastic substrates due to the conductive inks of C-SPEs. Then 5.0 µL of the resulted 1:1 mixture was deposited on the working electrode surface and dried at (20 ^{o}C) for 3 min, then Ag-ZnO NPs/MWCNTs was produced. The use of high temperatures can completely damage the SPE (Fanjul-Bolado *et al.* 2007). In the second step, the biosensor Lac/Ag-ZnO NPs/MWCNTs was prepared by deposition of 10 µL Lac on Ag-ZnO NPs/MWCNTs and allowed to dry at 4^{0} C for 3 hours. After drying, the electrodes were covered with 5 µL of glutaraldehyde and left to dry at room temperature for 10 minutes in order to avoid enzyme leakage. The fabrication of biosensor was illustrated in **Figure 4.3**.

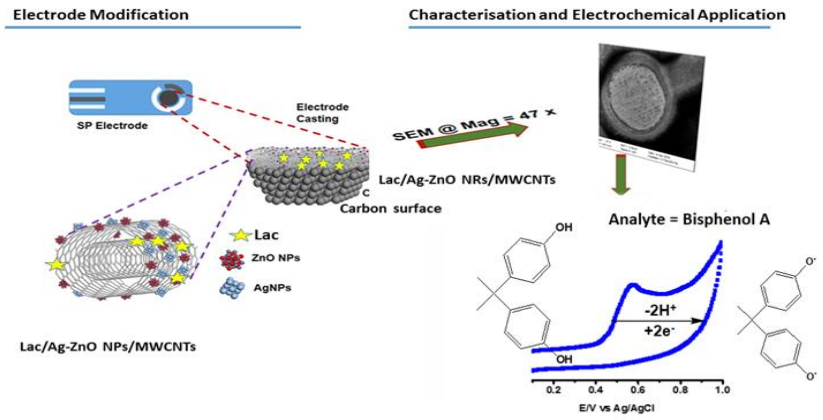

Figure 4.3 Modification of the screen printed electrode.

4.1.5.2 Design and fabrication of photo electrochemical sensor for BPS with MIP-ZnO NRs/FTO

The photo electrochemical sensor was constructed by using two steps molecular imprinted technique, (i) polymerization (ii) oxidation as shown on **Figure 4.4**.

(i) Polymerization

The cyclic voltammetry technique was used for the photo electrochemical and electrochemical polymerization of the monomer polypyrrole on the FTO surface in the absence and presence of the template (bisphenol S) using the modified method that was reported previously (Lu *et al.* 2013). Polymerization was achieved by the cycling the potential repeatedly between 0 and + 0.9 V at a scan rate of 100 mVs^{-1} for 12 voltammetric cycles, in the solution that contained 0.0001 M BPS, 3 M potassium chloride (KCl) and 0.01 M PPy. This electrode was then denoted as molecular imprinted polymer MIP-ZnO. In order to evaluate the imprinting effects, the control polymer named non-imprinted polymer NIP-ZnO is always prepared along with MIP. The NIP is prepared in same way as MIP but in the absence of a template BPS (route 1).

(ii) Oxidation

The removal of the template (BPS) from the monomer (PPy) after polymerization was carried by oxidation. This was achieved by electrochemical treatment (oxidation) at 1.5 V in 0.01 M sodium sulphate (Na_2SO_4). The sensor prepared in the presence of the template BPS was referred to as MIP-ZnO/FTO and the other one prepared in the absence of BPS the control sensor was referred to as NIP-ZnO/FTO.

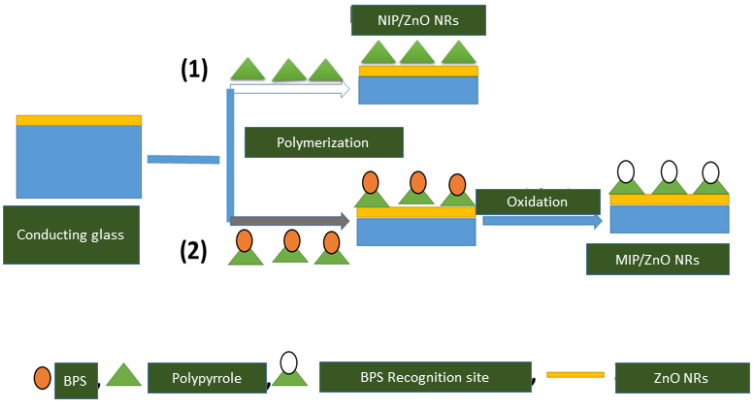

Figure 4.4 Schematic illustration for fabrication and selective mechanisms of the BPS sensor.

4.1.6 Electrochemical characterization

4.1.6.1 Cyclic voltammetry (CV)

Cyclic voltammetry was used to investigate the behaviour of analyte on the modified electrode surface. Analysis were carried out in 0.1 M PBS as the supporting solution in the potential range -0.4 to 1.0 V, scan rate 0.01 V. s^{-1}, with and without UV illumination.

4.1.6.2 Electrochemical Impedance Spectroscopy (EIS)

Electrochemical impedance spectroscopy (EIS) measurements, recorded using a two electrode system and results were analysed using FRA software. It was used to estimate the ionic conductivity of the synthesized ZnO synthesized in the presence and absence of polypyrrole in 0.1M PBS, at a perturbation amplitude of 150 mV within the frequency range of 100 kHz to 100 mHz.

4.1.6.3 Chronoamperometry

Chronoamperometry measurements were carried out in the three electrode system for the investigation of the electrochemical and photo electrochemical behaviour of BPS. The fixed potential of 0.5V and pulsed mode (20 s, 5 pulses) was imposed until the cathodic current became stable.

4.1.7 Electrochemical and photo electrochemical measurement of bisphenols

4.1.7.1 Electrochemical measurement of BPA with Lac/Ag-ZnO NPs/MWCNTs/C-SPE

All measurements were carried out at room temperature in a 10 mL electrochemical cell. To the electrochemical cell, 9.0 mL of 0.1 M PBS buffer solution (pH 6.0) and 10 µL standard solution of 5 mM BPA were added and thereafter electrochemical measurements were carried out by cyclic voltammetry (CV) in the potential range of 0.0 to 1500 mV vs. Ag/AgCl reference electrode at a scan rate of 50 $mV.s^{-1}$. Differential pulse voltammetry (DPV) scans were employed under the same potential range but at a scan rate of 100 $mV.s^{-1}$.

4.1.7.2 **Photo electrochemical measurement of BPS with MIP/ZnO NRs/FTO**

The response to target analyte BPS in a phosphate buffer solution (2mL, 0.1 M) was studied using chronoamperometry at the fixed potential of 0.5 V and pulsed mode (20 s, 5 pulses), analysis was performed with or without the UV illumination. The responses of 0.01 mM stock solution of BPS on ZnO NRs/FTO, MIP/ZnO NRs/FTO and NIP/ZnO NRs/FTO were recorded by successive addition of the appropriate analyte stock solution. All photo electrochemical experiments were carried out at 25 °C.

4.1.8 Extraction of BPA from mineral water bottles

The mineral water bottles were collected from a local disposal sites (Durban, South Africa). These samples were pre-cleaned by ultra-sonication in acetone, rinsed successively with alcohol, doubly distilled water and then dried at ambient temperature overnight. BPA was extracted from mineral water bottles using the reported method by Ntsendwana and co-workers (Ntsendwana *et al.* 2012) with minor modifications. Briefly, the samples were cut into small pieces, with an average size of 0.3 cm, from which approximately 1.0 g and 25 mL of deionized water was added into a round bottom flask. The flask was then fitted with a condenser placed into an oil bath heated to 70 ± 3^{o}C for 48 h. After cooling to room temperature; the condenser was washed with about 15 mL of deionized water into the same flask. Thereafter, the sample was filtered, through a 0.45 µm filter paper. Finally, the collected filtrate was made up to 50 mL and stored at 4 ^{o} C for further studies.

4.1.9 Interference studies

The interference of foreign species for detection of BPA and BPS was evaluated by using different concentration of metal ions (Cu^{2+}, Fe^{3+}, Bi^{3+}, Cd^{2+}, and K^{+}) and other phenolic compounds (catechol, 4-aminophenol, 2-nitrophenol, phenol, bisphenol C and 4,4-sulfonyldiphenol). Various concentration ranging from 0.5 to 10 mM of these foreign species were prepared. Each foreign species was mixed with the analyte of interest, current change was then monitored.

4.2 Computational studies

4.2.1 DFT calculations

The UV-Vis, Raman, and infra-red (IR) spectra were generated from DFT by means of optical and frequency calculation by computing a Hessian matrix during geometry optimization. For the frequency calculation, the Hessian elements were calculated by dislocating every atom in the infinite model and calculating a gradient vector. This procedure generates a comprehensive second derivative matrix (BIOVIA 2016). Upon the optimization, the Raman spectra can be generated from the lowest cluster's configuration, while IR spectra is generated from vibrational analysis tools along with 1.0 Å maximum amplitude and 'ultrafine' graphical quality.

4.2.1.1 Fluorine-doped tin oxide

(i) Structure and energetics

Dmol3 code was used for DFT calculation of FTO (Delley 2000) as MS software (BIOVIA 2016). It was used for the calculation of electronic properties of molecules such as crystalline solid materials, band structure and frontier orbitals (Delley 2000) as well as vibrational properties such as Raman and infra-red spectroscopy. DMol3 can both use gas phase boundary or 3d periodic boundary conditions for solids or simulations of lower-dimensional periodicity. The periodic structures were calculated using DFT method using Double Numerical plus Polarization (DNP) ver. 3.5 basis set and Generalized Gradient Approximations-Perdew-Burker-Ernnzerrhof (GGA-PBE) correlation energy functional (Perdew, Burke and Ernzerhof 1996). Metal oxide clusters have been calculated by the spin-unrestricted polarization method. This method is used to calculate different methods for different spins (Kang *et al.* 2015). DNP is the basis set that is comparable to 6-31G** basis set (Gaussian) in size and they are accurate (Benedek *et al.* 2005).

In order to perform large DFT calculation of FTO, geometry optimization of intrinsic structure is required to validate the used parameters. The 'gamma' type k-point of 1x1x1 was used for geometry optimization and structural properties calculations.

(ii) Electronics properties

The wurtzite ZnO bulk nanomaterial model was constructed based on its XRD plane values obtained from the experiment (0 0 2) using Materials Studio (BIOVIA 2016). The construction was made as the simplest as performed in order to avoid the time-restriction during the calculation. The ZnO (0 0 2) cluster was built along the 2 x 2-unit cell and C-plane orientations in order to facilitate periodic boundary box conditions with the following parameters; as a = 6.499 Å, b = 6.499 Å, c = 13.214 Å. Following, the calculations were done by spin-unrestricted DFT within Local Density Approximation implemented under DMol3 package. The Perdew-Wang (PWC) functional was employed without concerning the symmetry constraint. The double numerical basis set with polarization functions (DNP) was applied to describe all electron Kohn-Sham functions. The DNP function set is analogous with the 6-31G** basis set and since it is based on the atomic orbitals, the results are expected better than using Gaussian basis. Since it is based on the atomic orbitals, the results are expected better than using Gaussian basis. SCF tolerance was customized to be 10^{-5} eV/atom with 1,000 iterations. The atomic positions were relaxed to optimize the interatomic forces with the parameterized energy tolerance, force, as well as maximum displacement of energy to be 12 x 10^{-5} Ha, 4.0 x 10^{-3} Ha/Å, and 5.0 x 10^{-3} Å, respectively. The accuracy of this LDA/PWC has been investigated through testing the preliminary calculation toward the similar structure from low to fine quality predictions. The vibrational analysis was derived at 298 K along with the incidence light of 488 nm, which both are in similar values as observed in the experiment results. The HOMO-LUMO gap was calculated as an electric field function for the neutral ZnO by means of:

$$\Delta E_g^{DFT} = E_{lumo\ (eV)} - E_{homo\ (eV)}$$

The UV-Vis, Raman, and infra-red (IR) spectra were generated from DFT by means of optical and frequency calculation by computing a Hessian matrix during geometry optimization. For the frequency calculation, the Hessian elements were calculated by dislocating every atom in the infinite model and calculating a gradient vector. This procedure generates a comprehensive second derivative matrix (BIOVIA 2016). Upon the optimization, the Raman spectra can be generated from the lowest cluster's configuration, while IR spectra is generated from vibrational analysis tools along with 1.0 Å maximum amplitude and 'ultrafine' graphical quality.

CHAPTER 5

RESULTS AND DISCUSSION

This chapter presents the results and discussion of the experimental and computational findings. The experimental section involves characterization of the synthesized ZnO nanostructure (nanoparticles and nanorods), for the development of C-SPE and FTO based electrodes using multiwalled carbon nanotubes (MWCNTs) and polypyrrole (PPy) respectively. These electrodes were used to evaluate the electrochemical properties of BPA and BPS. Furthermore, DFT calculations were used to understand the optical properties of MIP/ZnO NRs.

5.1 Experimental

5.1.1 Characterisation of bare ZnO nanostructures

5.1.1.1 Optical and structural evaluation

(i) UV-visible analysis

The UV–visible spectrum of ZnO NPs dispersed in ethanol depicted in **Figure 5.1** shows an absorption peak (see curve-i) observed at 352 nm (3.237 eV), in agreement with the literature report (Siva Vijayakumar *et al.* 2013). On the other hand, the UV-visible spectrum of Ag-ZnO NPs (curve-ii) indicates a broader absorption peak observed at 357 nm (3.229 eV) with a red shift and low particle size as observed by Karami and Fakoori (Karami and Fakoori 2011). However, the band gap of ZnO NPs decreased from 3.237 eV to 3.229 eV when doped with Ag, due to the p-type conductivity of NPs, in accordance with those reported by Reddy and co-workers (Reddy *et al.* 2013). The band gap of the Ag-ZnO NPs decreases due to the downwards shifts of the conduction band.

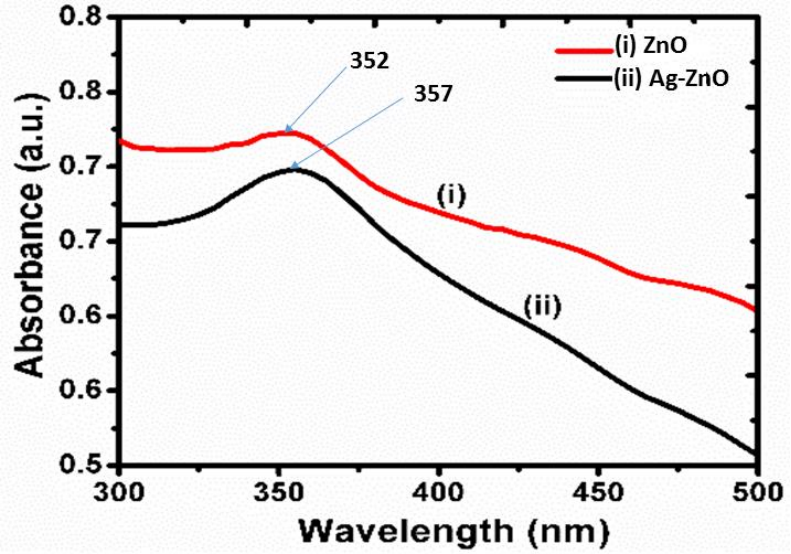

Figure 5.1 UV–visible absorption spectra of (i) ZnO NPs and (ii) Ag-ZnO NPs.

(ii) Fourier transform infrared analysis

The FTIR spectra of the synthesized ZnO NPs and Ag-ZnO NPs are shown in **Figure 5.2**. Reddy and co-worker observed similar spectra for ZnO NPs and Ag-ZnO NPs exhibiting absorbance at 1385 and 1395 cm^{-1} due to ZnO NPs (Reddy *et al.* 2013). The characteristic absorption peaks at 3349 cm^{-1} indicates -OH stretching vibrations (Reddy *et al.* 2013; Siva Vijayakumar *et al.* 2013), the band at 2873 cm^{-1} represents -CH stretching vibrations (Hosseini *et al.* 2015), while the sharper peak observed at 1582 cm^{-1} represents -C=O stretching vibration (Siva Vijayakumar *et al.* 2013; Hosseini *et al.* 2015). With the addition of Ag there is a minor shift towards lower frequencies, due to the partial substitution of the Ag^{+} ion in the ZnO lattice (Hosseini *et al.* 2015). The absence of Ag-O absorption bands at 460 to 565nm suggests no chemical bonding between Ag-O and Ag-ZnO NPs (Waterhouse, Bowmaker and Metson 2001; Yıldırım, Unalan and Durucan 2013).

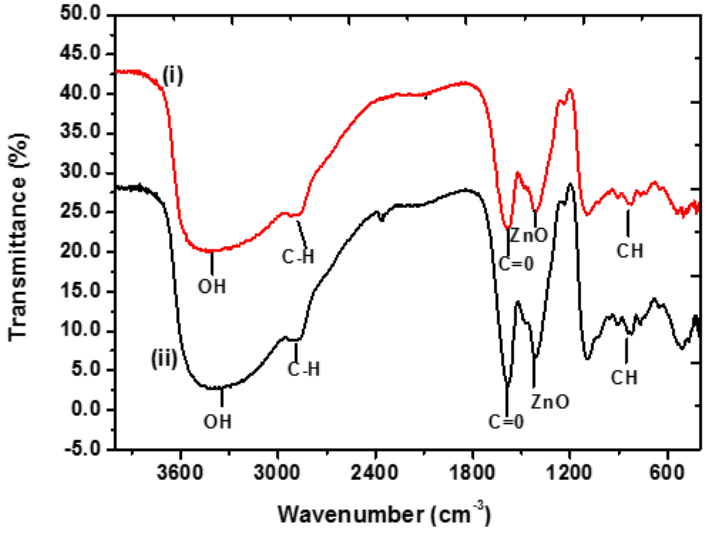

Figure 5.2 FTIR spectrum of pure (i) ZnO NPs and (ii) Ag-ZnO NPs.

(iii) Photoluminescence (PL)

Figure 5.3 shows the room temperature photoluminescence spectrum of ZnO NRs with an excitation wavelength of 355 nm in the wavelength ranging from 350 to 800 nm. The spectrum exhibits a single, intense and broad emission peak located at around 611 nm attributed to the presence of a single ionized oxygen species (Williams and Kamat 2009). The recombination of the photogenerated electron causes emission (Zhou *et al.* 2007). This supports the work of several authors where the absorption peaks are reported between 550 nm to 570 nm (Mamat *et al.* 2011; Troshyn *et al.* 2012). Photoluminescence (PL) analysis was performed on ZnO NRs deposited on FTO as a substrate.

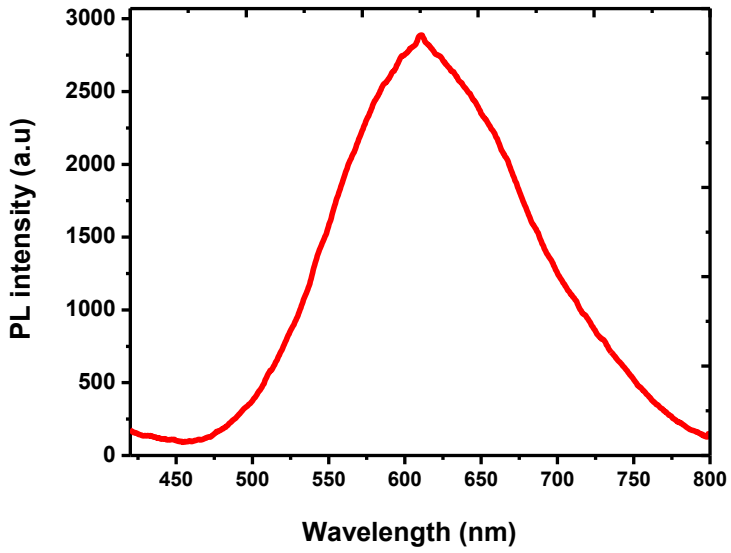

Figure 5.3 PL spectrum of ZnO NRs synthesized by hydrothermal method on the FTO substrate.

(iv) Raman spectroscopy

The structural defects and crystal perfection of the synthesized ZnO NRs were also evaluated using Raman spectroscopy as shown in **Figure 5.4**. The sharp peaks observed at 98 and 439 cm^{-1} are normally noticed in the wurzite structure of ZnO confirming the presence of low and high modes. The sharp peak at 439 cm^{-1} is assigned as the E_2 (high), showing the good crystal quality (Moulahi and Sediri 2014), while the intense band at 579 cm^{-1} is due to the oxygen vacancy in ZnO (Marie, Mandal and Manasreh 2015).

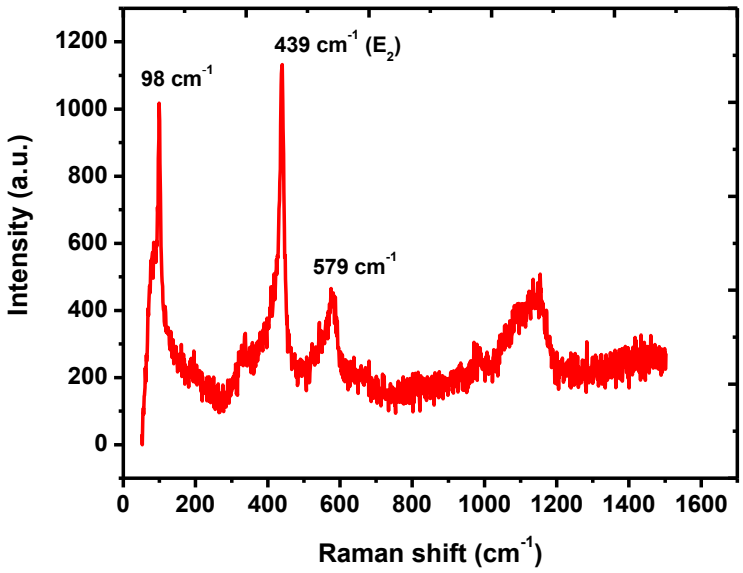

Figure 5.4 Raman shift of ZnO NRs.

(v) Grazing Incidence X-ray diffraction (GIX-RD)

The X-ray diffraction (XRD) analysis was carried out to investigate the crystalline structure of the synthesized ZnO NRs. The ZnO NRs structures showed orientation planes of (100), (002), (101), (102), (110), (103) and (112), in good agreement with the diffraction angles at 31.70, 34.51, 36.31, 47.67, 56.72, 66.87 and 68.12, as can be seen in **Figure 5.5**. The dominant peak observed at 34.410 (2θ) indicates that the synthesized ZnO NRs have a good crystalline structure. This crystalline structure is similar to the crystalline structure of ZnO NRs as reported by Warule and co-workers (Warule *et al.* 2009). Furthermore, XRD analysis of ZnO NRs revealed that the synthesized NRs has a hexagonal wurzite structure with the characteristic (002) peak confirming that c-axis is the preferred orientation (Mbuyisa, Ndwandwe and Cepek 2015; Narayanan, Ganesh and Karthigeyan 2016).

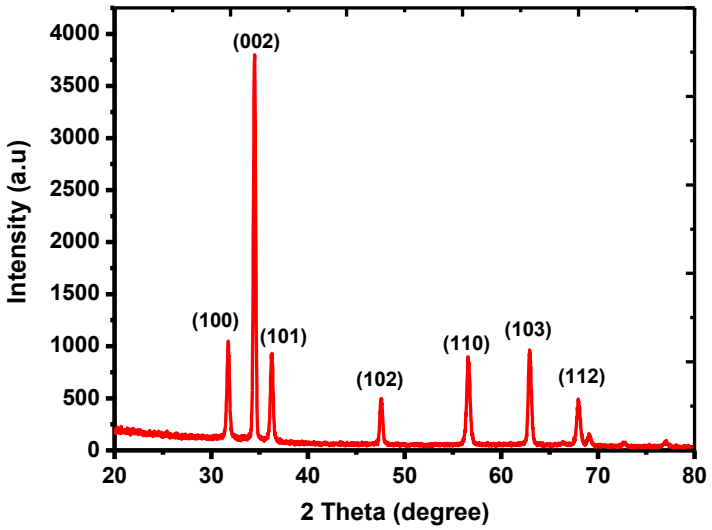

Figure 5.5 XRD pattern of ZnO NRs.

5.1.1.2 **Morphological evaluation**

(i) Scanning Electron Microscopy (SEM)

The SEM was used to examine the morphology of ZnO NRs grown on the ZnO seeded layer by hydrothermal method. SEM studies show that the synthesized ZnO NRs were fully grown onto the surface of the FTO seeded substrate. **Figure 5.6** (a) and (b) illustrates the SEM images of ZnO NRs at lower and higher magnifications. The uniformly well-aligned ZnO NRs with a diameter of 30 ± 15 nm and length of 800 ± 40 nm were observed. Similar results were reported by Ladanov and co-workers (Ladanov *et al.* 2011). The morphology revealed that the hexagonal wurtzite structure of ZnO NRs grows on the substrate along the c-axis direction, consistent with the recent work of Alimanesh and co-workers (Alimanesh, Hassan and Zainal 2017).

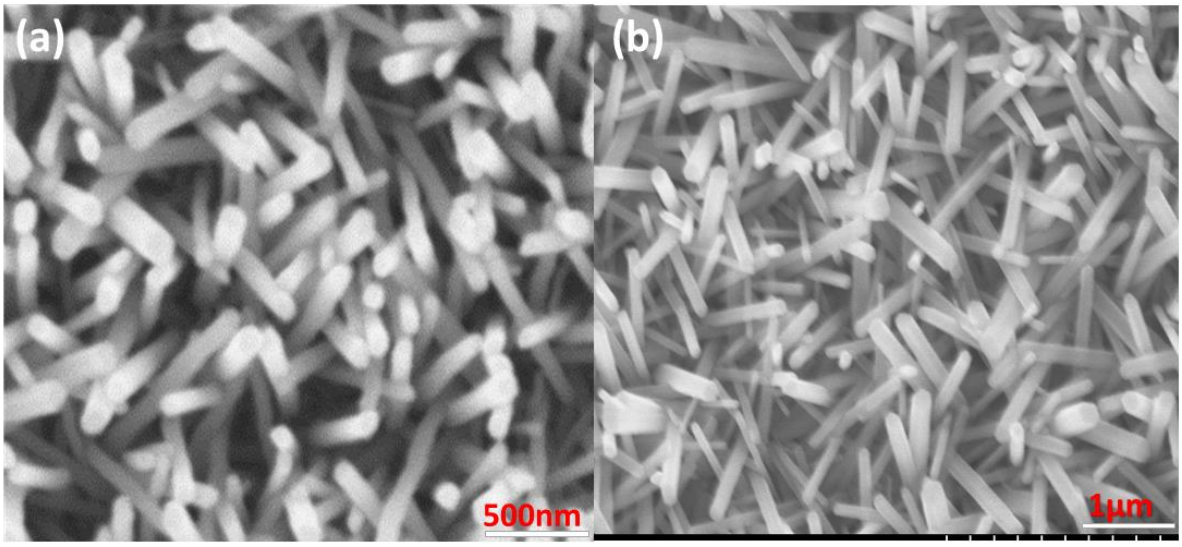

Figure 5.6 SEM images of ZnO NRs different magnifications, (a) 500 nm and (b) 1µm.

(ii) Transmission electron microscope (TEM)

The structural properties of the individual ZnO NRs were characterized using the high-resolution transmission electron microscopy (HRTEM) and selected area electron diffraction (SAED) pattern as shown on **Figure 5.7** (a) and (b). The images revealed that the synthesized ZnO NRs have a single high quality crystal structure growing along the [001] direction on the c-axis orientation, indicating that ZnO NRs have a hexagonal wurtzite structure. This is agreement with the XRD results shown in **Figure 5.5**, which is similar to the crystalline structure of ZnO NRs reported by other authors (Liu *et al.* 2005; Amin *et al.* 2012).

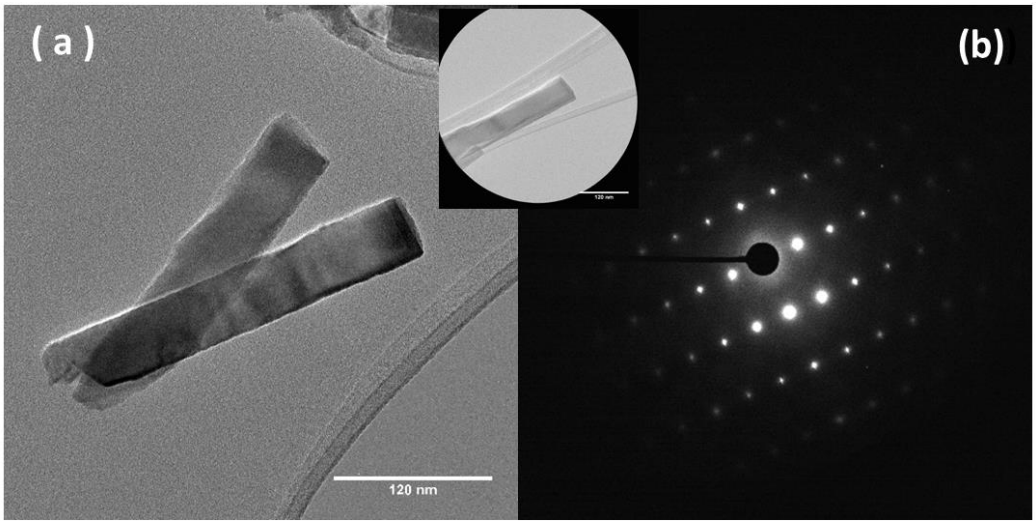

Figure 5.7 (a) TEM micrograph of individual ZnO NRs prepared on FTO substrate by a hydrothermal method and (b) selected area electron diffraction SAED pattern.

5.1.1.3 Electrochemical and photo electrochemical behaviour of ZnO NRs

The electrocatalytic behavior of ZnO NRs synthesized on the conducting glass was investigated in order to discover its possible applications. Fluorine doped tin oxide (FTO) substrate modified with ZnO NRs was used as the working electrode, platinum as the counter electrode and Ag/AgCl as the reference electrode in the presence of phosphate buffer (PBS). Different electrochemical techniques such as cyclic voltammetry (CV), electrochemical impedance spectroscopy (EIS) and chronoamperometry method have been used to characterize the synthesized ZnO NRs.

(i) Electrochemical characterization

Electrochemical behavior of ZnO NRs was investigated in a phosphate buffer by cyclic voltammetry as illustrated in **Figure 5.8**.The cyclic voltammograms (CVs) of ZnO NRs obtained with and without UV illumination are shown in **Figure 5.8** (i) and (ii) respectively, in the presence of 0.1 M PBS as the supporting electrolyte. A well-defined CV voltammogram for ZnO NRs is observed, suggesting that ZnO NRs have the electrocatalytic activity effects in the presence of PBS as the supporting electrolyte. The EIS is one of the most powerful tools for investigating the electron transfer across the electrolyte and the surface of the electrode. ZnO NRs impedance spectra in 0.1 M PBS within the frequency range of 100 kHz to 100 mHz. In **Figure 5.9** (ii), Nyquist plot shows a semicircle behavior at high frequency and straight line at low frequency, this implies that the electrochemical reaction at the ZnO electrode is controlled by two processes, charge transfer and diffusion limitations. **Figure 5.10** (ii) shows the chronoamperometric studies in the fixed potential of 0.5 V vs Ag/AgCl in PBS, with the current investigated at the positive potential. The chronoamperometric studies serve as an alternative probe of electron occupancy in ZnO NRs films. Greater current and quicker response time were observed. The transient current exhibited a fast phase in ZnO NRs, within few seconds at a positive potential.

(ii) Photo electrochemical characterization

The photopotential responses of ZnO NRs electrode were shown in **Figure 5.8** (i) and **Figure 5.10** (i). The photocurrent responses were observed because of the generated electron hole pair, this creates the competition between the recombination and the initial charge separation. In this process, both steps (recombination and initial charge separation) have to take place simultaneously. Therefore, this process is divided into two successive processes: (i) in the first process, transportation of charge in the non-illuminated ZnO NRs take place, (ii) in second process charge transport through the substrate FTO occurs. Without UV illumination low current was observed. Interestingly, under UV illumination, there is a substantial increase of photocurrent response in the same potential ranges. This shows that under UV illumination there is a more effective separation of photo induced electron-hole pairs and fast charge transport (Kang *et al.* 2015). The photo electrochemical mechanism is proposed as shown in **Figure 5.11**. With UV illumination, the photo−generated electrons are excited from valence band (VB) to conduction band (CB) in ZnO, this results in the formation of holes in the VB simultaneously. The photo−generated holes in the VB of ZnO transfer the signal fast to the PPy surface, since the VB potential of ZnO is more positive than of PPy. Thefore this increases the charge carrier transfer between the nanostructure and polymer, and allows the effective separation of photo−generated electron−hole pairs. The holes that are transferred and remained into the VB of ZnO can be used for the oxidation reaction of BPS. Some ZnO NR traps the photo-generated electrons, therefore, this facilitates the electron-hole separation and this improve the photo electrochemical reaction.

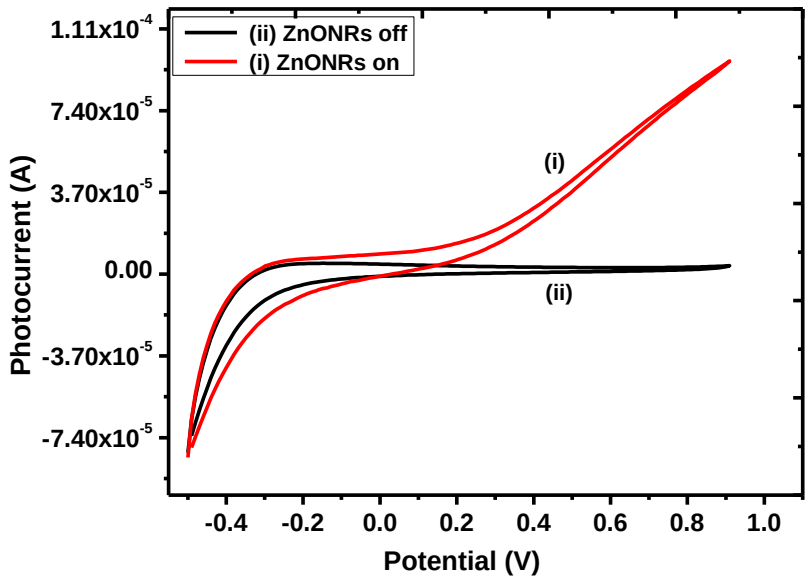

Figure 5.8 Cyclic voltmmograms of ZnO NRs in 0.1 M PBS at scan rate of 0.01V.s^{-1} with (i) and without (ii) UV illumination.

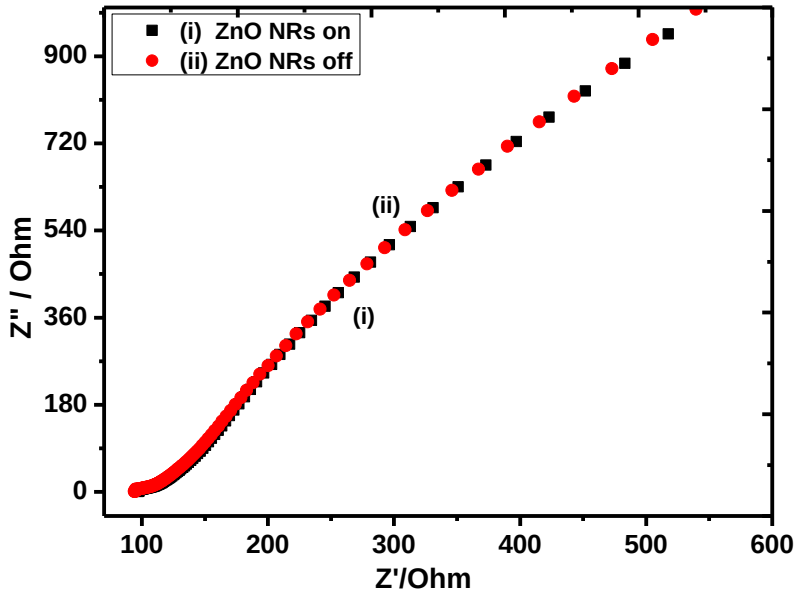

Figure 5.9 Nyquist plots of ZnO NRs in the presence of 0.1 M PBS as the electrolyte with UV (i) illumination and without UV illumination (ii).

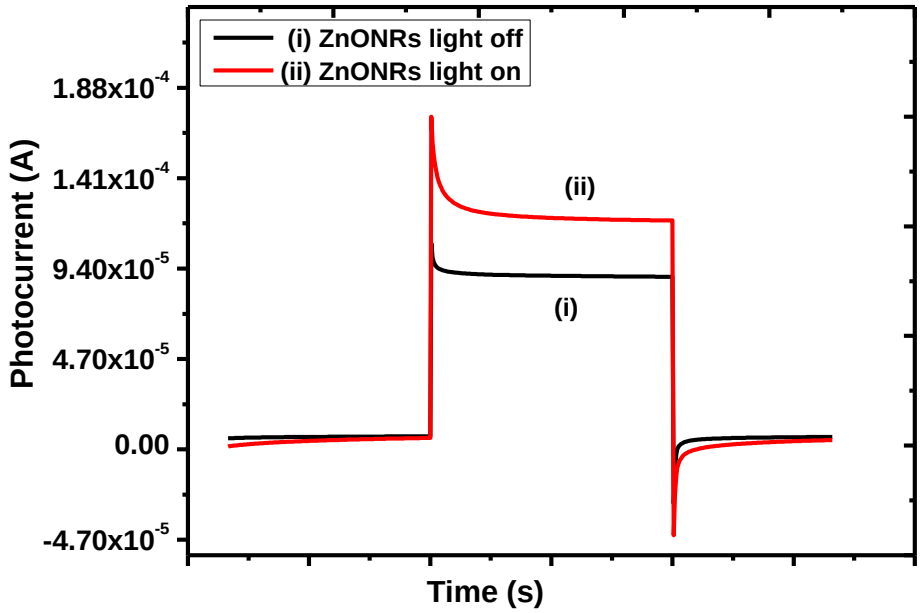

Figure 5.10 Chronoamperograms of ZnO NRs in 0.1 M PBS with (ii) UV illumination and without (i) UV illumination

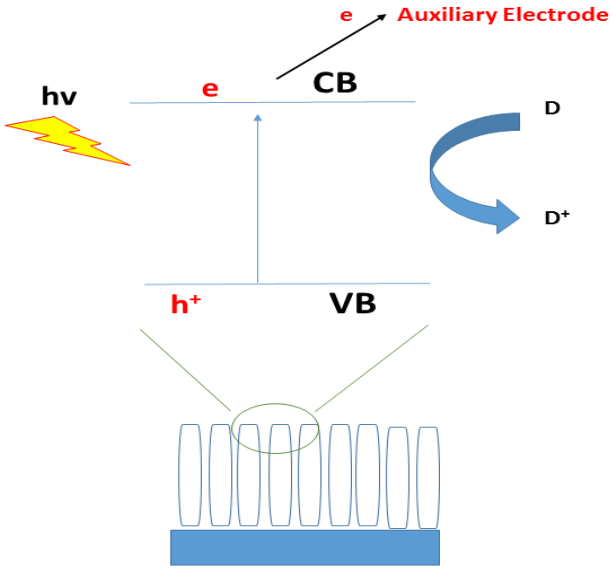

Figure 5.11 Photo electrochemical process on the substrate surface.

5.1.2 Characterization of the Lac/Ag-ZnO NPs/MWCNTs/C-SPE and MIP/ZnO NRs/FTO

5.1.2.1 Optimization of parameters for the synthesis of MIP/ZnO NRs/FTO

(i) The effect of the molar ratio functional monomer to template molecule

The template (BPS) and monomer (PPy) concentration ratio were used to control the amount of the recognition sites. This was achieved by varying the concentration of the template BPS and keeping the concentration of the monomer PPy constant at 0.01 M. Then, 0.01 mM PPy was used to investigate the photocurrent response changes at different concentration of BPS. The 0.0001 M BPS gives the highest current compared to other concentrations. Therefore, 0.0001 M BPS with 0.01 M PPy was chosen as the optimum polymerization solution for the entire experiment. After the removal of the template PPy and ZnO are still retained, this is valuable to the formation of more recognition cavities to BPS and offers transmission close to UV light, this makes a good use of ZnO NRs photoelectrocatalysis ability.

(ii) Polymerization

The effects of photo electrochemical and electrochemical polymerization of the monomer PPy on FTO surface in the absence and presence of the template (BPS) was achieved by performing numerous voltammetric cycles. After polymerization the blackish colour was observed on the electrode surface, this shows that the polymer was deposited on the surface of the electrode. **Figure 5.13** (a) and (b) shows the voltammograms for the polymerization of PPy on the FTO surface. Electropolymerization and photo electroplymerization of PPy films onto FTO surface was achieved by radical cation mechanism. In this process, the monomer (PPy) undergoes oxidation to form radical cations that form the insoluble polymer film onto the surface of the electrode. The growth of the PPy film was used to control the sensitivity of the electrode. The PPy thickness plays a crucial role in the sensitivity and selectivity of the electrode because it provides enough biding sites. The thicker imprinted polymer results in more imprinted sites. However, when the polymer is too thick it very hard to remove the template from the polymer. This makes it difficult for BPS to reach into the imprinted cavities due to the poor site and slow binding kinetics that are caused by the high mass–transfer resistance. The investigation of polymerization cycles was carried out from 5 to 30 cycles as shown in **Figure 5.12**. Photocurrent increases until it reached a maximum value at 12 cycles. After 12 scans, the current decreases and the even distribution of the film on the surface electrode were achieved which is shown by SEM pattern in **Figure 5.18** (a). This offers additional evidence that the FTO surface is

conductive and electrode fouling eliminated. As the cycles there is an increase of transfer resistance, and this causes the current to decrease. Therefore, 12 CV cycles were further used in the development of the MIP/ZnO NRs electrode. The scanning cycles were used to control the thickness of PPy film during electrochemical and photo electropolymerization process. To acquire a large surface area and keeping the nanorods structure, 0.01 M PPy concentration was prepared in 3 M KCl solution that was used as the electrolyte. During the multiply scan voltammetry there is an increase of the current which shows the formation of conducting polymer film on FTO surface. During electropolymerization an oxidation peak was observed at 0.5 V in the first cycle, however the peak disappeared in the second scan and the current decreases continuously as shown in **Figure 5.13** (b). The peak was due to the oxidation of BPS during electropolymerization. This oxidized BPS product attached itself to the MIP/ZnO NRs electrode and this result in the electrode passivation and therefore decreases the electropolymerization current. In the presence of UV light the photo electropolymerization current increases with the increase in CV cycles **Figure 5.13** (a), this shows the formation of the conductive polymer film on the surface of the electrode. After 12 scans, there was no obvious increase of current and the even distribution of the film on the surface electrode was achieved which is shown by SEM pattern in **Figure 5.18** (ii) and (iii), this offers additional evidence that the FTO surface is conductive and electrode fouling eliminated.

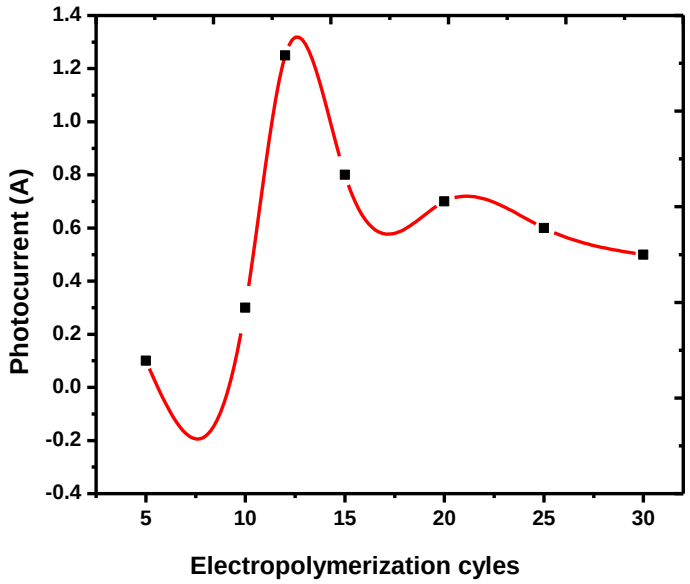

Figure 5.12 Effects of electropolymerization cycles.

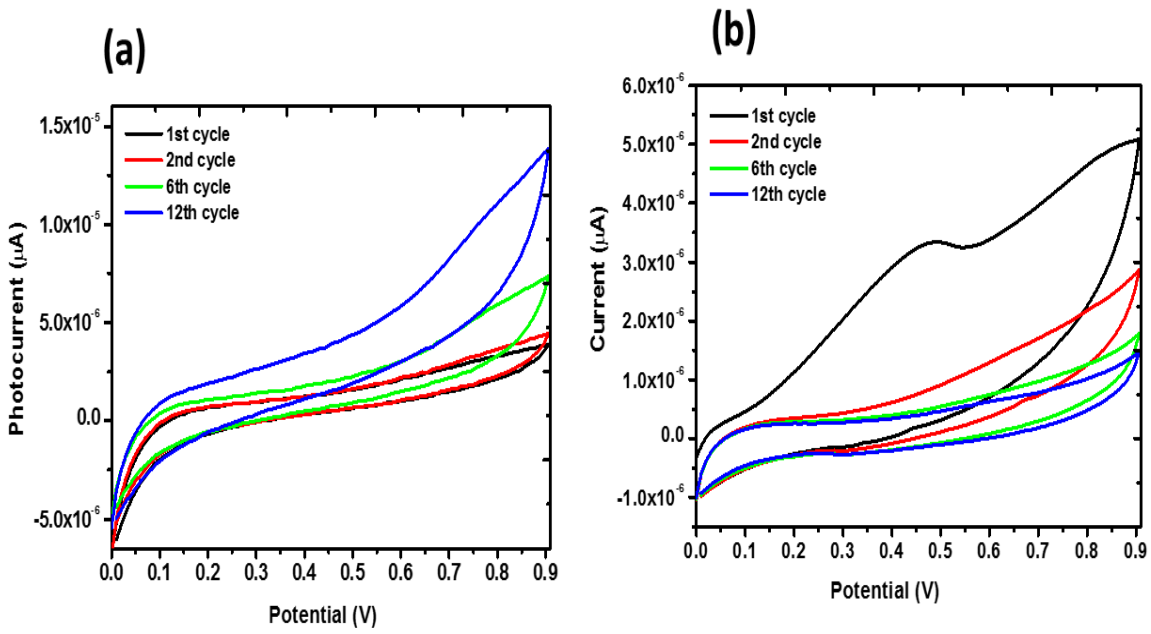

Figure 5.13 (a) Photo electropolymerization and (b) electropolymerization in 3 M KCl at scan rate 0.01 V s^{-1}.

(iii) Oxidation

Molecularly imprinted method plays a significant role in the molecular recognition capacity of the sensor, it increases the sensitivity and selectivity of the electrode. The formation of a hydrogen bond with BPS is formed by the combination of monomer polypyrrole and the template BPS and copolymerized on the surface of ZnO NRs. The imprinted cavities on the PPy film are formed by the removal of BPA templates and leaving the MIP with special recognition sites of BPS, in which only BPS can interact with the MIP. The removal of the template (BPS) from PPy was achieved by electrochemical and photo electrochemical treatment (oxidation) at 1.5 V in 0.01 M Na_2SO_4 as shown in **Figure 5.14**. To achieve the best cavities, electro and photo electrochemical oxidation time of BPS was studied. This was achieved by monitoring photocurrent and current changes. After 400 s of photo electrochemical treatment, photocurrent becomes constant. Therefore, 600 s was chosen as the optimum oxidation time for the entire experiment to ensure the complete removal of BPS template molecules, excess becomes a distinct polymer with holes that have a particular shape and size of the template. The recognition sites provide a sensitive and selective sensor. However, electrochemical treatment takes 1100 s for the current to be steady, this shows that the application of UV/light has a positive effect.

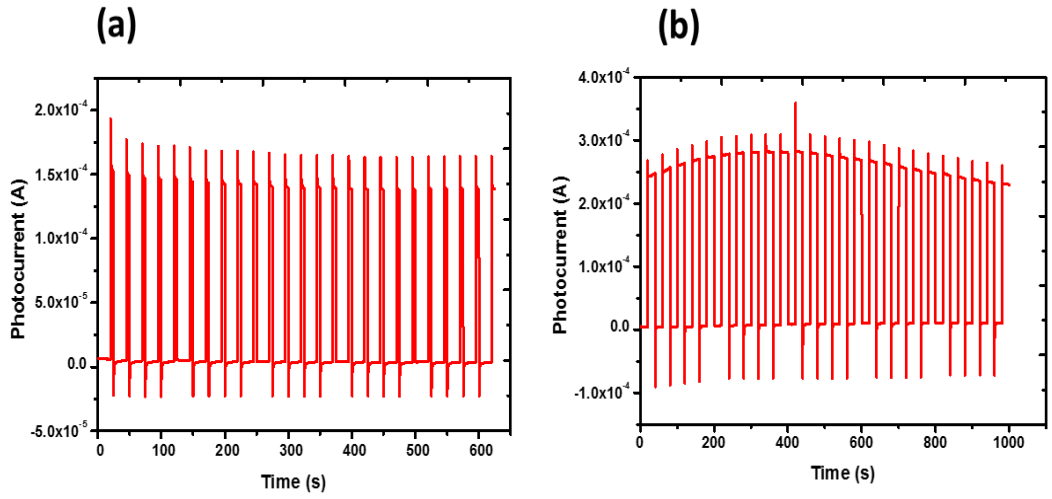

Figure 5.14 Oxidation (a) with UV illumination and (b) without UV illumination.

5.1.2.2 Optical and structural evaluation MIP/ZnO NRs/FTO

The optical and structural characterization of the sensor was studied by using different techniques such as spectroscopy, Photoluminescence (PL), Raman spectroscopy, Grazing incidence X-ray diffraction (GIX-RD).

(i) Characterization of sensor by photoluminescence and diffuse reflectance spectroscopy

The photoluminescence (PL) characterization was carried out to verify the polymerization on the surface of ZnO NRs, with the excitation wavelength of 355 nm. PL analysis is usually carried out in order to investigate the surface processes involved in electron–hole recombination of semiconductors. The strong absorption peak around 600 nm, as shown in **Figure 5.15** is due to the recombination of photo-excited holes with electrons occupying the singly ionized oxygen vacancies in ZnO. The PL intensity of the MIP/ZnO-decreases when compared with ZnO, which can be attributed to the reduction of the recombination process after the modification with the polymer. The decreases of the PL peak show a good crystal quality and good charge transport process this leads to a great performance of the electrode (Yahya AL-she'irey 2016). The polymerization does not alter the optical properties, because the PL peak emission does not shift. The diffuse reflectance spectra UV-vis of ZnO NRs and MIP/ZnO NRs nanocomposites are presented in **Figure 5.16**. **Figure 5.16** shows that both ZnO and MIP-ZnO absorb at UV-Vis region with the absorption band at about 450nm, corresponding to energy band gap of 3.22 and 3.16 eV respectively. The band gaps of the synthesized nanostructures were then calculated according to the previous report by Nasr and

co-workers (Nasr et al. 2016). There is a blue shift of absorption edge of ZnO after MIP deposition, this is due to the decreases of π-conjugation and a more aggregated structure that is caused by various intermolecular interaction between the functional group of BPS and the polymer. The decrease of intensity (hypochromic shift) was also observed on MIP. These results were similar to the results previous reported by Apodaca and co-workers (Apodaca et al. 2011). This shift is due to the occurrence of more conformational defects disrupting the π-conjugation.

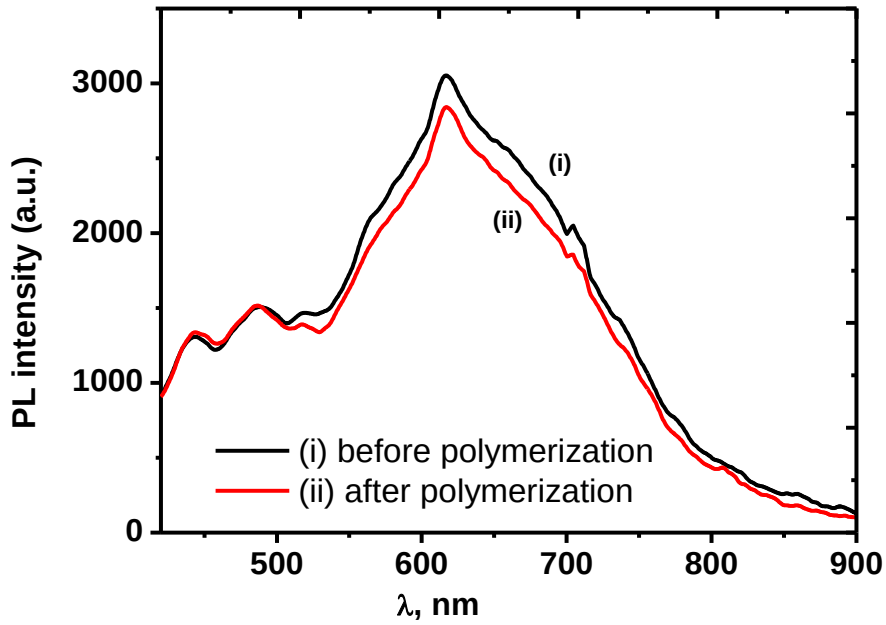

Figure 5.15 PL spectra of (i) ZnO NRs and (ii) MIP.

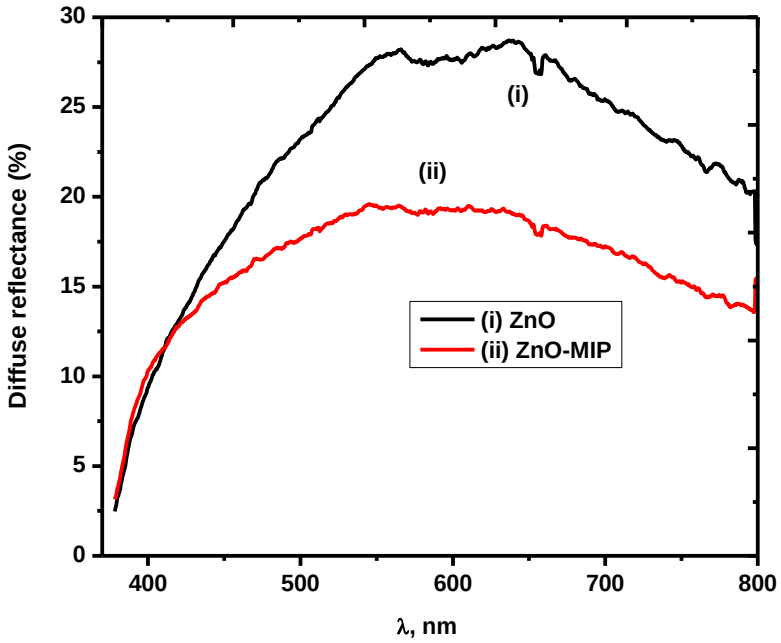

Figure 5.16 Diffuse reflectance of (i) Zno NRs and (i) MIP.

(ii) Raman spectroscopy and Grazing Incidence X-ray diffraction (GIX-RD) evaluation

Raman spectroscopy is a suitable tool to characterize oxide materials that have high Raman intensities, mainly for detection of electronic states and differentiate their crystal structures. Normally, Raman spectra of oxide materials display a peak at approximately 98 cm^{-1} and a peak at approximately 439 cm^{-1}, which suggest the wurzite crystalline structure of ZnO (Moulahi and Sediri 2014). These peaks represent low-and high mode (E_1, E_2) **Figure 5.17** shows that ZnO NRs produced two peaks at approximately 90 cm^{-1} and 400 cm^{-1} due to their oxide structures. However, MIPs/ZnO NRs does not show this characteristic peaks, this is due to the overcrowding of the polymer. The XRD pattern of ZnO NRs and MIP/ZnO NRs are similar, this indicates that the surface modification with a polymer does not alter the crystalline structure of ZnO NRs figure not shown here.

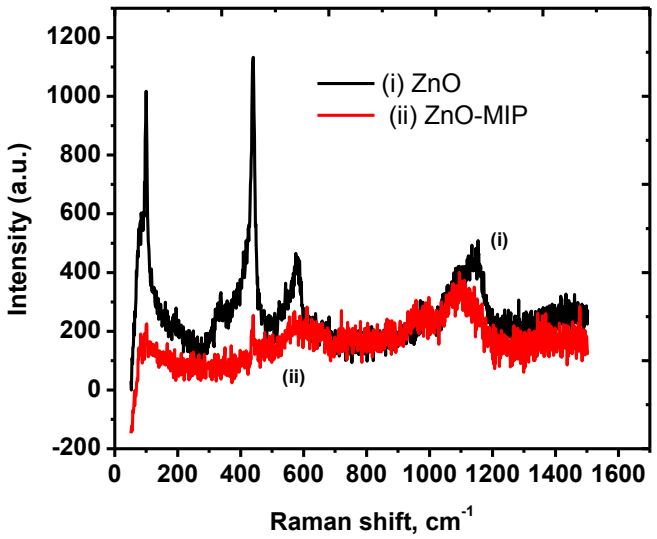

Figure 5.17 The Raman spectra of the (i) ZnO NRs and (ii) MIP.

5.1.2.3 Morphological characterization of the Lac/Ag-ZnO NPs/MWCNTs/C-SPE and MIP/ZnO NRs/FTO by SEM

The morphologies of ZnO NRs, NIPs-ZnO NRs and MIPs-ZnO NRs were studied by SEM, which are shown **Figure 5.18** (i), (ii) and (iii). The well-ordered uniform ZnO NRs with a diameter of 30±15 nm and 800±40 nm in length were observed as shown in **Figure 5.18** (i). After surface modification with PPy, the nanorods structure is still well retained and the polymer grows along the nanorods wall as shown in **Figure 5.18** (i) and (ii). This indicates that modification with PPy does not alter the structure of the nanorods. The surface morphologies of MIP were significantly different from that of NIP were observed. The rough surface of MIP was observed while NIP has a smoother surface, this indicates that MIP has a high surface area because of a highly porous surface. This can be further analysed by using a BET technique. The diameter of MIP and NIP were also studied and their average were 30±15 and 40±15 nm, respectively. The large diameter of NIP suggests that the template molecule BPS, had a positive effect on growth of the rods during polymerization (Pan *et al.* 2013). **Figure 5.19** represents the SEM images of bare C-SPE (see ii), Ag-ZnO NPs/MWCNTs/C-SPE (see iii) and Lac/Ag-ZnO NPs/C-SPE (see iv). The obtained SEM images clearly show the roughness of the coating increased from bare C-SPE to Lac/Ag-ZnO NPs/MWCNTs/C-SPE which is a good indicative of an increase in the surface area of the electrode with each modification. The SEM image shows that synthesized ZnO NPs is in nano scale.

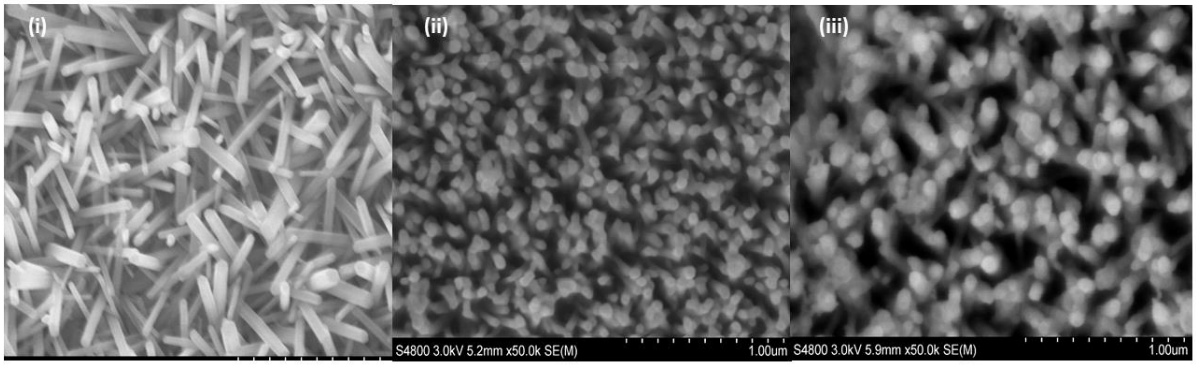

Figure 5.18 SEM images of (i) ZnO NRs, (ii) NIP/ZnO NRs and (iii) MIP/ZnO NRs.

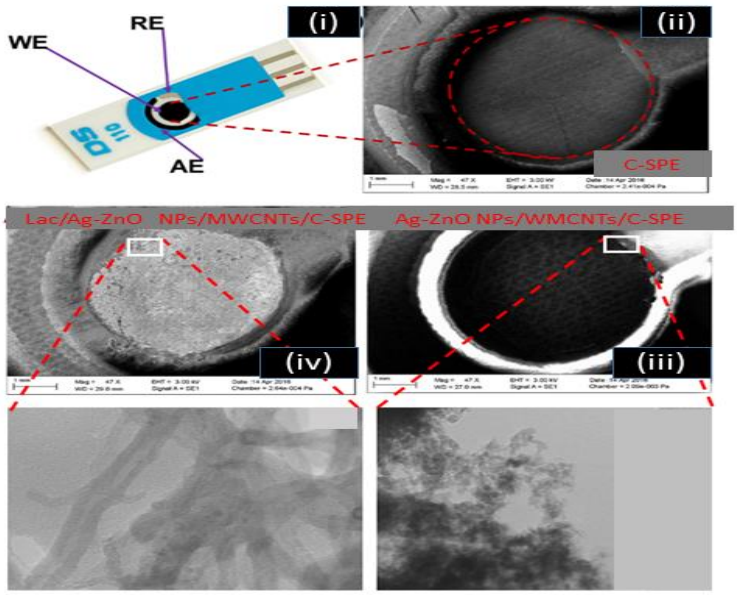

Figure 5.19 Image of (i) SPE, and SEM images of (ii) C-SPE, (iii) Ag-ZnO NPs/MWCNTs/C-SPE (iv) Lac/Ag-ZnO NPs/MWCNTs/C-SPE.

5.1.2.4 **Electrochemical behaviour of Lac/Ag-ZnO NPs/MWCNTs/C-SPE**

The main objective of this study was to develop a biosensor for selected phenolic compounds. **Figure 5.20** shows the cyclic voltammograms of BPA at the bare carbon-screen printed electrode (C-SPE), and Ag-ZnO NPs/MWCNTs/C-SPE and Lac/Ag-ZnO NPs/MWCNTs/C-SPE in aqueous PBS (0.1 M). The electrochemical behaviour of BPA was investigated in both the unmodified and modified electrode using a 0.5 mM BPA in 0.1 M PBS as the electrolyte. In the blank electrolyte, the oxidation peak was absent for both the modified and unmodified C-SPE, **Figure 5.20** (i) and (ii)) but after the addition of the analyte 0.5 mM BPA, the distinguished irreversible oxidation peak was observed in the modified and unmodified electrode as shown in **Figure 5.20** (iii),(iv) and (v). This shows that the oxidation peak belongs

to BPA. Cyclic voltammograms of bare electrode showed a low oxidation peak current, followed by Ag-ZnO NPs/MWCNTs/C-SPE composite and Lac/Ag-ZnO NPs/MWCNTs/C-SPE showing the highest oxidation peak current, this signifies an increased sensitivity. Low oxidation peak current that is not well defined peaks were observed in the C-SPE, **Figure 5.20** (iii). However, a well-defined oxidation peak was observed when Ag-ZnO NPs/MWCNTs/C-SPE and Lac/Ag-ZnO NPs/MWCNTs/C-SPE were introduced and the oxidation peak current increases significantly. This is due to the large surface and electrochemical conductivity of MWCNT and the catalytic activity of laccase. The strong adsorption effects of Ag-ZnO/MWCNTs/C-SPE and Lac/Ag-ZnO/MWCNTs/C-SPE results in the high oxidation current compared to the bare electrode.

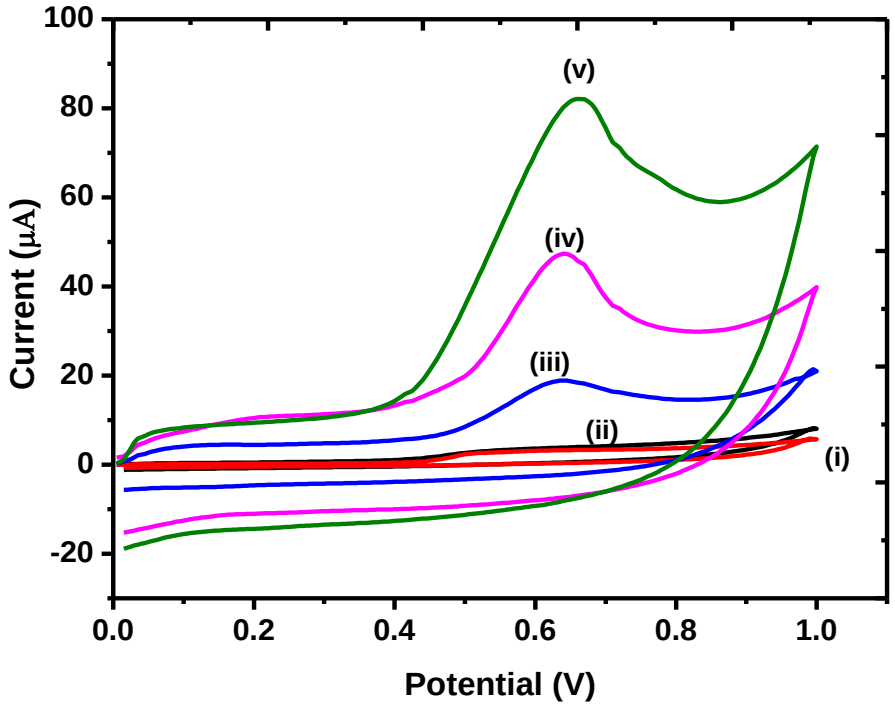

Figure 5.20 Cyclic voltammograms of blank at the bare C-SPE (curve i), Lac/Ag-ZnO/MWCNTs/C-SPE (ii) and of 0.5mM BPA at bare C-SPE (iii), Ag-ZnO/MWCNTs/C-SPE (curve iv) and Lac/Ag-ZnO/MWCNTs/C-SPE (curve v) in aq. PBS (0.1 M).

5.1.2.5 **Electrochemical and photo electrochemical behaviour of MIP/ZnO NRs/FTO**

The electrochemical and photo electrochemical features of the fabricated sensor (denoted MIP /ZnO NRs) was evaluated by amperometric i–t curve as shown in **Figure 5.21**. In dark conditions, low current responses were observed on all three sensors ZnO NRs, MIP /ZnO NRs and NIP/ZnO NRs under an applied voltage of 1.5 V. However, with UV illumination, a dramatic increase of current was observed on all the three sensors. This shows that electrochemical method requires high voltage compared to photo electrochemical methods. The electrodes that are modified with a polymer has similar photocurrent signal in 0.1 M PBS, due to their larger surface area than bare ZnO NRs electrode. The photocatalytic characteristic of ZnO NRs and PPy modification contributes to the dramatic increase of current. The greater sensitivity was initiated from the outstanding photocatalytic performance of well-crystallized ZnO NRs. Cyclic voltammetric examination results shown in **Figure 5.22** shows that without UV illumination, the weak current response was observed in the potential range -0. 4 to 1.0V. However, under UV illumination significant photocurrent response was observed on all the three electrodes in the same potential range. The photocurrent responses increase due to the outstanding photochemical performance of the ZnO NRs. Electrochemical impedance spectroscopy (EIS) was also used to monitor the sensor changes. In Nyquist plot, a semicircle corresponds to the electron-transfer limited resistance and a linear part corresponds to the diffusion process at low frequencies. **Figure 5.23** show the Nyquist diagram of the different electrode in the presence of 0.1 M PBS. The EIS of FTO/ZnO NRs have almost the straight line, this indicates that how is a fast electron-transfer kinetics on the surface of the electrode modified ZnO NRs. However, with the polymer film onto the FTO surface, the electron transfer and diffusion process were observed. This result indicates that polymer had the larger obstruction effect, which led to the decrease of electron transfer rate or an increase of the resistance of the electron flow. The formation of cavities facilitates the access of BPS, and this results in the high photocurrent and current response of MIP/ZnO NRs. However, both NIP /ZnO NRs/FTO and MIP/ZnO NRs/FTO produced high photocurrent more than of the ZnO NRs/FTO electrode. This is due to the conjugation effect of PPy, which can accelerate the electron separation and injection process and thus enhance the photocurrent response (Kang *et al.* 2015).

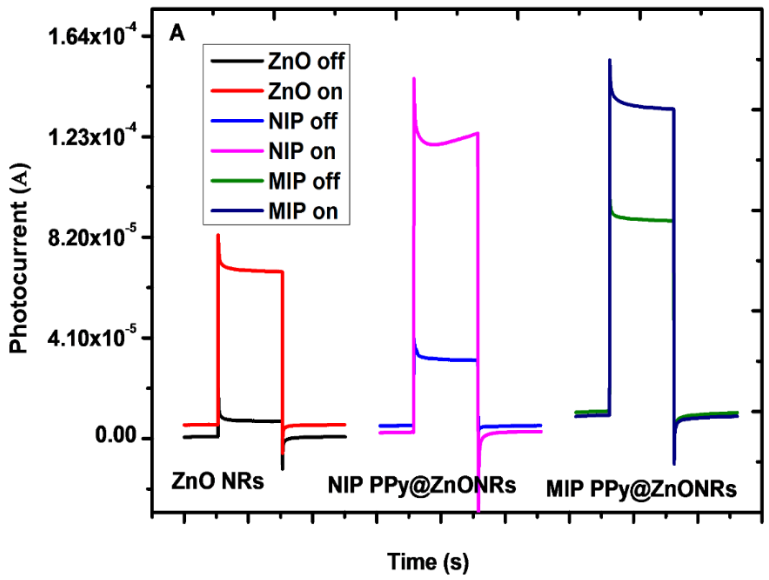

Figure 5.21 The photocurrent response of ZnO NRs, NIP/ZnO NRs and MIP/ZnO NRs in 0.1 M Na_2SO_4 solution.

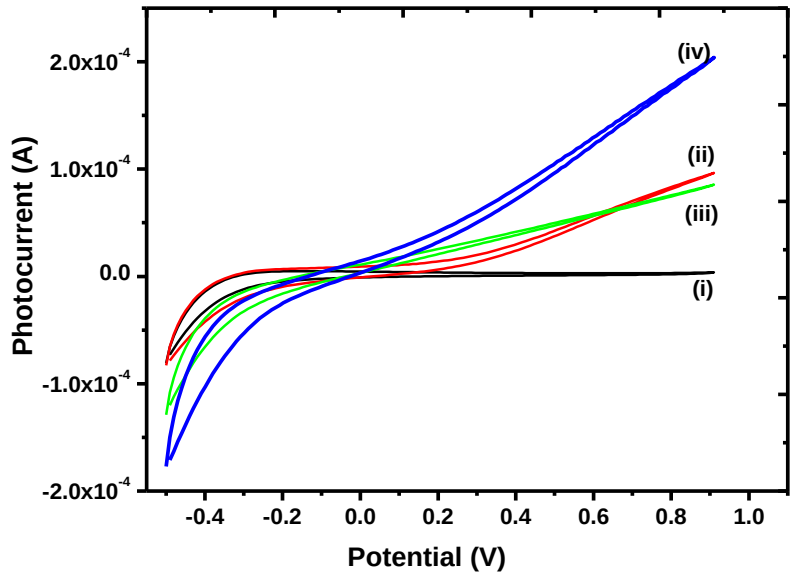

Figure 5.22 Cyclic voltamograms (i) NIP/ZnO NRs/FTO without UV illumination, (ii) NIP/ZnO NRs/FTO with UV illumination, (iii) MIP/ZnO NRs/FTO without UV illumination and (iv) MIP/ ZnO NRs/FTO with UV illumination.

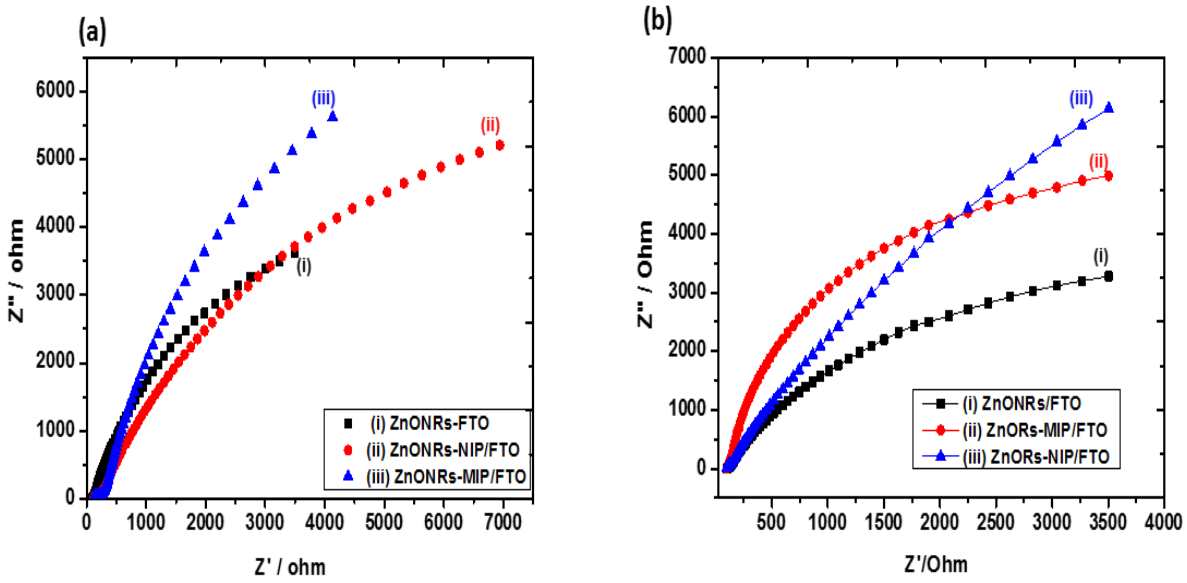

Figure 5.23 Nyquist plot of different electrodes in 0.1M PBS. (a) ZnO NRs/FTO (i), NIP/ZnO NRs/FTO (ii), MIP/ZnO NRs/FTO without UV illumination and (b) ZnO NRs/FTO (i), MIP ZnO NRs /FTO (ii), NIP/ZnO NRs/FTO with UV illumination.

5.1.3 Optimization of analytical parameters for Lac/Ag-ZnO NPs/MWCNTs/C-SPE

In order to fabricate a biosensor, laccase (Lac) was immobilized on the modified carbon screen printed electrode (C-SPE) with Ag-ZnO/MWCNTs. The final fabricated electrode was represented as Lac/Ag-ZnO/MWCNTs C-SPE. Numerous parameters such as pH, enzyme loading, temperature and deposition time were investigated because these parameters affect the analytical performances of the biosensor. In this study pH, scan rate, enzyme loading and deposition time were investigated and optimized by cyclic voltammetry measurements.

5.1.3.1 Effects of pH

The pH dependence of the laccase electrode was investigated between pH 3.0 and 10.0 in 0.1 M PBS in the presence of 0.5 mM BPA. The optimum current response was achieved at pH 6.0 as shown in **Figure 5.24**. These results are in good agreement with the reported study (Jaafar *et al.* 2007). Therefore, pH 6.0 was used for the entire experiments to obtain a maximum sensitivity.

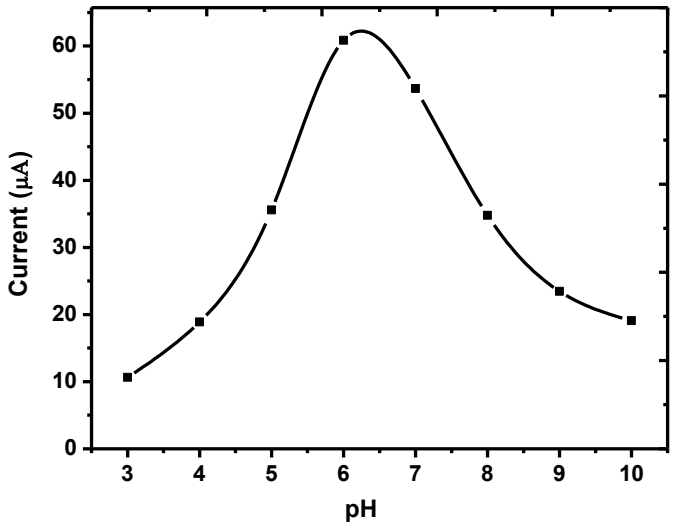

Figure 5.24 Effects of pH in 0.1 M PBS using Lac/Ag-ZnO/MWCNTs/C-SPE using 0.5 mM BPA.

5.1.3.2 **Effects of scan rates**

The relationship between the peak current and scan rate gives the valuable information that involves electrochemical mechanism. Hence, the effects of scan rate on the oxidation of BPA was studied using 0.5 mM BPA in PBS at pH 6.0, by monitoring the oxidation peak current. **Figure 5.25** (a) shows the cyclic voltammograms of 0.5 mM BPA at Lac/Ag-ZnO NPs/MWCNTs/C-SPE with different scan rates ranging from 0.01V.s^{-1} to 0.08 V.s^{-1}, the oxidation peak current increases with the increase of scan rate. The peak current of BPA increases linearly with the increase in the scan rate from 0.01V.s^{-1} to 0.08 V.s^{-1} as shown in **Figure 5.25** (b). This linear relationship confirms the adsorption of BPA onto the electrode surface. The linear relationship between a scan rate and oxidation peak current is confirmed by the regression equation y = 67.345x+0.41321 with the coefficient of R^2=0.9986. This indicates that the oxidation of BPA on the surface of the electrode is an adsorption-controlled process. The scan rate of 0.08 V. s^{-1} was chosen as the optimum. Literature reveals that the oxidation reaction of BPA involved two electron transfer (Xu *et al.* 2017). The possible reaction mechanisms for oxidation of BPA on the surface of the electrode is shown in **Scheme 5.1**.

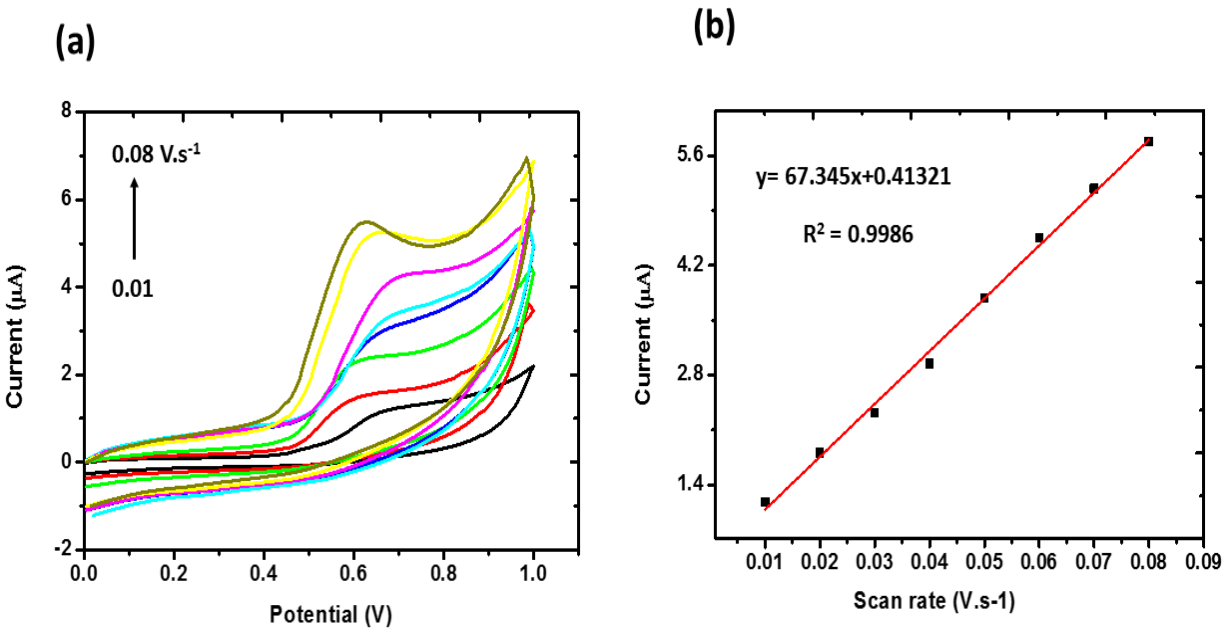

Figure 5.25 (a) Effects of scan rate from 0.01 to 0.08 $V.s^{-1}$ and (b) The relationship between scan rate and current on BPA.

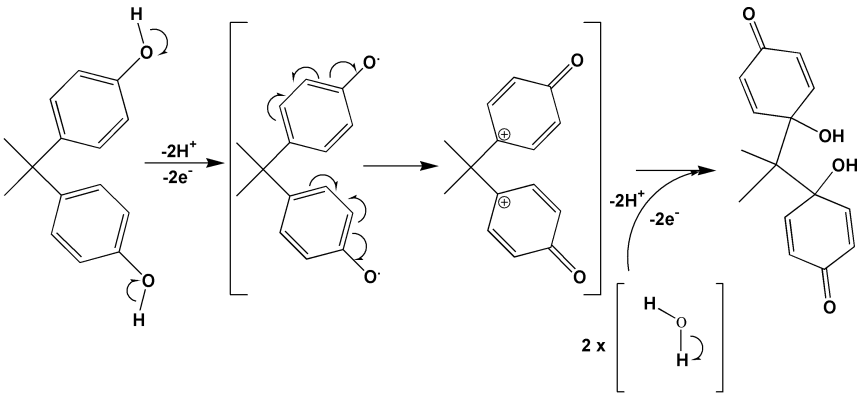

Scheme 5.1 Electrochemical oxidation reaction mechanism of BPA at Lac/Ag-ZnONPs/MWCNTs/C-SPE (Xu *et al.* 2017).

5.1.3.3 **Effects of deposition time**

The effects of deposition time were investigated in 0.5 mM BPA. **Figure 5.26** shows that the oxidation current increases gradually with the deposition time up to 25 s. The longer deposition time, the more BPA that is adsorbed onto the electrode surface. Beyond 25 s, the BPA oxidation peak current decreases due to the saturation of electrode surface with BPA. Deposition of 25 s was employed for the entire experiments.

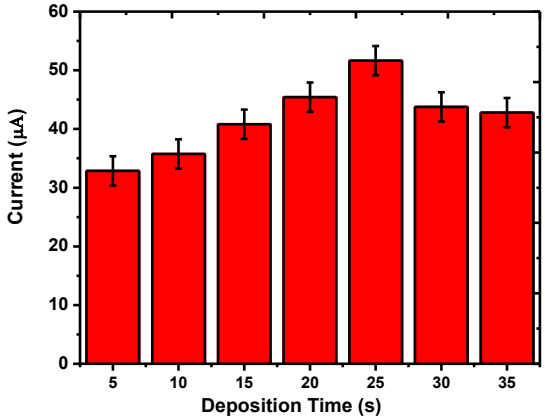

Figure 5.26 Effects of deposition time on the oxidation current in 0.5 mM BPA.

5.1.3.4 **Effect of enzyme loading**

The effects of the amount of the enzyme that was immobilized onto the surface of the electrode were investigated in order achieve a sensitive biosensor. Different concentration of enzyme from 1.0 to 7.0 mg mL^{-1} were prepared in 0.1 M phosphate buffer at pH 6.5 and the electrochemical response was then monitored as shown in **Figure 5.27**. The current increases until its reach the maximum value at 3.0 mg mL^{-1}, then the current decreases significant with the further increase of laccase. This is due to an increase in the film thickness and resulted in slow electron transfer due to interfacial electron transfer resistance (Yin *et al.* 2010). Therefore 3 mg mL^{-1} of laccase was immobilized onto the surface of the working electrode for the entire experiments and covered by glutaraldehyde as the cross linker.

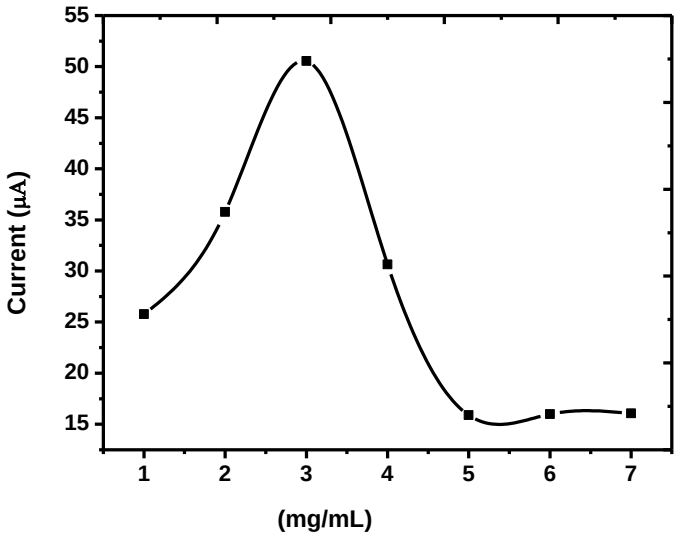

Figure 5.27 Effects of enzyme loading on the electrode.

5.1.4 Electrochemical behaviour of BPA at Lac/Ag-ZnO NPs/MWCNTs/C-SPE

5.1.4.1 Quantitative analysis of BPA

The current signal was investigated as a function of BPA concentration. **Figure 5.28** shows that the peak current increases with BPA concentration and thereafter current decreases at higher concentrations, due to higher amounts of phenoxy radicals. In this study the electrochemical responses of the electrode were measured as a function of the amount of BPA solutions (0.5, 0.99, 1.49, 1.99, 2.49, 2.99 µM) in 0.1 M PBS at pH 6.0. The oxidation peak current increases with the increase of BPA concentration up to 2.99 µM due to the increased electroactive species in a BPA solution. However, at high concentrations the peak current decreases, which suggests that the BPA is adsorbed on the electrode surface and there is a limited surface area on the electrode. This also confirms that the oxidation reaction is not limited by diffusion alone. The biosensor shows a linear concentration range of 0.5-2.99 µM with a correlation coefficient of 0.9943 and a low detection of limits of 0.08 µM. The LOD has been calculated as ratio signal/ noise (S/N) = 3. The LOD obtained is lower than the one reported in the literature by Portaccio and co-workers (Portaccio *et al.* 2013). A fabricated biosensor was used for quantitative analysis of real sample extracted from plastic water bottles. Two plastic bottles (sample I and II) from different commercial companies were collected and

extracted as described in section 4.1.8. The distinguishable peak of BPA was not found due to its low concentration of BPA in real samples. Then the samples were spiked with a known concentration of BPA in order to evaluate the accuracy of the biosensor. Three different concentrations of BPA were used for each sample, the obtained results are shown in **Table 5.1**. The recovery was between 89.3% and 111.1%, with the relative standard deviation (RSD) of 6 % for three consecutive measurements of the same sample.

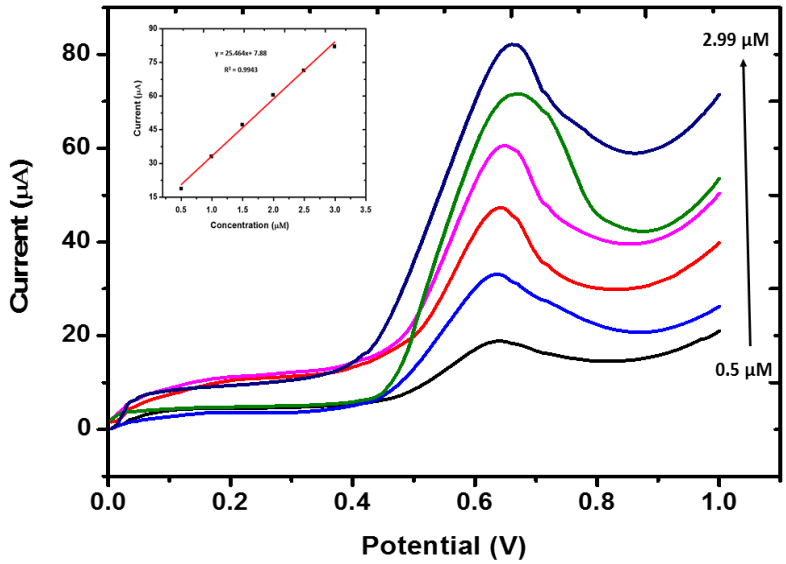

Figure 5.28 Biosensor response on BPA in 0.1 M PBS, pH 6.0, 3 mg/mL laccase. Insect: linear range of BPA response in the biosensor.

Table 5.1 Recovery studies of spiked plastic bottles.

Sample	BPA concentration added (µM)	BPA concentration found (µM)	Recovery (%)
Sample I	10	11.2	89.3
Sample I	20	19.0	105.3
Sample I	30	31.0	96.8
Sample II	10	9.0	111.1
Sample II	20	18.3	109.3
Sample II	30	28.7	104.5

5.1.4.2 Reproducibility and stability of Lac/Ag-ZnO NPs/MWCNTs/C-SPE

The reproducibility of Lac/Ag-ZnO NPs/MWCNTs/C-SPE was evaluated using same nanocomposites, but with different SPE's (carbon, platinum and gold) on the same day under the optimized parameters with 0.36 mM BPA (n = 6). A similar behavior was observed, but with lower currents. The Au-SPE had an outlier in the third measurement hence, the run was eliminated based on the Q-test. Overall relative standard deviation (%RSD) is in the order of Au-SPE>C-SPE>Pt-SPE, but the C-SPE with 0.86 % RSD chosen as the preferred electrode as it showed a much better current response in contrast to Au-SPE.

The stability of the Lac/Ag-ZnO NPs/MWCNTs/C-SPE was evaluated for five consecutive days using DPV. After using the Lac/Ag-ZnO NPs/MWCNTs/C-SPE for the determination of BPA on the first day, it was stored in the refrigerator set at 4 ^{o}C without rinsing for second day use. This process was repeated for five consecutive days. The experimental results show that there is a very small variation in the peak currents (30 %) at the end of the 5th day with % RSD of 0.595. The obtained results suggested that the electrochemical biosensor may be used for multiple analysis although it was designed for a single disposable electrode to make the method more economical.

5.1.4.3 Interferences study, effect of cleaning solvent

The interference of foreign species on the detection of BPA was evaluated by using a different concentration of metal ions (Cu^{2+}, Fe^{3+}, Bi^{3+}, Cd^{2+} and K^{+}) and other phenolic compounds (catechol, 4-aminophenol, 2-nitrophenol, phenol and 4,4-sulfonyldiphenol). The analytical data from this study reveals that 15.5% variation in the peak current was observed, indicating

an insignificant interference and thus enhancing the selectivity of Lac/Ag-ZnO NPs/MWCNTs/C-SPE for the detection of BPA in real samples.

Different organic solvents namely acetone, acetic acid, ethanol, deionized water and dimethylformamide (DMF) were checked for effectiveness in removing the analyte while retaining the nanocomposite modified onto the electrode surface. Among these solvents, acetone was the best solvent to rinse the electrode based on the current response which increases from 5.32 to 26.67 µA in comparison to deionized water and DMF as shown on **Figure 5.29**.

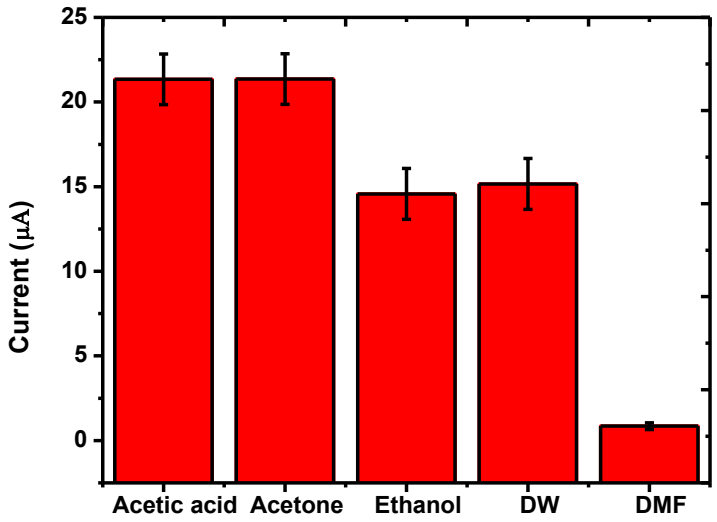

Figure 5.29 Effect of rinsing solvents on current signal between the runs of one modification.

5.1.5 Evaluation and analytical performance of the MIP/ZnO NRs/FTO

5.1.5.1 The linearity and sensitivity of the photo electrochemical sensor

The amperometric response of MIP against NIP in BPS sensing signify the successful imprinting of the polymer film. Both sensors MIP and NIP were exposed to different concentrations of BPS ranging from 2.5 to 12.5 µM. The change in the photocurrent at each concentration as shown in **Figure 5.30**. When MIP was exposed to different concentration of BPS, photocurrent increase linearly with increasing concentration of BPS. This shows that the template for BPS molecule was able to penetrate and bind with the cavities present within the imprinted polymer. However, NIP did not show any change in photocurrent response. This shows that NIP was not permitting BPS molecules to pass through due to the lack of cavities.

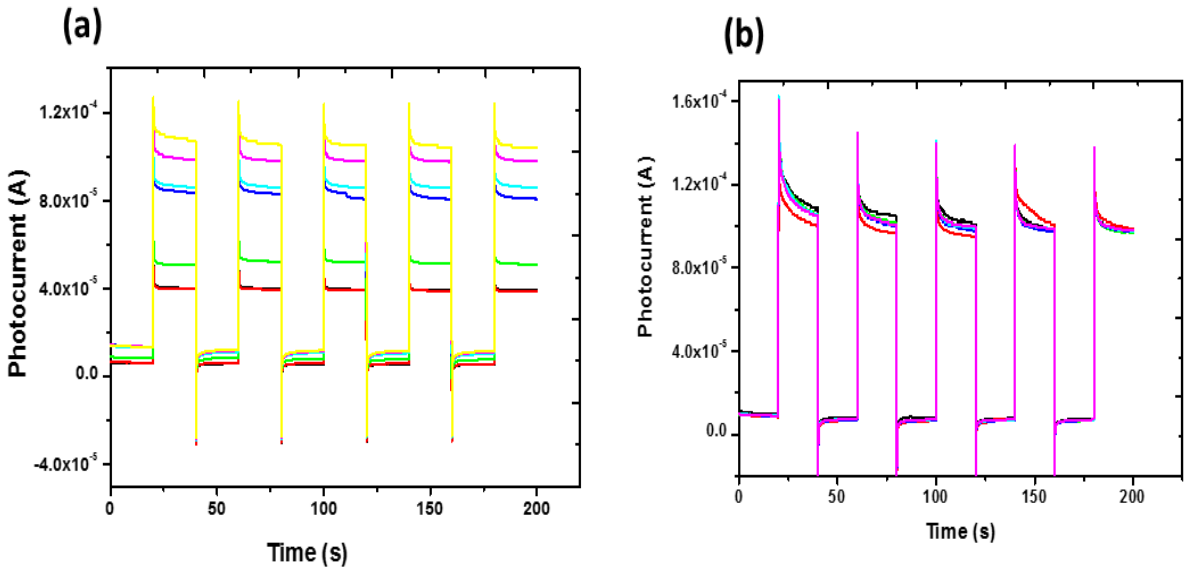

Figure 5.30 Amperometric response of (a) imprinted (MIP) and (b) non imprinted to BPS.

The amperometric method was used to quantitatively detect BPS in standard solutions. The analytical performance of the sensor was evaluated by measuring the photocurrent response of the as prepared MIP/ZnO NRs/FTO in BPS solution containing different concentration. The photocurrent increased gradually with the increasing BPS concentration ranging from 2.5 to 12.5 µM with a coefficient of R^2 = 0.989 as shown in **Figure 5.31**.The detection limit was calculated to be 0.7 µM based on 3σ/slope (σ, the standard deviation of the blank samples). This proposed sensor was then compared to other MIP sensors that have been reported in the literature as presented in **Table 5.2**.

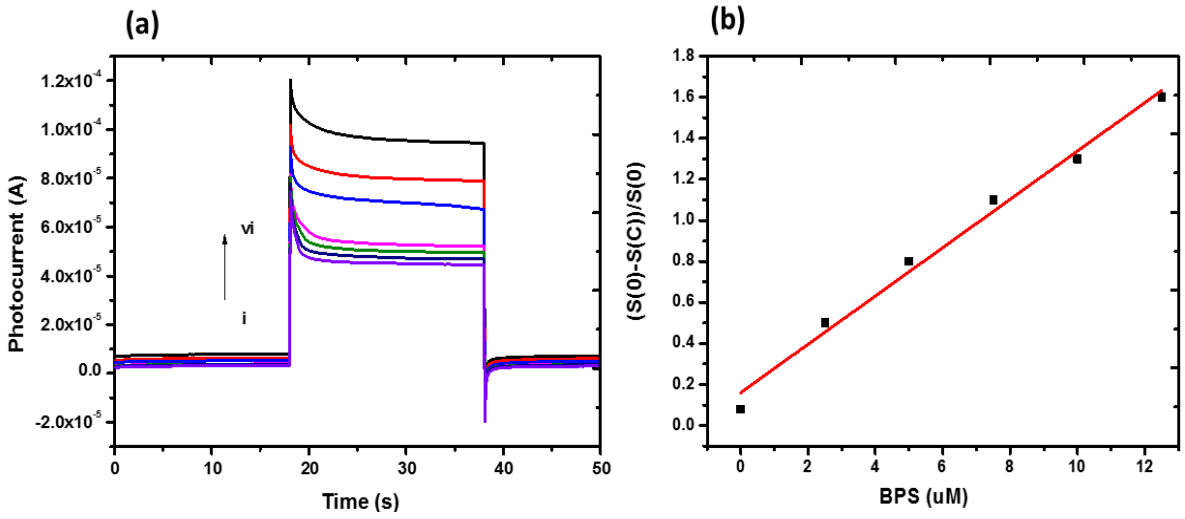

Figure 5.31 (a) Photocurrent response of the sensor in the presence of BPS with different concentrations (from i to vi: 2.5 to 12.5 µM). (b) Linear relationship plot between photocurrent and BPS concentration.

Table 5.2 Comparison of sensors based on molecularly imprinted polymers.

Method	LOD	Linear range	Reference
PEC	0.7 µM	2.5-12.5 µM	This work
EIS	0.42 mM	0 - 12 mM	(Apodaca *et al.* 2011)
SERS	0.53 µM	2.19 - 99.86 µM	(Xue *et al.* 2013)

5.1.5.2 **Reproducibility, repeatability, selectivity and application studies**

Selectivity, reproducibility and repeatability of the electrode are the key elements of the sensor. The reproducibility of MIP/ZnO NRs/FTO was investigated using four different electrodes prepared in the same conditions in the presence of 0.01 mM BPS in PBS (0.1 M). The relative standard deviation (RSD) was found to be 5.03 %, these results demonstrated that the prepared sensor has a good reproducibility. The repeatability of the sensor was investigated in 0.1 M PBS, the results revealed that the photocurrent response remained steady after 15 uninterrupted measurements with a relative standard deviation of 3.1%, as demonstrated in **Figure 5.32**.

To evaluate the selectivity of the sensor, organic molecules that have similar structures to BPS were investigated to see if they may interfere with the developed sensor. Photocurrent measurement was carried out in the presence of three phenolic compounds including 2-

nitropheno, bisphenol C (BPC), catechol and phenol (see **Figure 5.33** (a)). The amperometric technique was used to investigate the photocurrent of different phenolic compounds. **Figure 5.33** (b) shows that even when the sensor is exposed to 100 times excess of these phenolic compounds (0.01 mM versus 100 mM), the photocurrent response was extensively lower than of BPS. This shows that the PEC sensor has outstanding selectivity capacity towards BPS, this is due to the specific recognition surface of MIPs that are provided by the exclusive nanostructured ZnO NRs. On the other hand, it increases the hydrophilicity and enhanced the adsorption capacity of the MIP/ZnO NRs/FTO. The molecularly imprinted technique plays a significant part in the molecular recognition capacity of the PEC sensor. The formation of a hydrogen bond with BPs and copolymerized was achieved by using PPy as the monomer and BPS as the template. The imprinted cavities were formed after the removal of BPS template, and thus left distinct recognition sites in which only BPS can interact with the MIP/ZnO NRs. This distinct recognition sites can differentiate BPS from other phenolic compounds by molecular shape identification and functional group distribution, and interacts with BPS selectively by hydrogen bonds interaction. Then BPS was selectively adsorbed onto the surface of the sensor, while other phenolic compounds remained in the solution because they are not complementary with the cavities formed. The stability of the electrode was also investigated in the electrode that has been stored for a month, the photocurrent decrease with less than 6%. These experiments confirm a good stability, reproducibility and repeatability of the sensor towards BPS. The combination of PPy and ZnO NRs enhanced the sensitivity and the stability of the sensor. This is not only due to the cross-linked structure of PPy that is formed during photo polymerization, but also the stimulation of π bond of PPy that support the separation of photogenerated of ZnO NRs and this improve the stability of photo catalysis performance.

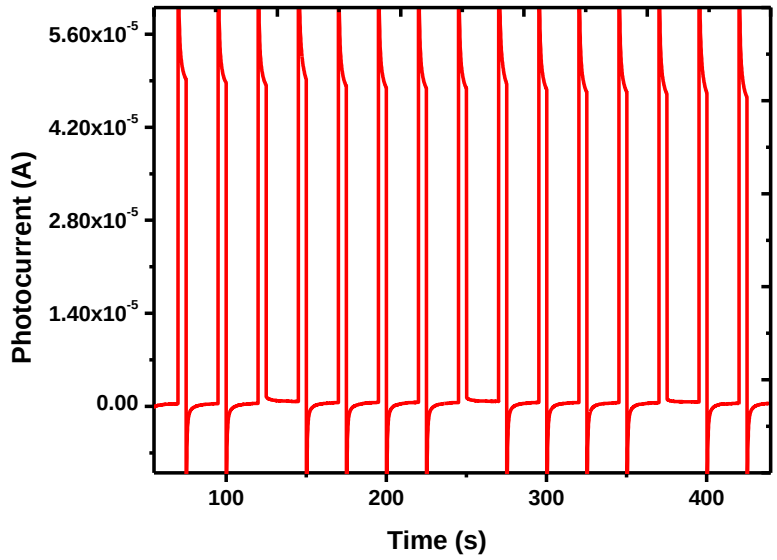

Figure 5.32 The photocurrent stability of the MIP/ZnO NRs/FTO sensor in 0.1 M PBS (n=15).

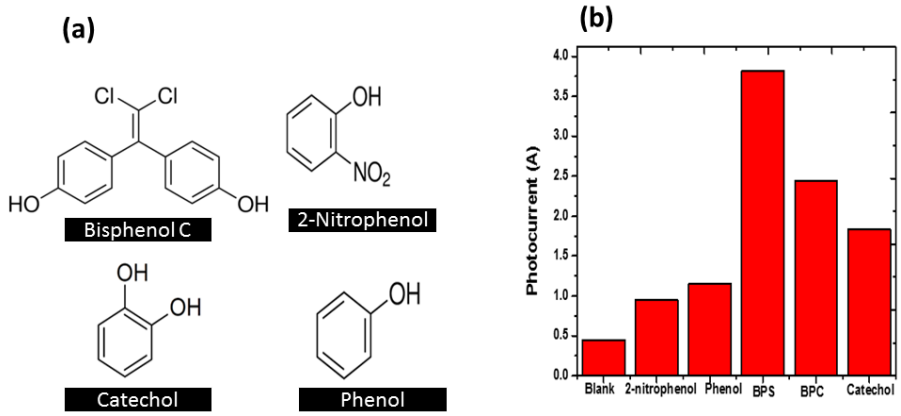

Figure 5.33 Molecular Structures of some phenolic compounds (a) and (b) Photocurrent ratio of MIP/ZnO NRs in 0.1M PBS containing different phenolic compounds.

5.2 Computational Studies

5.2.1 Calculated band gap and Raman vibrational modes using Density functional theory

The density functional theory DFT is commonly employed to calculate the atomic or molecular properties through solving the Schrodinger equations at the ground-state level. Instead of dealing with the many-body wave function $\Psi\ (r_1 \ldots\ldots, r_N)$, DFT leads to the direct calculation of the simplest electronic properties of atom or molecule, i.e. the electronic density. Since 1980, DFT has been established as one of the main tools for calculating the properties of solid state physics and molecules (Fiolhais, Nogueira and Marques 2003). For the metal oxide system, DFT has been widely used to observe not only the electronic properties but also vibrational frequencies of either pure or modified ZnO (Calzolari and Nardelli 2013). Herein, DFT calculations have been performed to validate the experimental band gap and Raman spectra. The use of LDA-PWC functionals opted to reproduce the accurate parameters in concordance with the existing experiment as well as previous studies (Srikant and Clarke 1998; Calzolari and Nardelli 2013). In this work, the experimental band gap (ΔE_g^{exp}) of ZnO single crystals were observed at 3.13 eV, similar to results previously reported by Srikant and Clarke (Srikant and Clarke 1998). The numerical based-DFT using LDA-PWC exhibited an underestimated band gap (ΔE_g^{DFT}) of 2.065 eV which corresponds to the common evidence of a standard DFT calculations. This may be due to an unphysical augmentation of the covalent character of the Zn-O bonds, instead of the lack of many-body corrections typical of DFT (Vogel*, et al.* 1996). The scissor operator was accordingly applied to evaluate the band gap discrepancy (Segall *et al.* 2002). The scissor operator attempts to correct the ZnO band gap *via* conducting the clear separation between valence and conduction bands shown in **Figure 5.34**. Herein, the scissor operator was set at 1.065 eV accounting for the difference between experimental (3.13 eV) and the calculated band gap energy values. Upon the application of scissor operator, the band gap of the nanocluster was significantly improved resulting in a value of 3.13 eV, in accordance with the experimental value. Hence, the calculated band gap is able to validate the experimental gap and further confirming semiconducting nature of the ZnO.

Due to its π-conjugated structure, polypyrrole has attracted great interest as a conductive polymer, which was emerged herein to improve the electrode capacity of the ZnO. The polymer PPy, exhibits highest band gap i.e. 3.500 eV which is highly comparable with the previous theoretical study (Ullah 2017).Whilst, functionalization of polypyrrole into the ZnO

nanocluster decreases the energy gap, from 2.067 eV to 1.285 eV (**Figure 5.35**). The lower band gap energy indicates higher reactivity of the functionalized system that enhances the electron's mobility in generating the electron transitions from a lower to higher orbitals (valence to conductance gap), thus producing more conductivity to the entire system, resulting in more redox reactions to occur. This result is in accordance with the trend of the experimental band gap and Electrochemical Impedance Spectroscopy (EIS) spectra, explaining the reduced charge transfer resistance owing to the PPy electrodeposited within the electrode system.

Raman spectroscopy is a commonly used technique to characterize the crystal structure of the oxidized materials including its defects and disorders, based on the emission or absorption of phonons (Saito *et al.* 2011). The calculated spectra of ZnO NRs are compared to the experiment in **Figure 5.36**, displaying a polarized Raman Spectra of ZnO and the active modes obtained at room temperature. There are four important peaks observed at around 100 cm^{-1}, 330 cm^{-1}, 437 cm^{-1}, and 580 cm^{-1}. The intense peak found around 100 cm^{-1} was assigned as the low frequency of E_2 (low) peak, commonly defining the Zn motion (**Figure 5.36 (I)**). The second peak observed at 332 cm^{-1} was attributed to the second order scattering of E_2 (high)-E_2 (low) mode (**Figure 5.36 (II)**). At around 450 cm^{-1}, a weak band was identified and indicated as the E_2 (high) of ZnO which corresponds to the wurtzite characteristic of the ZnO structure (**Figure 5.36 (III)**). As opposed to the experimental spectra, this band was found decrease, possibly correlated to the fluctuation effect of the nanocluster disorder upon structural optimization, accordingly. The next peak observed at around 581 cm^{-1} reflected the E_1 longitudinal optical (Fiolhais, Nogueira and Marques 2003) of the pure hexagonal ZnO (**Figure 5.36 (III)**), characterizing the intrinsic defects occurred on the ZnO crystal. Overall, these obtained theoretical Raman results are found in good agreement with those investigated in the experimental study.

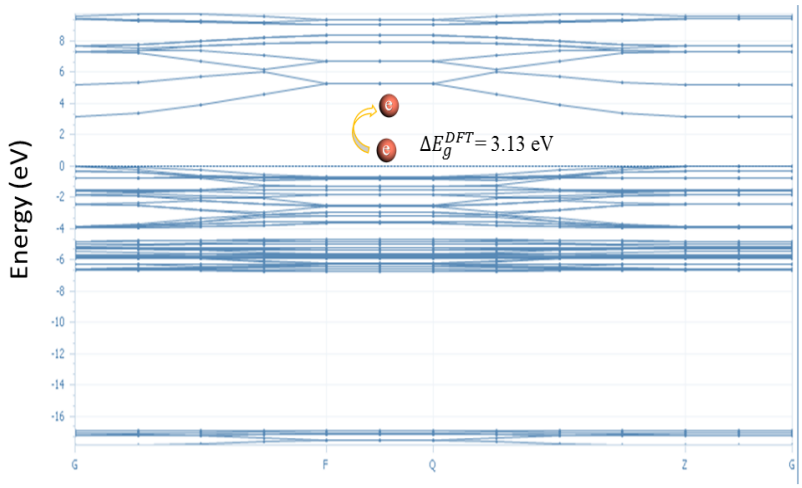

Figure 5.34 Band structure of ZnO NRs depicting the calculated band gap using LDA-PWC level of theory.

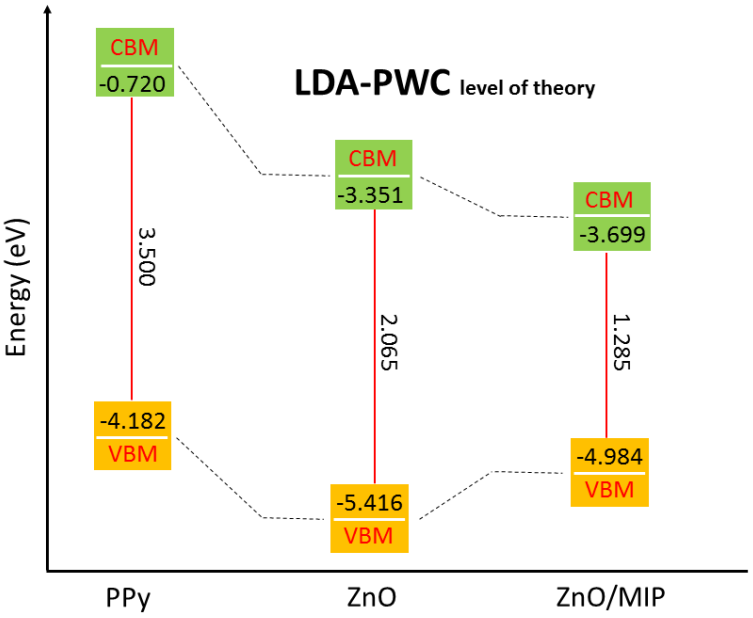

Figure 5.35 Energy band gaps of PPy, pure ZnO NRs, and MIP/ ZnO NRs.

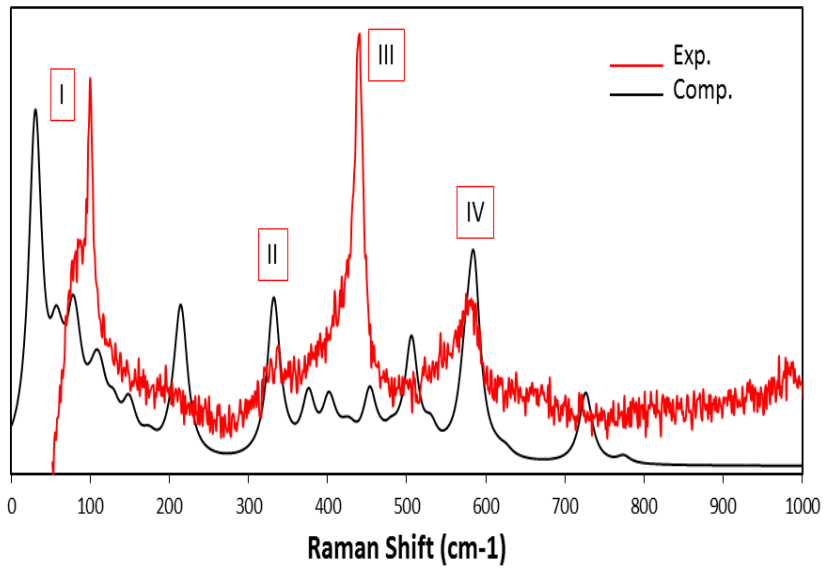

Figure 5.36 Experimental and calculated Raman spectra of ZnO NRs.

5.2.2 Optical UV-visible and IR properties

Quantum chemical calculations were carried out to further investigate the optical UV-visible followed by IR spectra. The similar basis set has been used to determine the first three low-lying excited states for observing the UV-visible absorption spectra of the native and modified ZnO (i.e. ZnO/PPy). The calculated results comprising of the oscillator strength, foremost contributions, and wavelength were generated and further compared to the native ZnO and polymerized system. The UV-visible absorption spectra derived from the computational prediction are shown in **Figure 5.37.** The broad absorption spectra at 398 nm and 454 nm are attributed to the interaction of ZnO and PPy (ZnO-PPy). This finding is comparable with the reference signature bands of ZnO-PPy at 379 nm and 415 nm (Shiigi *et al.* 2002; Joshi *et al.* 2009). The discrepancy is reasonable since the UV-visible spectra of the reference were derived from the experiment while our results were obtained from the theoretical calculations. Moreover, the peaks due to the formation of ZnO-PPy are shifted from 468 nm (native ZnO) to 454 nm (ZnO-PPy), suggesting a poor conjugation leading to the decrease of the computational band gap (**Figure 5.35**).

Further, the FT-IR spectra of the pure polypyrrole were computationally observed at several points (**Figure 5.38**) and compared with previous reports (Huang *et al.* 2014). The C=C and C-C bonds of PPy were observed at 1533.43 cm^{-1} and 1216.43 cm^{-1} respectively whereas, the others represented the pyrrole conjuctions (at 1433.76 cm^{-1}, 1172.76 cm^{-1}, and 1061.09 cm^{-1}).

The presence of peaks observed at 1164.26 cm^{-1} and 1122.60 cm^{-1} is due to the chemical interaction in the complex of ZnO and PPy, which are absent in pure ZnO.. Overall, these IR investigations pinpoint the chemical mechanism between the ZnO and PPy occurring at 1164.26 cm^{-1} and 1122.60 cm^{-1}, which are attributed to the atomic interactions delivering the greater impact of radicals throughout the polymerization process (Moghaddam *et al.* 2009).

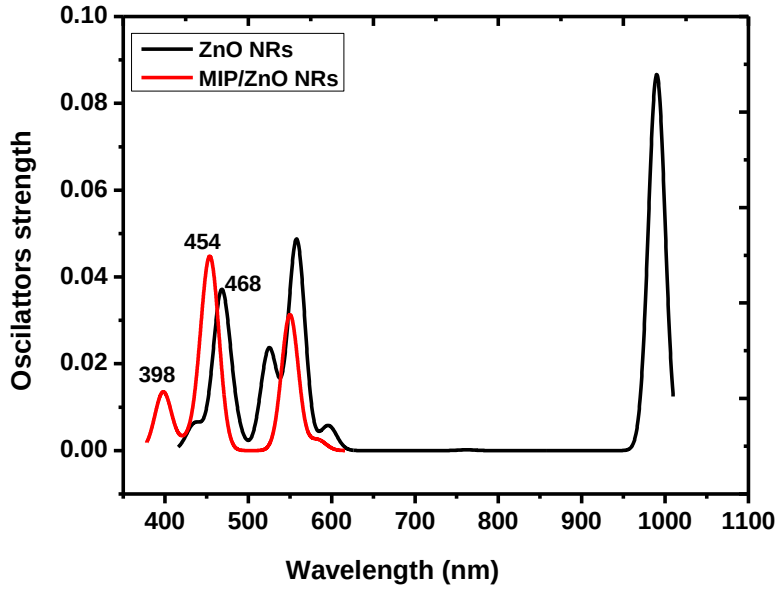

Figure 5.37 Calculated UV-Vis spectra of ZnO NRs and MIP/ZnO NRs.

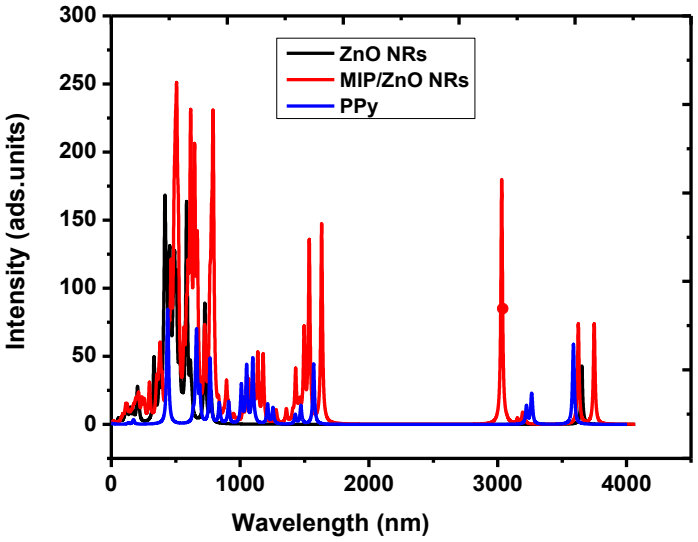

Figure 5.38 Calculated IR spectra of ZnO NRs, MIP/ZnO NRs, and PPy.

CHAPTER 6

CONCLUSION AND RECOMMENDATIONS

6.1 Concluding Remarks

The aim of this research was to develop a novel biosensor for the determination of phenolic compounds such as bisphenol A (BPA) and bisphenol S (BPS).

In summary, the electrochemical biosensor for the detection of phenolic compounds, BPA and BPS were successfully characterized using electrochemical, photo electrochemical, optical and morphological methods. This study was carried out in two stages:

The first approach of study involved the development of a biosensor for the detection of BPA by anchoring laccase enzyme onto Ag-ZnO NPs/MWCNTs nanocomposite. The fabricated electrochemical biosensor possessed high sensitivity for the determination of BPA. Under the optimised parameters the wide linear range (0.5 to 2.99 µM) with a low detection limit of 0.08 µM for the detection of BPA was obtained. The determination of BPA in real samples of plastic water bottles showed satisfactory recoveries ranging from 89.3% to 111.1 %. Results revealed that the bare electrode have a low current compared to the modified electrode. The electrodes modified with the MWCNTs and Ag-ZnO NPs composite and with the laccase enzyme showed well-defined and higher peak currents. This is due to the greater surface area and electrical conductivity provided, suggesting greater catalytic activity of silver doped zinc oxide/MWCNTs nanocomposite with the enzyme.

The second approach of this work involved the development of a novel and selective photo electrochemical (PEC) sensor to detect BPS based on the vertically aligned ZnO NRs (ZnO NRs), synthesized using a molecularly imprinted polymer for the first time. A highly sensitive PEC sensor for BPS attained a dynamic linear range from 2.5 to 12.5 µM with a low limit of detection of 0.7 µM. The proposed sensor exhibited excellent selectivity towards BPS. Moreover, 100-fold concentration of BPS analogues did not show any interference with phenolic compounds. Weak currents were observed on the electrode modified with ZnO NRs but when PPy was introduced onto the electrode, the current increased drastically. This is due to the photo catalytical characteristics and large surface area of ZnO NRs and electrical conductivity of PPy. The non-imprinted polymer did not show any sensitivity towards BPS,

due to lack of cavities towards BPS. However, MIP showed a good sensitivity towards BPS because of its cavities.

Characterization techniques such as SEM, photoluminescence (PL), Raman spectroscopy and X-RD shows that PPy modification does not alter the shape and the morphology of ZnO NRs. SEM images revealed that the synthesized ZnO NRs are vertically-aligned, this increase the specific surface area for PPy.

6.2 Recommendations for Further work

The further works could be directed toward experimental characterization of tunable surface at different temperatures as well as in conducting the interference study using real biological samples with the photo electrochemical biosensor. For this purpose, more advanced computational methods involving molecular docking and molecular dynamics simulations could be implemented for a better understanding of the sensitivity, reproducibility and selectivity of the developed biosensor.

REFERENCES

Abdullah, J., Ahmad, M., Karuppiah, N., Heng, L. Y. and Sidek, H. 2006. Immobilization of tyrosinase in chitosan film for an optical detection of phenol. *Sensors and Actuators B: Chemical*, 114 (2): 604-609.

Adhikari, B. and Majumdar, S. 2004. Polymers in sensor applications. *Progress in polymer science*, 29 (7): 699-766.

Adschiri, T., Hakuta, Y. and Arai, K. 2000. Hydrothermal synthesis of metal oxide fine particles at supercritical conditions. *Industrial & engineering chemistry research*, 39 (12): 4901-4907.

Agrawal, R. and Espinosa, H. D. 2011. Giant piezoelectric size effects in zinc oxide and gallium nitride nanowires. A first principles investigation. *Nano Letters*, 11 (2): 786-790.

Ahuja, T. and Kumar, D. 2009. Recent progress in the development of nano-structured conducting polymers/nanocomposites for sensor applications. *Sensors and Actuators B: Chemical*, 136 (1): 275-286.

Al-Bat'hi, S. A. 2015. Electrodeposition of Nanostructure Materials. In: *Electroplating of Nanostructures*. InTech, DOI: 10.5772/61389

Alimanesh, M., Hassan, Z. and Zainal, N. 2017. Electrochemical growth of controlled tip shapes of ZnO nanorod arrays on silicon substrate and enhanced photoluminescence emission from nanopyramid arrays compared with flat-head nanorods. *Optical Materials*, 72 (Supplement C): 276-282.

Alkasir, R. S. J., Ganesana, M., Won, Y.-H., Stanciu, L. and Andreescu, S. 2010. Enzyme functionalized nanoparticles for electrochemical biosensors: A comparative study with applications for the detection of bisphenol A. *Biosensors and Bioelectronics*, 26 (1): 43-49.

Almansa, E., Kandelbauer, A., Pereira, L., Cavaco-Paulo, A. and Guebitz, G. M. 2004. Influence of structure on dye degradation with laccase mediator systems. *Biocatalysis and Biotransformation*, 22 (5-6): 315-324.

Amin, G., Sandberg, M., Zainelabdin, A., Zaman, S., Nur, O. and Willander, M. 2012. Scale-up synthesis of ZnO nanorods for printing inexpensive ZnO/polymer white light-emitting diode. *Journal of Materials Science*, 47 (11): 4726-4731.

Angelopoulos, M. 2001. Conducting polymers in microelectronics. *IBM Journal of Research and Development*, 45 (1): 57-75.

Anh, T. M., Dzyadevych, S. V., Van, M. C., Renault, N. J., Duc, C. N. and Chovelon, J.-M. 2004. Conductometric tyrosinase biosensor for the detection of diuron, atrazine and its main metabolites. *Talanta*, 63 (2): 365-370.

Apodaca, D. C., Pernites, R. B., Ponnapati, R., Del Mundo, F. R. and Advincula, R. C. 2011. Electropolymerized molecularly imprinted polymer film: EIS sensing of bisphenol A. *Macromolecules*, 44 (17): 6669-6682.

Arıca, M. Y., Altıntas, B. and Bayramoğlu, G. 2009. Immobilization of laccase onto spacer-arm attached non-porous poly(GMA/EGDMA) beads: Application for textile dye degradation. *Bioresource Technology*, 100 (2): 665-669.

Arora, D. S. and Sharma, R. K. 2010. Ligninolytic fungal laccases and their biotechnological applications. *Applied biochemistry and biotechnology*, 160 (6): 1760-1788.

Arribas, A. S., Martínez-Fernández, M. and Chicharro, M. 2012. The role of electroanalytical techniques in analysis of polyphenols in wine. *TrAC Trends in Analytical Chemistry*, 34: 78-96.

Ates, M., Karazehir, T. and Sezai Sarac, A. 2012. Conducting polymers and their applications. *Current Physical Chemistry*, 2 (3): 224-240.

B Djurisic, A., Y Chen, X. and H Leung, Y. 2012. Recent progress in hydrothermal synthesis of zinc oxide nanomaterials. *Recent patents on nanotechnology*, 6 (2): 124-134.

Bagheri, H. and Saraji, M. 2001. New polymeric sorbent for the solid-phase extraction of chlorophenols from water samples followed by gas chromatography–electron-capture detection. *Journal of Chromatography A*, 910 (1): 87-93.

Banerjee, D., Lao, J., Wang, D., Huang, J., Ren, Z., Steeves, D., Kimball, B. and Sennett, M. 2003. Large-quantity free-standing ZnO nanowires. *Applied Physics Letters*, 83 (10): 2061-2063.

Baruwati, B., Kumar, D. K. and Manorama, S. V. 2006. Hydrothermal synthesis of highly crystalline ZnO nanoparticles: A competitive sensor for LPG and EtOH. *Sensors and Actuators B: Chemical*, 119 (2): 676-682.

Belický, Š., Katrlík, J. and Tkáč, J. 2016. Glycan and lectin biosensors. *Essays in biochemistry*, 60 (1): 37-47.

Benedek, N., Snook, I., Latham, K. and Yarovsky, I. 2005. Application of numerical basis sets to hydrogen bonded systems: a density functional theory study. *The Journal of chemical physics*, 122 (14): doi.org/10.1063/1061.1876152.

Bernal, A. J. and Jirtle, R. L. 2010. Epigenomic disruption: the effects of early developmental exposures. *Birth defects research Part A: Clinical and molecular teratology*, 88 (10): 938-944.

Bhakat, C. and Singh, P. P. 2012. Zinc Oxide Nanorods: Synthesis and Its Applications in Solar Cell. *International Journal of Modern Engineering Research*, 2: 2452-2454.

BIOVIA, D. 2016. *Material Studio Modelling*: San Diego: Dassault Systemes.

Bisetty, K., Sabela, M., Khulu, S., Xhakaza, M. and Ramsarup, L. 2011. Multivariate optimization of voltammetric parameters for the determination of total polyphenolic content in wine samples using an immobilized biosensor. *International Journal of Electrochemical Science*, 6: 3631-3643.

Bonefeld-Jørgensen, E. C., Long, M., Hofmeister, M. V. and Vinggaard, A. M. 2007. Endocrine-disrupting potential of bisphenol A, bisphenol A dimethacrylate, 4-n-nonylphenol, and 4-n-octylphenol in vitro: new data and a brief review. *Environmental health perspectives*, 115 (Suppl 1): 69.

Botello-Méndez, A. R., Martínez-Martínez, M. T., López-Urías, F., Terrones, M. and Terrones, H. 2007. Metallic edges in zinc oxide nanoribbons. *Chemical Physics Letters*, 448 (4): 258-263.

Brena, B., González-Pombo, P. and Batista-Viera, F. 2013. Immobilization of enzymes: a literature survey. In: *Immobilization of Enzymes and Cells: Third Edition*. 15-31.

Buzea, C., Pacheco, I. I. and Robbie, K. 2007. Nanomaterials and nanoparticles: Sources and toxicity. *Biointerphases*, 2 (4): MR17-MR71.

Cajthaml, T., Křesinová, Z., Svobodová, K. and Möder, M. 2009. Biodegradation of endocrine-disrupting compounds and suppression of estrogenic activity by ligninolytic fungi. *Chemosphere*, 75 (6): 745-750.

Calzolari, A. and Nardelli, M. B. 2013. Dielectric properties and Raman spectra of ZnO from a first principles finite-differences/finite-fields approach. *Scientific Reports*, 3: DOI: 10.1038/srep02999.

Cao, G., Zhuang, Y. and Liu, B. 2014. Simultaneous determination of bisphenol A and bisphenol S in environmental water using ratio derivative ultraviolet spectrometry. *South African Journal of Chemistry*, 67 (1): 99-103.

Cembrero, J., Elmanouni, A., Hartiti, B., , M., M. and , M., amp, x and B. 2004. Nanocolumnar ZnO films for photovoltaic applications. *Thin Solid Films*, 451–452: 198-202.

Chauhan, N. and Pundir, C. S. 2011. An amperometric biosensor based on acetylcholinesterase immobilized onto iron oxide nanoparticles/multi-walled carbon nanotubes modified gold electrode for measurement of organophosphorus insecticides. *Analytica Chimica Acta*, 701 (1): 66-74.

Chawla, S., Rawal, R., Sharma, S. and Pundir, C. S. 2012. An amperometric biosensor based on laccase immobilized onto nickel nanoparticles/carboxylated multiwalled carbon nanotubes/polyaniline modified gold electrode for determination of phenolic content in fruit juices. *Biochemical engineering journal*, 68: 76-84.

Chen, D., Jiao, X. and Cheng, G. 1999. Hydrothermal synthesis of zinc oxide powders with different morphologies. *Solid State Communications*, 113 (6): 363-366.

Chen, Y., Tuan, N., Segawa, Y., Ko, H.-j., Hong, S.-k. and Yao, T. 2001. Stimulated emission and optical gain in ZnO epilayers grown by plasma-assisted molecular-beam epitaxy with buffers. *Applied Physics Letters*, 78 (11): 1469-1471.

Cheynier, V., Tomas-Barberan, F. A. and Yoshida, K. 2015. Polyphenols: from plants to a variety of food and nonfood uses. *Journal of Agricultural and Food Chemistry*, 63 (35): 7589-7594.

Chiu, W. S., Khiew, P. S., Cloke, M., Isa, D., Tan, T. K., Radiman, S., Abd-Shukor, R., Hamid, M. A. A., Huang, N. M., Lim, H. N. and Chia, C. H. 2010. Photocatalytic study of two-dimensional ZnO nanopellets in the decomposition of methylene blue. *Chemical Engineering Journal*, 158 (2): 345-352.

Ciosek, P. and Wróblewski, W. 2011. Potentiometric electronic tongues for foodstuff and biosample recognition—An overview. *Sensors*, 11 (5): 4688-4701.

COŞKUN, C., GÜNEY, H., GÜR, E. and and TÜZEMEN, S. 2009. Effective annealing of ZnO thin films grown by electrochemical deposition technique. *Turkish Journal of Physics*, 33 (1): 49-56.

Cremer, D. and He, Z. 1996. Sixth-Order Møller− Plesset Perturbation Theory On the Convergence of the MP n Series. *The Journal of Physical Chemistry*, 100 (15): 6173-6188.

de Rijke, E., Out, P., Niessen, W. M. A., Ariese, F., Gooijer, C. and Brinkman, U. A. T. 2006. Analytical separation and detection methods for flavonoids. *Journal of Chromatography A*, 1112 (1): 31-63.

Delley, B. 2000. From molecules to solids with the DMol 3 approach. *The Journal of chemical physics*, 113 (18): 7756-7764.

Di Fusco, M., Tortolini, C., Deriu, D. and Mazzei, F. 2010. Laccase-based biosensor for the determination of polyphenol index in wine. *Talanta*, 81 (1): 235-240.

Dick, K. A., Deppert, K., Larsson, M. W., Mårtensson, T., Seifert, W., Wallenberg, L. R. and Samuelson, L. 2004. Synthesis of branched'nanotrees' by controlled seeding of multiple branching events. *Nature materials*, 3 (6): 380-384.

Ding, Y., Ayon, A. and García, C. D. 2007. Electrochemical detection of phenolic compounds using cylindrical carbon-ink electrodes and microchip capillary electrophoresis. *Analytica Chimica Acta*, 584 (2): 244-251.

Dreizler, R. M. and da Providencia, J. 2013. *Density functional methods in physics*. Springer Science & Business Media.

Durán, N., Rosa, M. A., D'Annibale, A. and Gianfreda, L. 2002. Applications of laccases and tyrosinases (phenoloxidases) immobilized on different supports: a review. *Enzyme and microbial technology*, 31 (7): 907-931.

Eladak, S., Grisin, T., Moison, D., Guerquin, M.-J., N'Tumba-Byn, T., Pozzi-Gaudin, S., Benachi, A., Livera, G., Rouiller-Fabre, V. and Habert, R. 2015. A new chapter in the bisphenol A story: bisphenol S and bisphenol F are not safe alternatives to this compound. *Fertility and sterility*, 103 (1): 11-21.

Elias, J., Bechelany, M., Utke, I., Erni, R., Hosseini, D., Michler, J. and Philippe, L. 2012. Urchin-inspired zinc oxide as building blocks for nanostructured solar cells. *Nano Energy*, 1 (5): 696-705.

Espitia, P. J. P., Soares, N. d. F. F., dos Reis Coimbra, J. S., de Andrade, N. J., Cruz, R. S. and Medeiros, E. A. A. 2012. Zinc oxide nanoparticles: synthesis, antimicrobial activity and food packaging applications. *Food and Bioprocess Technology*, 5 (5): 1447-1464.

Fadeel, B. 2014. *Handbook of Safety Assessment of Nanomaterials: From Toxicological Testing to Personalized Medicine*. USA: CRC Press.

Fahoume, M., Maghfoul, O., , A., M., , Hartiti, B., Chraïbi, F. and and Ennaoui, A. 2006. Growth and characterization of ZnO thin films prepared by electrodeposition technique. *Solar Energy Materials and Solar Cells*, 90 (10): 1437-1444.

Fan, H., Li, Y., Wu, D., Ma, H., Mao, K., Fan, D., Du, B., Li, H. and Wei, Q. 2012. Electrochemical bisphenol A sensor based on N-doped graphene sheets. *Analytica Chimica Acta*, 711: 24-28.

Fanjul-Bolado, P., Hernández-Santos, D., Lamas-Ardisana, P. J., Martín-Pernía, A. and Costa-García, A. 2008. Electrochemical characterization of screen-printed and conventional carbon paste electrodes. *Electrochimica Acta*, 53 (10): 3635-3642.

Fanjul-Bolado, P., Queipo, P., Lamas-Ardisana, P. J. and Costa-García, A. 2007. Manufacture and evaluation of carbon nanotube modified screen-printed electrodes as electrochemical tools. *Talanta*, 74 (3): 427-433.

Fernández, M., Bianchi, M., Lux-Lantos, V. and Libertun, C. 2009. Neonatal exposure to bisphenol a alters reproductive parameters and gonadotropin releasing hormone signaling in female rats. *Environmental health perspectives*, 117 (5): 757.

Ferreira, F. D. P., Silva, L. I. B., Freitas, A. C., Rocha-Santos, T. A. P. and Duarte, A. C. 2009. High performance liquid chromatography coupled to an optical fiber detector coated with laccase for screening catecholamines in plasma and urine. *Journal of Chromatography A*, 1216 (42): 7049-7054.

Ferreira, V. C., Melato, A. I., Silva, A. F. and Abrantes, L. M. 2011. Conducting polymers with attached platinum nanoparticles towards the development of DNA biosensors. *Electrochemistry Communications*, 13 (9): 993-996.

Fiolhais, C., Nogueira, F. and Marques, M. A. 2003. *A primer in density functional theory*. Springer Science & Business Media.

Fonseca, F. N., Kato, M. J., Oliveira, L., Neto, N. P. and Tavares, M. F. M. 2001. Critical assessment of electrolyte systems for the capillary electrophoresis analysis of phenolic compounds in herbal extracts. *Journal of Microcolumn Separations*, 13 (6): 227-235.

Foo, K. L., Hashim, U., Muhammad, K. and Voon, C. H. 2014. Sol–gel synthesized zinc oxide nanorods and their structural and optical investigation for optoelectronic application. *Nanoscale Research Letters*, 9 (1): doi.org/10.1186/1556-1276X-1189-1429.

Frade, T., Jorge, M. M. and Gomes, A. 2012. One-dimensional ZnO nanostructured films: Effect of oxide nanoparticles. *Materials Letters*, 82: 13-15.

Franklin, J. B., Zou, B., Petrov, P., McComb, D. W., Ryan, M. P. and and McLachlan, M. A. 2011. Optimised pulsed laser deposition of ZnO thin films on transparent conducting substrates. *Journal of Materials Chemistry*, 21 (22): 8178-8182.

Gabriel, F. L., Cyris, M., Giger, W. and Kohler, H. P. E. 2007. ipso-Substitution: A General Biochemical and Biodegradation Mechanism to Cleave α-Quaternary Alkylphenols and Bisphenol A. *Chemistry & biodiversity*, 4 (9): 2123-2137.

Gaddam, V., Kumar, R. R., Parmar, M., Nayak, M. and Rajanna, K. 2015. Synthesis of ZnO nanorods on a flexible Phynox alloy substrate: influence of growth temperature on their properties. *RSC Advances*, 5 (109): 89985-89992.

Gao, P. X., Ding, Y., Mai, W., Hughes, W. L., Lao, C. and Wang, Z. L. 2005. Conversion of zinc oxide nanobelts into superlattice-structured nanohelices. *Science*, 309 (5741): 1700-1704.

Gao, X., Ma, J., Chen, Y. and Hong-Sheng, W. 2015. Rapid responses and mechanism of action for low-dose bisphenol S on ex vivo rat hearts and isolated myocytes: evidence of female-specific proarrhythmic effects. *Environmental health perspectives*, 123 (6): 571-578.

Geens, T., Goeyens, L. and Covaci, A. 2011. Are potential sources for human exposure to bisphenol-A overlooked? *International Journal of Hygiene and Environmental Health*, 214 (5): 339-347.

Geetha, S., Rao, C. R. K., Vijayan, M. and Trivedi, D. C. 2006. Biosensing and drug delivery by polypyrrole. *Analytica Chimica Acta*, 568 (1): 119-125.

Gerard, M., Chaubey, A. and Malhotra, B. D. 2002. Application of conducting polymers to biosensors. *Biosensors and Bioelectronics*, 17 (5): 345-359.

Girault, H. H. 2004. *Analytical and physical electrochemistry*. CRC Press.

Glausiusz, J. 2014. The plastics puzzle. *Nature*, 508 (7496): 306-308.

Gordon, R. G. 2000. Criteria for choosing transparent conductors. *MRS bulletin*, 25 (08): 52-57.

Grignard, E., Lapenna, S. and Bremer, S. 2012. Weak estrogenic transcriptional activities of Bisphenol A and Bisphenol S. *Toxicology in Vitro*, 26 (5): 727-731.

Gudiksen, M. S., Lauhon, L. J., Wang, J., Smith, D. C. and Lieber, C. M. 2002. Growth of nanowire superlattice structures for nanoscale photonics and electronics. *Nature*, 415 (6872): 617-620.

Gurav, K., Gang, M., Shin, S., Patil, U., Deshmukh, P., Agawane, G., Suryawanshi, M., Pawar, S., Patil, P. and Lokhande, C. 2014. Gas sensing properties of hydrothermally grown ZnO nanorods with different aspect ratios. *Sensors and Actuators B: Chemical*, 190: 439-445.

Han, L., Mei, F., Liu, C., Pedro, C. and and Alves, E. 2008. Comparison of ZnO thin films grown by pulsed laser deposition on sapphire and Si substrates. *Physica E: Low-dimensional Systems and Nanostructures*, 40 (3): 699-704.

Hao, Y., Meng, G., Wang, Z. L., Ye, C. and Zhang, L. 2006. Periodically Twinned Nanowires and Polytypic Nanobelts of ZnS: The Role of Mass Diffusion in Vapor− Liquid− Solid Growth. *Nano Letters*, 6 (8): 1650-1655.

Harrison, N. 2003. An introduction to density functional theory. *Nato Science Series Sub Series III Computer And Systems Science*, 187: 45-70.

Harvey, J. N. 2006. On the accuracy of density functional theory in transition metal chemistry. *Annual Reports Section" C"(Physical Chemistry)*, 102: 203-226.

Hashimoto, M., Tsukagoshi, K., Nakajima, R. and Kondo, K. 1999. Compact detection cell using optical fiber for sensitization and simplification of capillary electrophoresis–chemiluminescence detection. *Journal of Chromatography A*, 832 (1): 191-202.

Hasnidawani, J. N., Azlina, H. N., Norita, H., Bonnia, N. N., Ratim, S. and Ali, E. S. 2016. Synthesis of ZnO Nanostructures Using Sol-Gel Method. *Procedia Chemistry*, 19: 211-216.

Hohenberg, P. and Kohn, W. 1964. Inhomogeneous electron gas. *Physical Review*, 136 (3B): doi: org/10.1103.

Hossain, M., Ghosh, S., Boontongkong, Y., Thanachayanont, C. and Dutta, J. 2005. Growth of zinc oxide nanowires and nanobelts for gas sensing applications. In: Proceedings of *Journal of Metastable and Nanocrystalline Materials*. Trans Tech Publ, 27-30.

Hosseini, S., Sarsari, I. A., Kameli, P. and Salamati, H. 2015. Effect of Ag doping on structural, optical, and photocatalytic properties of ZnO nanoparticles. *Journal of Alloys and Compounds*, 640: 408-415.

Huang, M. H., Wu, Y., Feick, H., Tran, N., Weber, E. and Yang, P. 2001. Catalytic growth of zinc oxide nanowires by vapor transport. *Advanced Materials*, 13 (2): 113-116.

Huang, Z.-B., Yin, G.-F., Liao, X.-M. and Gu, J.-W. 2014. Conducting polypyrrole in tissue engineering applications. *Frontiers of Materials Science*, 8 (1): 39-45.

Iwakura, T., Iwafuchi, M., Muraoka, D., Yokosuka, M., Shiga, T., Watanabe, C. and Ohtani-Kaneko, R. 2010. Effect of bisphenol A on developing hypothalamic neurons. *Neuroscience Research*, 68: e281-e334.

Iwuoha, E. I., Williams-Dottin, A. R., Hall, L. A., Morrin, A., Mathebe, G. N., Smyth, M. R. and Killard, A. 2004. Electrochemistry and application of a novel monosubstituted squarate electron-transfer mediator in a glucose oxidase-doped poly (phenol) sensor. *Pure and applied chemistry*, 76 (4): 789-799.

Jaafar, A., Musa, A., Lee Yook, H., Nadarajah, K. and Hamidah, S. 2007. An Optical Biosensor based on Immobilization of Laccase and MBTH in Stacked Films for the Detection of Catechol. *Sensors*, 7: 2238-2250.

Jaffrezic-Renault, N. and Dzyadevych, S. V. 2008. Conductometric microbiosensors for environmental monitoring. *Sensors*, 8 (4): 2569-2588.

Jensen, F. 2016. *Introduction to computational chemistry*. Three ed. John wiley & sons.

Joshi, A., Aswal, D. K., Gupta, S. K., Yakhmi, J. V. and Gangal, S. A. 2009. ZnO-nanowires modified polypyrrole films as highly selective and sensitive chlorine sensors. *Applied Physics Letters*, 94 (10): doi.org/10.1063/1061.3093499

Junghanns, C., Moeder, M., Krauss, G., Martin, C. and Schlosser, D. 2005. Degradation of the xenoestrogen nonylphenol by aquatic fungi and their laccases. *Microbiology*, 151 (1): 45-57.

Kang, Z., Gu, Y., Yan, X., Bai, Z., Liu, Y., Liu, S., Zhang, X., Zhang, Z., Zhang, X. and Zhang, Y. 2015. Enhanced photoelectrochemical property of ZnO nanorods array synthesized on reduced graphene oxide for self-powered biosensing application. *Biosensors and Bioelectronics*, 64: 499-504.

Kansal, S. K., Ali, A. H., Kapoor, S. and Bahnemann, D. W. 2011. Synthesis of flower like zinc oxide nanostructure and its application as a photocatalyst. *Separation and Purification Technology*, 80 (1): 125-130.

Karami, H. and Fakoori, E. 2011. Sythesis and characterization of ZnO nanorods based on a new gel pyrolysis method. *Journal of Nanomaterials*, 2011 (2011): doi.org/10.1155/2011/628203.

Kaur, G., Mitra, A. and and Yadav, K. L. 2015. Pulsed laser deposited Al-doped ZnO thin films for optical applications. . *Progress in Natural Science: Materials International*, 25 (1): 12-21.

Keis, K., Magnusson, E., Lindström, H., Lindquist, S.-E. and Hagfeldt, A. 2002. A 5% efficient photoelectrochemical solar cell based on nanostructured ZnO electrodes. *Solar Energy Materials and Solar Cells*, 73 (1): 51-58.

Kinch, C. D., Ibhazehiebo, K., Jeong, J.-H., Habibi, H. R. and Kurrasch, D. M. 2015. Low-dose exposure to bisphenol A and replacement bisphenol S induces precocious hypothalamic neurogenesis in embryonic zebrafish. *Proceedings of the National Academy of Sciences*, 112 (5): 1475-1480.

Klejdus, B., Mikelová, R., Petrlová, J., Potěšil, D., Adam, V., Stiborová, M., Hodek, P., Vacek, J., Kizek, R. and Kubáň, V. 2005. Determination of isoflavones in soy bits by fast column high-performance liquid chromatography coupled with UV–visible diode-array detection. *Journal of Chromatography A*, 1084 (1): 71-79.

Kohn, W. and Sham, L. J. 1965. Self-Consistent Equations Including Exchange and Correlation Effects. *Physical Review*, 140 (4A): A1133-A1138.

Kołodziejczak-Radzimska, A. and Jesionowski, T. 2014. Zinc oxide—from synthesis to application: a review. *Materials*, 7 (4): 2833-2881.

Kong, X. Y., Ding, Y., Yang, R. and Wang, Z. L. 2004. Single-crystal nanorings formed by epitaxial self-coiling of polar nanobelts. *Science*, 303 (5662): 1348-1351.

Kong, X. Y. and Wang, Z. L. 2003. Spontaneous polarization-induced nanohelixes, nanosprings, and nanorings of piezoelectric nanobelts. *Nano Letters*, 3 (12): 1625-1631.

Kuch, H. M. and Ballschmiter, K. 2001. Determination of endocrine-disrupting phenolic compounds and estrogens in surface and drinking water by HRGC−(NCI)− MS in the picogram per liter range. *Environmental science & technology*, 35 (15): 3201-3206.

Kumar, S. S., Venkateswarlu, P., Rao, V. R. and and Rao, G. N. 2013. Synthesis, characterization and optical properties of zinc oxide nanoparticles. *International Nano Letters*, 3 (1): 30.

Ladanov, M., Ram, M. K., Matthews, G. and Kumar, A. 2011. Structure and Opto-electrochemical Properties of ZnO Nanowires Grown on n-Si Substrate. *Langmuir*, 27: 9012-9017.

Larsson, K., Ljung Björklund, K., Palm, B., Wennberg, M., Kaj, L., Lindh, C. H., Jönsson, B. A. G. and Berglund, M. 2014. Exposure determinants of phthalates, parabens, bisphenol A and triclosan in Swedish mothers and their children. *Environment International*, 73: 323-333.

Lei, Y., Chen, W. and Mulchandani, A. 2006. Microbial biosensors. *Analytica Chimica Acta*, 568 (1): 200-210.

Levy, M. 1979. Universal variational functionals of electron densities, first-order density matrices, and natural spin-orbitals and solution of the v-representability problem. *Proceedings of the National Academy of Sciences*, 76 (12): 6062-6065.

Levy, M. 1982. Electron densities in search of Hamiltonians. *Physical Review A*, 26 (3): 1200-1208.

Li, D., Luo, L., Pang, Z., Ding, L., Wang, Q., Ke, H., Huang, F. and Wei, Q. 2014. Novel phenolic biosensor based on a magnetic polydopamine-laccase-nickel nanoparticle loaded carbon nanofiber composite. *ACS applied materials & interfaces*, 6 (7): 5144-5151.

Li, Y.-F., Liu, Z.-M., Liu, Y.-L., Yang, Y.-H., Shen, G.-L. and Yu, R.-Q. 2006. A mediator-free phenol biosensor based on immobilizing tyrosinase to ZnO nanoparticles. *Analytical biochemistry*, 349 (1): 33-40.

Liao, C. and Kannan, K. 2013. Concentrations and profiles of bisphenol A and other bisphenol analogues in foodstuffs from the United States and their implications for human exposure. *Journal of Agricultural and Food Chemistry*, 61 (19): 4655-4662.

Liao, C., Liu, F. and Kannan, K. 2012. Bisphenol S, a new bisphenol analogue, in paper products and currency bills and its association with bisphenol A residues. *Environmental science & technology*, 46 (12): 6515-6522.

Liu, F., Cao, P., Zhang, H., Shen, C., Wang, Z., Li, J. and Gao, H. 2005. Well-aligned zinc oxide nanorods and nanowires prepared without catalyst. *Journal of crystal growth*, 274 (1): 126-131.

Liu, Y., Qu, X., Guo, H., Chen, H., Liu, B. and Dong, S. 2006. Facile preparation of amperometric laccase biosensor with multifunction based on the matrix of carbon nanotubes–chitosan composite. *Biosensors and Bioelectronics*, 21 (12): 2195-2201.

Liu, Z.-h., Kanjo, Y. and and Mizutani, S. 2009. Removal mechanisms for endocrine disrupting compounds (EDCs) in wastewater treatment — physical means, biodegradation, and chemical advanced oxidation: A review. . *Science of The Total Environment*, 407 (2): 731-748.

Lotti, N., Colonna, M., Fiorini, M., Finelli, L. and Berti, C. 2011. Poly (butylene terephthalate) modified with ethoxylated bisphenol S with increased glass transition temperature and improved thermal stability. *Polymer*, 52 (4): 904-911.

Lu, B., Liu, M., Shi, H., Huang, X. and Zhao, G. 2013. A novel photoelectrochemical sensor for bisphenol A with high sensitivity and selectivity based on surface molecularly imprinted polypyrrole modified TiO2 nanotubes. *Electroanalysis*, 25 (3): 771-779.

Lu, J. G., Chang, P. and Fan, Z. 2006. Quasi-one-dimensional metal oxide materials—Synthesis, properties and applications. *Materials Science and Engineering: R: Reports*, 52 (1): 49-91.

Lundqvist, S. and March, N. H. 2013. *Theory of the inhomogeneous electron gas*. Springer Science & Business Media.

Luong, J. H., Male, K. B. and Glennon, J. D. 2008. Biosensor technology: technology push versus market pull. *Biotechnology advances*, 26 (5): 492-500.

Lupetti, K. O., Rocha, F. R. and Fatibello-Filho, O. 2004. An improved flow system for phenols determination exploiting multicommutation and long pathlength spectrophotometry. *Talanta*, 62 (3): 463-467.

Ma, R. and Sasaki, T. 2010. Nanosheets of oxides and hydroxides: Ultimate 2D charge-bearing functional crystallites. *Advanced Materials*, 22 (45): 5082-5104.

Madhavi, V. and Lele, S. 2009. Laccase: properties and applications. *BioResources*, 4 (4): 1694-1717.

Maffini, M. V., Rubin, B. S., Sonnenschein, C. and Soto, A. M. 2006. Endocrine disruptors and reproductive health: the case of bisphenol-A. *Molecular and cellular endocrinology*, 254: 179-186.

Mahalingam, T., John, V., Raja, M., Su, Y.-K. and and Sebastian, P. 2005. Electrodeposition and characterization of transparent ZnO thin films. *Solar Energy Materials and Solar Cells*, 88 (2): 227-235.

Mamat, M. H., Khusaimi, Z., Musa, M. Z., Malek, M. F. and Rusop, M. 2011. Fabrication of ultraviolet photoconductive sensor using a novel aluminium-doped zinc oxide nanorod–nanoflake network thin film prepared via ultrasonic-assisted sol–gel and immersion methods. *Sensors and Actuators A: Physical*, 171 (2): 241-247.

Marie, M., Mandal, S. and Manasreh, O. 2015. An electrochemical glucose sensor based on zinc oxide nanorods. *Sensors*, 15 (8): 18714-18723.

Mayorga-Martinez, C. C., Guix, M., Madrid, R. E. and Merkoçi, A. 2012. Bimetallic nanowires as electrocatalysts for nonenzymatic real-time impedancimetric detection of glucose. *Chemical Communications*, 48 (11): 1686-1688.

Mbuyisa, P., Ndwandwe, O. and Cepek, C. 2015. Controlled growth of zinc oxide nanorods synthesised by the hydrothermal method. *Thin Solid Films*, 578: 7-10.

McNeill, R., Siudak, R., Wardlaw, J. and Weiss, D. 1963. Electronic conduction in polymers. I. The chemical structure of polypyrrole. *Australian Journal of Chemistry*, 16 (6): 1056-1075.

Mehrotra, P. 2016. Biosensors and their applications – A review. *Journal of Oral Biology and Craniofacial Research*, 6 (2): 153-159.

Mei, L.-P., Feng, J.-J., Wu, L., Zhou, J.-Y., Chen, J.-R. and Wang, A.-J. 2015. Novel phenol biosensor based on laccase immobilized on reduced graphene oxide supported palladium–copper alloyed nanocages. *Biosensors and Bioelectronics*, 74: 347-352.

Meulenkamp, E. A. 1998. Synthesis and growth of ZnO nanoparticles. *The Journal of Physical Chemistry B*, 102 (29): 5566-5572.

Moghaddam, A. B., Nazari, T., Badraghi, J. and Kazemzad, M. 2009. Synthesis of ZnO Nanoparticles and Electrodeposition of Polypyrrole/ZnO Nanocomposite Film. *International Journal of Electrochemical Science*, 4: 247-257.

Morozova, O., Shumakovich, G., Shleev, S. and Yaropolov, Y. I. 2007. Laccase-mediator systems and their applications: a review. *Applied Biochemistry and Microbiology*, 43 (5): 523-535.

Moulahi, A. and Sediri, F. 2014. ZnO nanoswords and nanopills: Hydrothermal synthesis, characterization and optical properties. *Ceramics International*, 40 (1): 943-950.

Mu, B. and Wang, A. 2016. Adsorption of dyes onto palygorskite and its composites: a review. *Journal of Environmental Chemical Engineering*, 4 (1): 1274-1294.

Narayanan, G. N., Ganesh, R. S. and Karthigeyan, A. 2016. Effect of annealing temperature on structural, optical and electrical properties of hydrothermal assisted zinc oxide nanorods. *Thin Solid Films*, 598: 39-45.

Nasr, M., Viter, R., Eid, C., Warmont, F., Habchi, R., Miele, P. and Bechelany, M. 2016. Synthesis of novel ZnO/ZnAl 2 O 4 multi co-centric nanotubes and their long-term stability in photocatalytic application. *RSC Advances*, 6 (105): 103692-103699.

Naveen, M. H., Gurudatt, N. G. and Shim, Y.-B. 2017. Applications of conducting polymer composites to electrochemical sensors: A review. *Applied Materials Today*, 9 (Supplement C): 419-433.

Neilson, A. H., Allard, A. S., Hynning, P. Å. and Remberger, M. 1991. Distribution, fate and persistence of organochlorine compounds formed during production of bleached pulp. *Toxicological & Environmental Chemistry*, 30 (1-2): 3-41.

Ntsendwana, B., Mamba, B., Sampath, S. and Arotiba, O. 2012. Electrochemical detection of bisphenol A using graphene-modified glassy carbon electrode. *International Journal of Electrochemical Science*, 7 (4): 3501-3512.

Okada, H., Tokunaga, T., Liu, X., Takayanagi, S., Matsushima, A. and Shimohigashi, Y. 2008. Direct evidence revealing structural elements essential for the high binding ability of bisphenol A to human estrogen-related receptor-γ. *Environmental health perspectives*, 116 (1): 32.

Olea, N., Pulgar, R., Pérez, P., Olea-Serrano, F., Rivas, A., Novillo-Fertrell, A., Pedraza, V., Soto, A. M. and Sonnenschein, C. 1996. Estrogenicity of resin-based composites and sealants used in dentistry. *Environmental health perspectives*, 104 (3): 298.

Opeolu, B., Fatoki, O. and Odendaal, J. 2010. Development of a solid-phase extraction method followed by HPLC-UV detection for the determination of phenols in water. *International Journal of Physical Sciences*, 5 (5): 576-581.

Osipov, E., Polyakov, K., Kittl, R., Shleev, S., Dorovatovsky, P., Tikhonova, T., Hann, S., Ludwig, R. and Popov, V. 2014. Effect of the L499M mutation of the ascomycetous Botrytis aclada laccase on redox

potential and catalytic properties. *Acta Crystallographica Section D: Biological Crystallography*, 70 (11): 2913-2923.

Otero, T. F. 2000. Electrochemomechanical devices based on conducting polymers. In: *Polymer Sensors and Actuators*. Springer, 295-323.

Otero, T. F. 2009. Soft, wet, and reactive polymers. Sensing artificial muscles and conformational energy. *Journal of Materials Chemistry*, 19 (6): 681-689.

Ou, J., Hu, L., Hu, L., Li, X. and Zou, H. 2006. Determination of phenolic compounds in river water with on-line coupling bisphenol A imprinted monolithic precolumn with high performance liquid chromatography. *Talanta*, 69 (4): 1001-1006.

Özgür, Ü., Alivov, Y. I., Liu, C., Teke, A., Reshchikov, M., Doğan, S., Avrutin, V., Cho, S.-J. and Morkoc, H. 2005. A comprehensive review of ZnO materials and devices. *Journal of Applied Physics*, 98 (4): doi.org/10.1063/1061.1992666

Pan, G., Guo, Q., Cao, C., Yang, H. and Li, B. 2013. Thermo-responsive molecularly imprinted nanogels for specific recognition and controlled release of proteins. *Soft Matter*, 9 (14): 3840-3850.

Pan, X. and Zhao, X. 2015. Ultra-High Sensitivity Zinc Oxide Nanocombs for On-Chip Room Temperature Carbon Monoxide Sensing. *Sensors*, 15 (4): 8919-8930.

Perdew, J. P., Burke, K. and Ernzerhof, M. 1996. Generalized gradient approximation made simple. *Physical review letters*, 77 (18): 3865.

Perednis, D. and Gauckler, L. J. 2005. Thin Film Deposition Using Spray Pyrolysis. *Journal of Electroceramics*, 14 (2): 103-111.

Pietruszka, R., Witkowski, B. S., Gieraltowska, S., Caban, P., Wachnicki, L., Zielony, E., Gwozdz, K., Bieganski, P., Placzek-Popko, E. and Godlewski, M. 2015. New efficient solar cell structures based on zinc oxide nanorods. *Solar Energy Materials and Solar Cells*, 143: 99-104.

Piontek, K., Antorini, M. and Choinowski, T. 2002. Crystal structure of a laccase from the fungusTrametes versicolor at 1.90-Å resolution containing a full complement of coppers. *Journal of Biological Chemistry*, 277 (40): 37663-37669.

Pivnenko, K., Pedersen, G. A., Eriksson, E. and Astrup, T. F. 2015. Bisphenol A and its structural analogues in household waste paper. *Waste Management*, 44: 39-47.

PlasticsEurope. Manufactures, A. o. P. 2007. *Application of Bisphenol A*.

Pohanka, M. and Skládal, P. 2008. Electrochemical biosensors–principles and applications. *Journal of Applied Biomedicine*

6(2): 57-64.

Polshettiwar, V., Baruwati, B. and Varma, R. S. 2009. Self-assembly of metal oxides into three-dimensional nanostructures: synthesis and application in catalysis. *ACS nano*, 3 (3): 728-736.

Portaccio, M., Di Tuoro, D., Arduini, F., Moscone, D., Cammarota, M., Mita, D. G. and Lepore, M. 2013. Laccase biosensor based on screen-printed electrode modified with thionine–carbon black nanocomposite, for Bisphenol A detection. *Electrochimica Acta*, 109: 340-347.

Puurunen, R. L. 2005. Surface chemistry of atomic layer deposition: A case study for the trimethylaluminum/water process. *Journal of Applied Physics*, 97 (12): doi.org/10.1063/1061.1940727

Quan, D. and Shin, W. 2004. Amperometric Detection of Catechol and Catecholamines by Immobilized Laccase from DeniLite. *Electroanalysis*, 16 (19): 1576-1582.

Rani, S., Suri, P., Shishodia, P. and Mehra, R. 2008. Synthesis of nanocrystalline ZnO powder via sol–gel route for dye-sensitized solar cells. *Solar Energy Materials and Solar Cells*, 92 (12): 1639-1645.

Rasmussen, J. W., Martinez, E., Louka, P. and Wingett, D. G. 2010. Zinc oxide nanoparticles for selective destruction of tumor cells and potential for drug delivery applications. *Expert opinion on drug delivery*, 7 (9): 1063-1077.

Rechberger, F. and Niederberger, M. 2017. Synthesis of aerogels: from molecular routes to 3-dimensional nanoparticle assembly. *Nanoscale Horizons*, 2 (1): 6-30.

Reddy, S., Reddy, V., Reddy, K. and Kumari, P. 2013. Synthesis, structural, optical properties and antibacterial activity of co-doped (Ag, Co) ZnO nanoparticles. *Research Journal of Material Science*, 1 (1): 11-20.

Richter, C. A., Birnbaum, L. S., Farabollini, F., Newbold, R. R., Rubin, B. S., Talsness, C. E., Vandenbergh, J. G., Walser-Kuntz, D. R. and vom Saal, F. S. 2007. In vivo effects of bisphenol A in laboratory rodent studies. *Reproductive toxicology*, 24 (2): 199-224.

Rochester, J. R. 2013. Bisphenol A and human health: A review of the literature. *Reproductive toxicology*, 42: 132-155.

Rochester, J. R. and Bolden, A. L. 2015. Bisphenol S and F: a systematic review and comparison of the hormonal activity of bisphenol A substitutes. *Environmental health perspectives*, 123 (7): 643-650.

Rodríguez-Delgado, M. M., Alemán-Nava, G. S., Rodríguez-Delgado, J. M., Dieck-Assad, G., Martínez-Chapa, S. O., Barceló, D. and Parra, R. 2015. Laccase-based biosensors for detection of phenolic compounds. *TrAC Trends in Analytical Chemistry*, 74: 21-45.

Rodriguez-Mozaz, S., de Alda, M. L. and Barceló, D. 2005. Analysis of bisphenol A in natural waters by means of an optical immunosensor. *Water Research*, 39 (20): 5071-5079.

Rubianes, M. and Rivas, G. 2000. Amperometric Biosensor for Phenols and Catechols Based on Iridium-Polyphenol Oxidase-Modified Carbon Paste. *Electroanalysis*, 12 (14): 1159-1162.

Saito, R., Hofmann, M., Dresselhaus, G., Jorio, A. and Dresselhaus, M. S. 2011. Raman spectroscopy of graphene and carbon nanotubes. *Advances in Physics*, 60 (3): 413-550.

Sambe, H., Hoshina, K., Hosoya, K. and Haginaka, J. 2006. Simultaneous determination of bisphenol A and its halogenated derivatives in river water by combination of isotope imprinting and liquid chromatography–mass spectrometry. *Journal of Chromatography A*, 1134 (1): 16-23.

Sarafraz-Yazdi, A., Dizavandi, Z. R. and Amiri, A. 2012. Determination of phenolic compounds in water and urine samples using solid-phase microextraction based on sol–gel technique prior to GC-FID. *Analytical Methods*, 4 (12): 4316-4325.

Schlettwein, D., Oekermann, T., Yoshida, T., Tochimoto, M. and Minoura, H. 2000. Photoelectrochemical sensitisation of ZnO–tetrasulfophthalocyaninatozinc composites prepared by electrochemical self-assembly. *Journal of Electroanalytical Chemistry*, 481 (1): 42-51.

Segall, M. D., Lindan, P. J., Probert, M. A., Pickard, C. J., Hasnip, P. J., Clark, S. J. and Payne, M. C. 2002. First-principles simulation: ideas, illustrations and the CASTEP code. *Journal of Physics: Condensed Matter*, 14 (11): 2717.

Segets, D., Gradl, J., Taylor, R. K., Vassilev, V. and Peukert, W. 2009. Analysis of optical absorbance spectra for the determination of ZnO nanoparticle size distribution, solubility, and surface energy. *ACS nano*, 3 (7): 1703-1710.

Sharma, S., Dalal, V. S. and Mahajan, V. 2016. Synthesis of Zinc oxide nano flower for photovoltaic applications. *Materials Today: Proceedings*, 3 (6): 1359-1362.

Shayeh, J. S., Ehsani, A., Ganjali, M., Norouzi, P. and Jaleh, B. 2015. Conductive polymer/reduced graphene oxide/Au nano particles as efficient composite materials in electrochemical supercapacitors. *Applied Surface Science*, 353: 594-599.

Shi, R., Yang, P., Dong, X., Ma, Q. and Zhang, A. 2013. Growth of flower-like ZnO on ZnO nanorod arrays created on zinc substrate through low-temperature hydrothermal synthesis. *Applied Surface Science*, 264: 162-170.

Shiigi, H., Kishimoto, M., Yakabe, H., Deore, B. and Nagaoka, T. 2002. Highly Selective Molecularly Imprinted Overoxide Polypyrrole Colloids: One -Step Preparation Technique. *Analytical Science*, 18 (1): 41-44.

Singh, O., Kohli, N. and and Singh, R. C. 2013. Precursor controlled morphology of zinc oxide and its sensing behaviour. *Sensors and Actuators B: Chemical*, 178: 149-154.

Siva Vijayakumar, T., Karthikeyeni, S., Vasanth, S., Ganesh, A., Bupesh, G., Ramesh, R., Manimegalai, M. and Subramanian, P. 2013. Synthesis of silver-doped zinc oxide nanocomposite by pulse mode ultrasonication and its characterization studies. *Journal of Nanoscience*, 2013: doi.org/10.1155/2013/785064.

Skledar, D. G. and Mašič, L. P. 2016. Bisphenol A and its analogs: Do their metabolites have endocrine activity? *Environmental toxicology and pharmacology*, 47: 182-199.

Sokolov, P., Baranov, A., Dobrokhotov, Z. V. and Solozhenko, V. 2010. Synthesis and thermal stability of cubic ZnO in the salt nanocomposites. *Russian Chemical Bulletin*, 59 (2): 325-328.

Soltaninezhad, M. and Aminifar, A. 2011. Study nanostructures of semiconductor zinc oxide (ZnO) as a photocatalyst for the degradation of organic pollutants. *International Journal of Nano Dimension*, 2: 137-145.

Srikant, V. and Clarke, D. R. 1998. On the optical band gap of zinc oxide. *Journal of Applied Physcics*, 83 (10): 5447-5451.

Stuart, J. D., Capulong, C. P., Launer, K. D. and Pan, X. 2005. Analyses of phenolic endocrine disrupting chemicals in marine samples by both gas and liquid chromatography–mass spectrometry. *Journal of Chromatography A*, 1079 (1): 136-145.

Švegl, F., Orel, B. and Hutchins, M. 1997. Structural and electrochromic properties of Co-oxide and Co/Al/Si-oxide films prepared by the sol-gel dip coating technique. *Journal of Sol-Gel Science and Technology*, 8 (1): 765-769.

Tan, Y., Deng, W., Ge, B., Xie, Q., Huang, J. and Yao, S. 2009. Biofuel cell and phenolic biosensor based on acid-resistant laccase–glutaraldehyde functionalized chitosan–multiwalled carbon nanotubes nanocomposite film. *Biosensors and Bioelectronics*, 24 (7): 2225-2231.

Tang, L., Zeng, G., Liu, J., Xu, X., Zhang, Y., Shen, G., Li, Y. and Liu, C. 2008. Catechol determination in compost bioremediation using a laccase sensor and artificial neural networks. *Analytical and bioanalytical chemistry*, 391 (2): 679-685.

Thurston, C., F. 1994. The structure and function of fungal laccases. *Microbiology*, 140: 19-20.

Troshyn, O., Kovalenko, A., Dorofeev, S. and Baranov, A. 2012. Sensitization of ZnO nanorods with CdSe quantum dots. *Inorganic materials*, 48 (7): 709-715.

Tsukagoshi, K., Kameda, T., Yamamoto, M. and Nakajima, R. 2002. Separation and determination of phenolic compounds by capillary electrophoresis with chemiluminescence detection. *Journal of Chromatography A*, 978 (1): 213-220.

Tsukamoto, T., Ishikawa, Y., Sengoku, Y. and Kurita, N. 2009. A combined DFT/Green's function study on electrical conductivity through DNA duplex between Au electrodes. *Chemical Physics Letters*, 474 (4): 362-365.

Ullah, H. 2017. Inter-molecular interaction in Polypyrrole/TiO 2: a DFT study. *Journal of Alloys and Compounds*, 692: 140-148.

Valls, J., Millán, S., Martí, M. P., Borràs, E. and Arola, L. 2009. Advanced separation methods of food anthocyanins, isoflavones and flavanols. *Journal of Chromatography A*, 1216 (43): 7143-7172.

Vandenberg, L. N., Hauser, R., Marcus, M., Olea, N. and Welshons, W. V. 2007. Human exposure to bisphenol A (BPA). *Reproductive toxicology*, 24 (2): 139-177.

Vernitskaya, T. y. V. and Efimov, O. N. 1997. Polypyrrole: a conducting polymer; its synthesis, properties and applications. *Russian chemical reviews*, 66 (5): 443-457.

Vílchez, J. L., Zafra, A., González-Casado, A., Hontoria, E. and del Olmo, M. 2001. Determination of trace amounts of bisphenol F, bisphenol A and their diglycidyl ethers in wastewater by gas chromatography–mass spectrometry. *Analytica Chimica Acta*, 431 (1): 31-40.

Viñas, P., Campillo, N., Martínez-Castillo, N. and Hernández-Córdoba, M. 2010. Comparison of two derivatization-based methods for solid-phase microextraction–gas chromatography–mass spectrometric determination of bisphenol A, bisphenol S and biphenol migrated from food cans. *Analytical and bioanalytical chemistry*, 397 (1): 115-125.

Wagner, R. and Ellis, W. 1964. Vapor-liquid-solid mechanism of single crystal growth. *Applied Physics Letters*, 4 (5): 89-90.

Wahab, R., Ansari, S. G., Kim, Y. S., Seo, H. K., Kim, G. S., Khang, G. and Shin, H.-S. 2007. Low temperature solution synthesis and characterization of ZnO nano-flowers. *Materials Research Bulletin*, 42 (9): 1640-1648.

Wang, J., Sun, X. W., Wei, A., Lei, Y., Cai, X., Li, C. M. and Dong, Z. L. 2006. Zinc oxide nanocomb biosensor for glucose detection. *Applied Physics Letters*, 88 (23): doi.org/10.1063/1061.2210078.

Wang, Q., Wang, G., , J., J., , Han, X., Xu, B. and and Hou, J. G. 2005. Annealing effect on optical properties of ZnO films fabricated by cathodic electrodepositio. *Thin Solid Films*, 492 (1): 61-65.

Wang, R., Ren, D., Xia, S., Zhang, Y. and Zhao, J. 2009. Photocatalytic degradation of Bisphenol A (BPA) using immobilized TiO2 and UV illumination in a horizontal circulating bed photocatalytic reactor (HCBPR). *Journal of Hazardous Materials*, 169 (1–3): 926-932.

Wang, Z. L. and Song, J. 2006. Piezoelectric nanogenerators based on zinc oxide nanowire arrays. *Science*, 312 (5771): 242-246.

Warule, S. S., Chaudhari, N. S., Kale, B. B. and More, M. A. 2009. Novel sonochemical assisted hydrothermal approach towards the controllable synthesis of ZnO nanorods, nanocups and nanoneedles and their photocatalytic study. *CrystEngComm*, 11 (12): 2776-2783.

Watabe, Y., Kondo, T., Morita, M., Tanaka, N., Haginaka, J. and Hosoya, K. 2004. Determination of bisphenol A in environmental water at ultra-low level by high-performance liquid chromatography with an effective on-line pretreatment device. *Journal of Chromatography A*, 1032 (1): 45-49.

Waterhouse, G. I., Bowmaker, G. A. and Metson, J. B. 2001. The thermal decomposition of silver (I, III) oxide: a combined XRD, FT-IR and Raman spectroscopic study. *Physical Chemistry Chemical Physics*, 3 (17): 3838-3845.

Weng, Y.-I., Hsu, P.-Y., Liyanarachchi, S., Liu, J., Deatherage, D. E., Huang, Y.-W., Zuo, T., Rodriguez, B., Lin, C.-H. and Cheng, A.-L. 2010. Epigenetic influences of low-dose bisphenol A in primary human breast epithelial cells. *Toxicology and applied pharmacology*, 248 (2): 111-121.

Willander, M., Zhao, Q. and Nur, O. 2007. *Zinc oxide nanostructures at the forefront of new white light-emitting technology*. SPIE Newsroom.

Williams, G. and Kamat, P. V. 2009. Graphene− semiconductor nanocomposites: excited-state interactions between ZnO nanoparticles and graphene oxide. *Langmuir*, 25 (24): 13869-13873.

Wissiack, R., Rosenberg, E. and Grasserbauer, M. 2000. Comparison of different sorbent materials for on-line solid-phase extraction with liquid chromatography–atmospheric pressure chemical ionization mass spectrometry of phenols. *Journal of Chromatography A*, 896 (1): 159-170.

Wong, E. M., Bonevich, J. E. and Searson, P. C. 1998. Growth kinetics of nanocrystalline ZnO particles from colloidal suspensions. *The Journal of Physical Chemistry B*, 102 (40): 7770-7775.

Wu, C., Liu, Z., Sun, H., Wang, X. and Xu, P. 2016. Selective determination of phenols and aromatic amines based on horseradish peroxidase-nanoporous gold co-catalytic strategy. *Biosensors and Bioelectronics*, 79: 843-849.

Xu, H., Wang, H., Zhang, Y., He, W., Zhu, M., Wang, B. and Yan, H. 2004. Hydrothermal synthesis of zinc oxide powders with controllable morphology. *Ceramics International*, 30 (1): 93-97.

Xu, Y., Lei, W., Zhang, Y., Fan, H., Hao, Q. and Gao, S. 2017. Bamboo Fungus-Derived Porous Nitrogen-Doped Carbon for the Fast, Sensitive Determination of Bisphenol A. *Journal of The Electrochemical Society*, 164 (5): B3043-B3048.

Xue, J., Wan, Y. and Kannan, K. 2016. Occurrence of bisphenols, bisphenol A diglycidyl ethers (BADGEs), and novolac glycidyl ethers (NOGEs) in indoor air from Albany, New York, USA, and its implications for inhalation exposure. *Chemosphere*, 151: 1-8.

Yahya AL-she'irey, A. 2016. Effect of Methylammonium Iodide (CH3NH3PbI3) Perovskite Concentration on the Performance of Perovskite Solar Cell. *KnE Engineering*, 2016 (1): DOI: 10.18502/keg.v18501i18501.18502.

Yakimova, R., Selegård, L., Khranovskyy, V., Pearce, R., Lloyd Spetz, A. and Uvdal, K. 2012a. ZnO materials and surface tailoring for biosensing. *Frontiers in Bioscience*, 4 (1): 254-278.

Yakimova, R., Selegård, L., Khranovskyy, V., Pearce, R., Lloyd Spetz, A. and Uvdal, K. 2012b. ZnO materials and surface tailoring for biosensing. *Frontiers in bioscience (Elite edition)*, 4 (1): 254-278.

Yang, R. D., Tripathy, S., Li, Y. and Sue, H.-J. 2005. Photoluminescence and micro-Raman scattering in ZnO nanoparticles: The influence of acetate adsorption. *Chemical Physics Letters*, 411 (1–3): 150-154.

Yıldırım, Ö. A., Unalan, H. E. and Durucan, C. 2013. Highly Efficient Room Temperature Synthesis of Silver-Doped Zinc Oxide (ZnO: Ag) Nanoparticles: Structural, Optical, and Photocatalytic Properties. *Journal of the American Ceramic Society*, 96 (3): 766-773.

Yin, H., Zhou, Y., Xu, J., Ai, S., Cui, L. and Zhu, L. 2010. Amperometric biosensor based on tyrosinase immobilized onto multiwalled carbon nanotubes-cobalt phthalocyanine-silk fibroin film and its application to determine bisphenol A. *Analytica Chimica Acta*, 659 (1): 144-150.

Young, D. 2001. *Computational chemistry: A practical guide for applying techniques to real world problems*. USA: John Wiley & Sons.

Yu, C., Gou, L., Zhou, X., Bao, N. and Gu, H. 2011. Chitosan–Fe 3 O 4 nanocomposite based electrochemical sensors for the determination of bisphenol A. *Electrochimica Acta*, 56 (25): 9056-9063.

Zhai, J., Yong, D., Li, J. and Dong, S. 2013. A novel colorimetric biosensor for monitoring and detecting acute toxicity in water. *Analyst*, 138 (2): 702-707.

Zhang, A., Wan, L., Wu, C., Fang, Y., Han, G., Li, H., Zhang, Z. and Wang, H. 2013. Simultaneous determination of 14 phenolic compounds in grape canes by HPLC-DAD-UV using wavelength switching detection. *Molecules*, 18 (11): 14241-14257.

Zhang, H., Yang, D., Ma, X., Ji, Y., Xu, J. and Que, D. 2004. Synthesis of flower-like ZnO nanostructures by an organic-free hydrothermal process. *Nanotechnology*, 15 (5): 622.

Zhang, X. L., Qiao, R., Kim, J. C. and Kang, Y. S. 2008. Inorganic cluster synthesis and characterization of transition-metal-doped ZnO hollow spheres. *Crystal Growth and Design*, 8 (8): 2609-2613.

Zhang, Y., Zeng, G.-M., Tang, L., Huang, D.-L., Jiang, X.-Y. and Chen, Y.-N. 2007. A hydroquinone biosensor using modified core–shell magnetic nanoparticles supported on carbon paste electrode. *Biosensors and Bioelectronics*, 22 (9): 2121-2126.

Zhao, M.-H., Wang, Z.-L. and Mao, S. X. 2004. Piezoelectric characterization of individual zinc oxide nanobelt probed by piezoresponse force microscope. *Nano Letters*, 4 (4): 587-590.

Zhou, J., Zhao, F., Wang, Y., Zhang, Y. and Yang, L. 2007. Size-controlled synthesis of ZnO nanoparticles and their photoluminescence properties. *Journal of luminescence*, 122: 195-197.

Zhou, Y., Tang, L., Zeng, G., Chen, J., Cai, Y., Zhang, Y., Yang, G., Liu, Y., Zhang, C. and Tang, W. 2014. Mesoporous carbon nitride based biosensor for highly sensitive and selective analysis of phenol and catechol in compost bioremediation. *Biosensors and Bioelectronics*, 61: 519-525.

Zhou, Y., Yang, L., Lu, J., Wu, Y., Li, C., Liu, Y. and Li, M. 2016. Photoelectric properties of three-dimensional urchin-like zinc oxide/titanium dioxide composite micronanostructures. *Micro & Nano Letters*, 11 (5): 277-280.

Zucca, P. and Sanjust, E. 2014. Inorganic Materials as Supports for Covalent Enzyme Immobilization: Methods and Mechanisms. *Molecules*, 19 (9): 14139-14194.